UNIVERSITY OF CALIFORNIA SAN DIEGO

Modular Nucleic Acid Nano-Complexes Self-Assembling from Small RNA and DNA Motifs

A dissertation submitted in partial satisfaction of the requirements
for the degree Doctor of Philosophy

in

Materials Science and Engineering

by

Shi Chen

Committee in Charge:

Professor Thomas Hermann, Chair
Professor Michael Gilson
Professor Jeffrey Rinehart
Professor Akif Tezcan
Professor Jerry Yang

2021

The dissertation of Shi Chen is approved, and it is acceptable in quality and form for publication on microfilm and electronically.

University of California San Diego

2021

Dedication

This dissertation is dedicated to my beloved parents,

my father and my mother,

for their endless love and support

Table of Contents

List of Abbreviations

AFM: Atomic Force Microscopy

APS: Ammonium Persulfate

Cryo-EM: Cryogenic Electron Microscopy

DNA: Deoxyribonucleic Acid

FRET: Förster Resonance Energy Transfer

HCV: Hepatitis C Virus

IRES: Internal Ribosome Entry Sites

PAGE: Polyacrylamide Gel Electrophoresis

RNA: Ribonucleic Acid

SEM: Scanning Electron Microscopy

SVV: Seneca Valley Virus

ssRNA: Single-stranded RNA

TAMRA: Tetramethylrhodamine

TEM: Transmission Electronic Microscopy

TEMED: Tetramethylethylenediamine

List of Figures

List of Tables

Acknowledgements

I want to thank Prof. Thomas Hermann for being a truly great mentor. His genuine interest in science mentored my growth to be a scientist and his wisdom in life mentored my growth as a person.

I also want to thank all my lab mates who were in my life for the last six years. Their help and support were incredible. I want to especially thank Mark Boerneke, a great scientist graduated from Hermann lab, for helping me start my research in Hermann lab.

The material in Chapter 2, in full, is a reprint of material as it appears in Methods (2021) titled "A simple screening strategy for complex RNA-DNA hybrid nanoshapes" with Alba Monferrer and Thomas Herman as co-authors. The dissertation author was the primary investigator and author of this material. Prof. Hermann was the corresponding author.

The material in Chapter 3, in full, is a reprint of material as it appears in Nano Research (2021, 14(1), 46-51) titled "Complex RNA-DNA hybrid nanoshapes from iterative mix-and-match screening" with Zhiyuan Zhang, Eugene Alforque and Thomas Hermann as co-authors. The dissertation author was the primary investigator and author of this material. Prof. Hermann was the corresponding author.

The material in Chapter 4, in part, is currently prepared for submission with Thomas Hermann as co-author. The dissertation author was the primary investigator and author of this material. Prof. Hermann was the corresponding author.

The material in Chapter 5, in part, has been published in Nanoscale titled "RNA–DNA hybrid nanoshapes that self-assemble dependent on ligand binding" with Thomas Hermann as co-

author. The dissertation author was the primary investigator and author of this material. Prof. Hermann was the corresponding author.

The material in Chapter 6, in part, is currently submitted for a publication with Li Xing, Alba Monferrer and Thomas Hermann as co-authors. The dissertation author was the primary investigator and author of this material. Prof. Hermann was the corresponding author.

Vita

2014 Bachelor of Science, Beijing University of Chemical Technology

2016 Master of Science, University of California San Diego

2021 Doctor of Philosophy, University of California San Diego

Publications

1. S. Chen, L. Xing, A. Monferrer, T. Hermann, "Nano-sandwich composite by kinetic-trapping assembly from protein and nucleic acid", under review.
2. S. Chen, T. Hermann, "Transform RNA-DNA Hybrid Nano-Complexes through Swift Replacements of Nucleic Acid Modules", under review.
3. S. Chen, Z. Zhang, E. Alforque, T. Hermann, "Complex RNA-DNA Hybrid Nano-Constructs Determined by Consecutive Screening Process", *Nano Research.* 14, 46–51 (2021).
4. S. Chen, T. Hermann, "RNA-DNA hybrid Nano-Shapes that Self-Assemble Dependent on Ligand Binding", *Nanoscale,* 2020, 12, 3302-3307.
5. S. Chen, A. Monferrer, T. Hermann, "A Simple Screening Strategy for Complex RNA-DNA Hybrid Nanoshapes", *Methods*, in press, 2021.

Abstract of the Dissertation

Modular Nucleic Acid Nano-Complexes Self-Assembling from Small RNA and DNA Motifs

by

Shi Chen

Doctor of Philosophy in Materials Science and Engineering

University of California San Diego, 2021

Professor Thomas Hermann, Chair

Nucleic acid has emerged as a new biomaterial to construct new functional biomaterials through mainly Watson-Crick base pairing between complementary sequences. Different from past efforts that used DNA and RNA largely separately to create nucleic acid nano-assemblies, this dissertation outlines a new research direction that sought to assemble discrete DNA and RNA modules to RNA-DNA hybrid nanoparticles. The new direction that marries the structural diversified RNA motifs as architectural joints and chemical flexible DNA modules as functional

components gives rise to nanoparticle entities enriched with structural varieties and functional potentials at the sub-10 nanometer scale. The screening methods and multi-step assembly strategy described in the dissertation laid the foundation for designing and preparing complex RNA-DNA hybrid nanoparticles, as well as composite materials based on RNA-DNA hybrid nanoparticles.

Chapter 1: Introduction to Nucleic Acid Nanotechnology

Nucleic acid nanotechnology seeks to design and prepare artificial nanoparticles with well-defined structures and various functions from nucleic acid building blocks to solve general engineering problems in the nanotechnology world and basic science problems in biochemistry and biology. In this field, nucleic acid is considered as a water-soluble polymer material whose growth and branching can be precisely controlled at atomic accuracy, rather than a conventional carrier of gene instructions.

The formation of nucleic acid nanoparticles relies on the predictable folding and self-assembly of the biopolymer through base paring between complementary oligonucleotide segments, which are encoded within the primary sequence of nucleic acids. To design and develop diverse nanoparticles that are self-assembled from DNA and RNA arising from natural folding of polynucleotide chains, an in-depth understanding of nucleic acid structure is instrumental.

1.1 DNA and RNA structure

As two different types of nucleic acids, DNA and RNA are similar in chemical components. With monomeric units called nucleotides, DNA is naturally composed of two polynucleotide chains and RNA contains a single polymeric chain of monomers in nature. Each nucleotide is made up of one of four nitrogenous bases (cytosine [C], guanine [G], adenine [A] or thymine [T] for DNA nucleotides and uracil [U] for RNA nucleotides), a ribose sugar with 5 carbons numbered from 1' to 5', and a phosphate residue. The nitrogenous base is covalently bonded to 1' position, while one phosphate residue is bonded to 3' position of one sugar group and 5' position of another sugar group by covalent bonds too.

Watson-Crick base pair formed through hydrogen bonding between nucleobases is fundamental to nucleic acid's structure. Purine (A and G)-pyrimidine (C and T in DNA or U in RNA) base pairing of GC and AT (or AU in RNA) results in unique double helical structure that

is essential to nucleic acid's function. For example, the double helix of DNA facilitates the association and disassociation of base pairs between DNA and incoming nucleotides, allowing for the replication of DNA(1) and the transcription from DNA to RNA(2).

Nucleic acid's structure is usually described from four levels. The primary structure is the linear sequences of nucleotides that are connected by a phosphate diester from a nucleotide's 5'-phosphate group to the 3'-hydroxyl group of one neighbor and a second phosphate diester from the nucleotide's 3'-hydroxyl group to another neighbor's 5'-phosphate group. The primary sequence of nucleic acid is usually described from the 5' end of a polymeric chain to the 3' end. The secondary structure is formed by Watson-Crick base paring between complementary regions from different polymeric chains or within the same chain. DNA's secondary structure is usually formed through base paring between two single strands, while RNA has various secondary segments that are usually consisted of one single polynucleotide having both single-stranded regions and double-stranded regions. For example, an RNA stem-loop secondary structure, a common RNA secondary structure and a building block for hierarchical structural motifs, is a double helix ends in a short unpaired loop(3). The variety of the secondary structure contributes to even more diversified structures of RNA at the tertiary level. Nucleic acids tertiary structure refers to the three-dimensional arrangements of secondary structures. While double helix is the dominant tertiary structure for DNA, RNA has a vast of diversified tertiary structures, including helical duplexes, triple-stranded structures and so on, through tertiary interactions, such as coaxial stacking(4). Precise three-dimensional shapes of nucleic acids are fundamental to their functions ranging from molecular recognition and catalyst. Quaternary structure of nucleic acid refers to higher level of arrangements and interactions of DNA and RNA motifs, such as kissing-loop interactions between two stem-loop segments.

The structural diversity of RNA over DNA comes from two chemical components that are different in the two types of nucleic acids: 1) uracil (U) in RNA has one less methyl group than thymine (T) in DNA; 2) ribose sugar of RNA has one more hydroxyl group at 2' carbon than deoxyribose sugar of DNA. These two minor differences in chemical components result in large distinctions between the structure of RNA and DNA, especially at the tertiary level.

Firstly, in addition to the regular Watson-Crick base pairing between uracil and adenine, uracil in RNA has been widely seen to form a wobble base pair with guanine(5). Those G-U wobble base pairs, along with other non-Watson-Crick base pairs involving uracil, play an important role in stabilizing RNA tertiary structures(6). Secondly, the unique hydroxyl group increases the ability of RNA in forming hydrogen bonds since it can be both a hydrogen-bond donor and acceptor. The additional hydrogen bonds structurally and thermal dynamically stabilize RNA tertiary structure, as the evidence has been widely seen in the crystal structure of RNAs(7). Besides, the unique hydroxyl group in RNA provides an extra binding site for divalent metals, such as Mg^{2+}, which drive different secondary motifs to a close proximity to form some specific tertiary structures.

1.2 DNA Nanotechnology

Since Nadrian Seeman brought up the idea of using immobile DNA junctions to crystallize proteins(8), DNA nanotechnology has been established as an important field in nanoscience owing to its remarkable ability and accuracy to control materials assembly. The fabrication of nano-assemblies from DNA building blocks uses two different approaches, bottom-up approach and top-down approach. The bottom-up approach mainly relies on immobile DNA junctions, such as Holliday junctions(9), and sticky ends, the short single strands extended from the end of DNA junctions, to assemble large nanoparticles with well-defined topologies from small DNA pieces.

This approach was dominant in making DNA nano-assemblies ranging from polygonal shapes to 2D arrays(10,11) until the emerging of DNA origami technique that was brought up in 2006 by Paul Ruthemund(12). The new top-down approach seeks to fold a long DNA strand, scaffold, to a designed pattern with the assistance of short staple strands. The long scaffold containing thousands of bases is usually derived from viral DNA, typically the 7,249 bp genomic DNA of M13 bacteriophage(13), and hundreds of DNA staple strands bind the scaffold at various positions to facilitate the formation of pre-defined two- or three-dimensional shapes. The new approach that is fully dependent on primary sequence of DNA quickly changed the landscape of DNA nanotechnology, providing a robust method in making diverse nanoparticles(14–17).

Although DNA naturally lacks structural versatility, its chemical robustness allows for straightforward chemical modifications and binding to a variety of functional materials to achieve applications in a range of areas from biomedicine to materials science(18). A vast array of work have been reported to deposit or incorporate organic ligands, metal nanoparticles, metal ions, polymers and proteins to DNA nano-complexes(16), showing great promising of DNA nanotechnology in solving generous problems in the field of nanoscience.

1.3 RNA Nanotechnology

RNA's role in nucleic acid nanotechnology has been overlooked until Eric Westhof, Luc Jaeger and their colleague proposed the concept of RNA tectonics(19). In this proposal, the author discussed the RNA structural information that was associated with their primary sequence and suggested RNA molecules that naturally folded into specific shapes could assemble to supramolecular architectures directed by a pre-defined governing rule. RNA's diverse secondary and tertiary structures give rise to numerous small RNA motifs enriched with structural versality, providing a vast of diversified building blocks for nano-assemblies and making RNA

nanotechnology mainly stick to a bottom-up assembling strategy. To explore the structural potential of RNA in building topological and hierarchical nano-objects, a library of building bricks (RNA motifs) needs to be collected and interactions directing the assembly of biological macromolecules need to be defined.

To date, a number of RNA motifs with diversified structures have been discovered and collected for constructing RNA nanoparticles. Among them, a pRNA 3-way junction (3WJ) that was discovered in a hexametric ring RNA structure associated with the bacteriophage phi29 DNA packaging motor was one of the most widely motifs applied for RNA nano-assemblies(20). It can be assembled from three individual RNA oligos at room temperature and remain as a stable junction with a high melting temperature (Tm = 58), making it a distinct robust architectural unit(21). Peixuan Guo group firstly used it to design and prepare three circularly closed planar RNA structures, triangle, square and pentagon (Fig.1.1A)(22). With a long internal guide strand having specific hybridization bases, three RNA shorter external strands selectively assembled into a homogeneous triangular nanoparticle that was consisted of three copies of the pRNA-3WJ motif. Square and pentagon were also formed in a selective and efficient manner with increasing number of external strands and hybridization sites on the internal guide strand. The formation of diverse shapes demonstrated the 3WJ motif existed as a flexible state in solution with the angle between two closest arms varying from 60 to 108 degrees, indicating the architectural potential of a single RNA motif can be significant. The size of the square was tunable from 5nm to 20nm by changing the length of the internal long strand(23), which affected the biodistribution of RNA nanoparticles in vivo(24). Due to the branched nature of the 3WJ, each corner of the closed nano-shapes has an extended arm available for further hybridization and chemical modifications. Another work from Peixuan Guo group demonstrated that six pRNA 3WJ nano-triangles could constitute a hexamer

through the hybridization of the extended branches among six triangles(25), which can be further arranged to form a nano-array with honeycomb pattern. Other types of two-dimensional structures, such as an RNA dendrimer, have also been successfully made from the pRNA 3WJ motif(26). Moreover, rational designed 3-dimensional nanoparticles, such as nanoprism (Fig.1.1B), made from the pRNA 3WJ motif with precise shape and size have been fabricated and used for cancer targeting and small RNAs delivery(27,28). Apart from the pRNA, 3-way junction structures in other RNA motifs have also been used to construct functional RNA nano-objects(29).

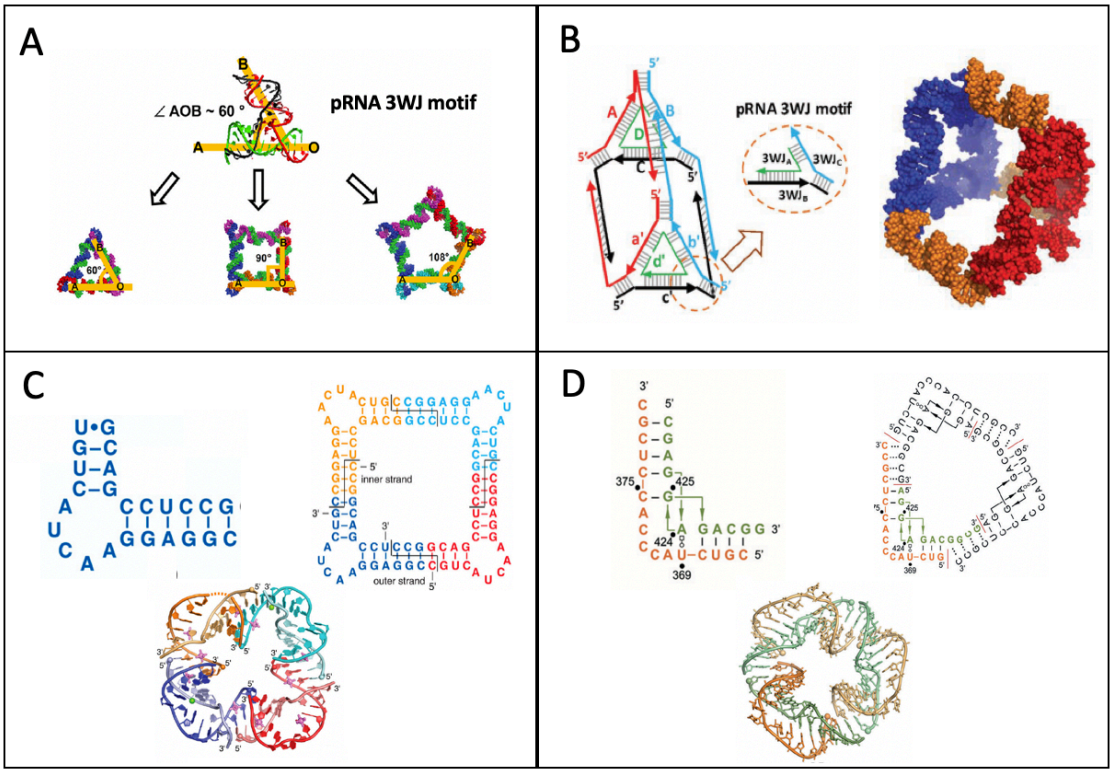

Figure 1.1. RNA nanoparticles made from naturally occurring RNA motifs. (A) Two-dimensional RNA nano-triangle, square and pentagon made from the pRNA 3WJ motif[18]. (B) Three-dimensional RNA nanoprism made from the pRNA 3WJ motif[24]. (C) Secondary structure of an RNA bent motif from hepatitis C virus (HCV), and secondary and crystal structure of an RNA square consisted of four copies of the bent motif[31]. (D) Secondary structure of an RNA bent motif from Seneca Valley virus (SVV), and secondary and crystal structure of an RNA triangle made with three copies of the bent motif[33].

In addition to pRNA 3WJ, various RNA structural motifs derived from viral RNAs have also been added to the library of RNA building blocks. For example, Thomas Hermann and colleagues resolved the crystal structure of the domain IIa bulge in the internal ribosome entry site (IRES) of the hepatitis C virus (HCV) RNA genome(30), which adopts a unique bend structure at 90 degrees (Fig. 1.1C). Four copies of such a domain were arranged to self-assemble into an RNA nano-square(31). Additionally, Hermann group identified another bend RNA structure (Fig. 1.1D), domain IIa from the IRES element of Seneca Valley virus through x-ray crystallography(32). The crystal structure led to a design of a triangular nanoparticle consisted of three copies of such a domain(33). Both RNA nano-square and nano-triangle were crystallized and investigated by x-ray

diffraction, showing the RNA internal loop motifs in the square and triangle were both separated by a straight double helix with 10 base pairs. This was in consistent with a full turn of an A-form double helix. Adding one more base pair between internal loops could lead the architectural joints to rotate out of the plane and end up as a spiral structure. Such a designing principle has been widely applied in the construction of both planar RNA and DNA nanoparticles. To make sure that all motifs are co-planar in a two-dimensional nano-shape, architectural joints are usually connected with a rigid dimer that extends one or multiple full turns or half turns of a helix. A full turn helix leads the architectural units to a cis conformation, while a half turn helix leads to a trans conformation(34).

Apart from naturally occurring RNA structures, artificially designed and prepared RNA structural motifs were also a major source to the library of building bricks. For example, Chengde Mao group de novo designed an RNA tile that was consisted of three straight helical regions (Pa, Pb and Pc), two internal loops (Lab and Lbc) that locked at 90 degrees and two single strands (Ta and Tb) for further hybridization between tiles(35). Four tiles assembled into a square through the base pairing between the Ta tail and the internal loop. Self-complementary single strand Tc then homo-dimerized to connect two squares to an octameric prism. Similarly, Elisa Franco, Kirill Afonin and their colleagues also reported an artificial nanometer-scale RNA tile that eventually assembled into large lattices(36).

Owing to the superb structural flexibility, artificial branched motifs, such as 3-way junction motifs, are of significant interest to researchers. A flexible 3-way junction region consisted of 9 uridines was firstly introduced to generate RNA nanotubes designed on the basis of computational three-dimensional models(37). Computational studies using a coarse-gained method indicated that linkers with less than two uridines on one side of the junction could trigger electrostatic repulsion

between negatively charged phosphate groups, leading to significant steric clashes(38). Addition of uridines in the linker resulted in an overall more flexible and stable 3-way junction region. Therefore, a library of nanoparticles from triangles to hexagons with diverse functions, such as drug delivery and controlled neuro-immunomodulatory properties, have been fabricated with flexible 3-way junctions that have three or four uridines in each arm(39–41).

A recent example of an artificial branched structure was a branched kissing-loop (bKL) motif reported by Yossi Weizmann group(42). The bKL motif that obtained a T-shape was modified from an RNA kissing loop complex by replacing the two-adenosine linker in one loop with an RNA double helix. The branched KL motif was used to successfully fabricate multiple hierarchical nano-assemblies, including an RNA ladder, an RNA ring, and an RNA tetrameric nanocage.

Robust assembly of RNA nanoparticles from RNA structural motifs also requires defining interactions directing the assembly of biological macromolecules. While the library or RNA structural motifs is expanding at an accelerating rate, the interactions that govern the assembly remain within two major classes.

The first class is the kissing loop interaction, an interaction formed between two stem-loops through Watson-Crick base pairing. Early conceptional work on RNA nanoparticles assembled from kissing loop interactions demonstrated the possibility of such interaction on directing the assembly of linear and circular RNA nano-objects(43,44). In 2004, Luc Jeager group reported programmable jigsaw puzzles consisted of four tectoRNA units that made from a right angle (RL) motif bending at 90 degrees and derivatives of human immunodeficiency virus (HIV) RNA(45). The assembly of the square structure was guided by 6-bp kissing loop interactions between stem-loops of each unit. As the kissing interactions are typically consisted of 4 to 7 Watson-Crick base

pairs that arise from 9 to 11-nucleotide loops, the angles between two stems can vary from 90 degrees to 180 degrees by moving the kissing regions along the stem-loop, leading to different conformations of assemblies. For example, with the same stem-loop motif derived from HIV RNA, head to head kissing loop interaction that resulted in an angle at 180 degrees between stems constituted an RNA linear fiber, while two stem loops that locked at an angle of 120 degrees led to a closed hexametric ring(46).

The second class of interaction that directs the RNA assembly is the sticky-end interaction. Sticky-end is a few unpaired nucleotides that extend from the end of one RNA motif, which can be used as a non-covalent connector to form a rigid dimer with the sticky-end from another RNA motif. Compared to the kissing-loop interaction that can be locked at different angles, the sticky-end interaction has higher flexibility in length, as the shortest tail only contains 4 nucleotides(31,33,35), while the longest tail can be infinite in theory.

The fast-expanding library of RNA motifs and increasing understanding of RNA interactions allows for the construction of novel RNA nano-complexes at an unprecedent hierarchical level. For example, Luc Jaeger group reported a series of nano-hearts made from six RNA units through multiple kissing loop interactions(47). A bunch of other symmetric and asymmetric nano-objects were also constructed through the combination of different RNA units, including aptamers, 3WJs, Triple helixes, etc.

In addition to RNA tectonics, it is also worth noting the development of another strategy of building RNA nano-objects, RNA origami. DNA origami that plays an essential role in the success of DNA nanotechnology has achieved remarkable progress in using short ‘staple’ DNA strands to guide the folding of a long DNA strand into artificial two- and three-dimensional constructs(48). However, RNA origami majorly focuses on the single-stranded origami technique

that relies on the folding of single RNA long strand in a designed manner based on the information encoded in the primary sequence.

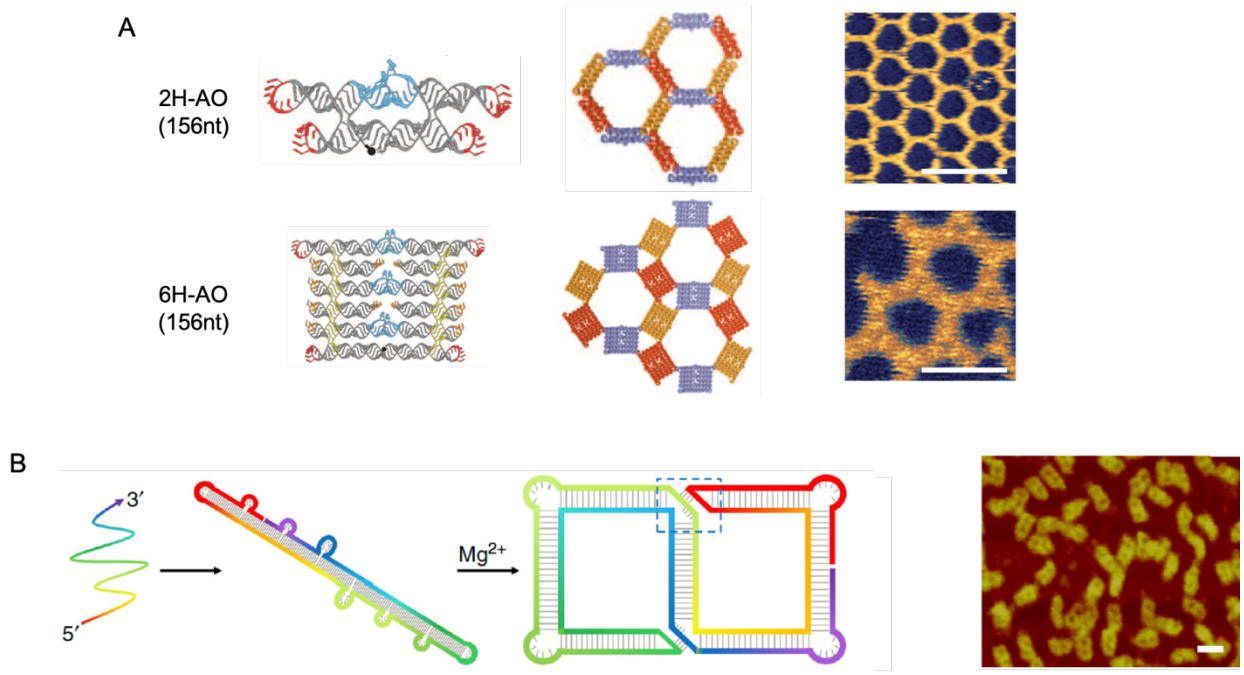

Figure 1.2. Single-stranded RNA origami structures. (A) Atomic models of tiles (left) and tile assemblies (mid), and AFM images of purified tiles assemblies (right)[49]. (B) The folding pathway of an origami structure from a single-stranded RNA (left) and AFM image of the origami structure (right)[53]. Scale bar is 20nm.

The first work about RNA origami was reported by Ebbe S. Anderson group(49), in which a single-stranded RNA folded into an origami tile that was conversed from multiple-stranded RNA double crossover tiles. The conversion was achieved through the connection of outer helix ends and the substitution from an inter-crossover domain to a 180-degree kissing loop interaction. Based on this conversion, five long single-stranded RNA oligos ranging from 156 nucleotides(2H-AO, Fig.1.2A) to 660 nucleotides(6H-AO, Fig.1.2A) folded into different tiles with two, four and six helical tall, which can further associate into periodic arrays through a simple kissing interaction at the corner of the tiles. A simplified design based on the two-helical origami tile was later reported and used as a platform for a FRET system and an artificial anticoagulant(50,51).

To date, the longest single-stranded RNA origami structure was reported by Peng Yin, Hao Yan and their colleagues which contained 6337 nucleotides(52).

An important advantage of the RNA origami technique, as well as the RNA nanotechnology over DNA nanotechnology, is RNA that naturally exists in vivo as a single strand can be transcribed in cells and readily fold into a programmable nano-structure. For example, Chengde Mao group reported a strategy to produce multiple well-defined RNA nanostructures self-assembled from single-stranded RNAs transcribed from gene-encoded DNA duplexes in vivo (Fig.1.2B)(53). The strategy allowed the single-stranded RNA to firstly fold into hairpins which were not only thermodynamically stable but also kinetically feasible during the transcription. Due to the simple structure that only involved local interactions, single-stranded RNAs can quickly re-arrange from alternative structural forms to the target hairpin structure, which largely avoided the kinetic traps along the folding pathway. After the natural folding of hairpins, the remaining unpaired residues were then hybridized to form the final RNA nanostructures as designed. The strategy that mimics the natural process of RNA hairpin ribozymes and protein production avoided the expensive large-scale production of single-stranded RNA in vitro and the complicated process of delivering RNAs into cells, providing a cost-effective method to produce and apply hierarchical RNA nanostructures in vivo.

1.4 RNA-DNA Hybrid Nano-Complexes

Although RNA and DNA have been largely used separately as building blocks for nanoparticles, RNA-DNA hybrid assemblies have recently emerged as promising new materials for reversible nano-materials and vehicles of biomolecules. The strategy that harasses the hybridization between two types of nucleic acids has been proved to possess two important advantages. The first advantage is to stabilize single-stranded RNA and double-stranded RNA by

base paring or replacing with a DNA strand. Studies have shown that RNA-DNA hybrids have higher resistance to RNase than that of single-stranded RNA and RNA-RNA duplexes(54). Based on this, Shapiro and his colleagues developed a strategy to split the small interfering RNAs (siRNAs) into two RNA-DNA hybrids(55). Delivering two RNA-DNA hybrids into cells overcame the potential intravascular degradation of the double-stranded siRNA. After the delivery, two siRNA single strands were released by a toe-hold interaction and re-associated to functional double stranded siRNA in cells. Due to the involvement of DNA strands, additional functionalities can be achieved through the modification of the DNA strands. For example, introducing two fluorescent compounds to the DNA toe-hold strands can trigger the FRET effect when the siRNAs were releasing, monitoring the position and rate of the release of siRNA(56).

Another advantage is to make dynamic reversible nucleic acids nano-assemblies through the addition and removal of RNA in the RNA-DNA hybrids. To date, most work in the field of nucleic acid nanotechnology has been focusing on the addition of components to construct a topological particle. However, to reduce the toxicity and accumulation of nano-assemblies, controllable degradation of the nano-assemblies in vivo is also of great importance in future applications of those nano-assemblies. RNA's nature of instability and degradation upon enzymes gives it an advantage in making degradable nano-assemblies. Elisa Franco and her colleagues used RNA-DNA hybridized linkers to connect double crossover DNA tiles to yield micron-long nanotubes(57). Those nanotubes can form and disassociate upon the addition and removal of the RNA. In this work, RNA in the RNA-DNA hybrid linkers was hydrolyzed by an RNA-degrading enzyme, RNase-H. Pre-formed nanotubes were observed to degrade at a rate that was controlled by the concentration of RNase-H. It is worth noting that the micro-long RNA-DNA hybrid

nanotube can form and degrade isothermally at 37 degrees, indicating its promising potential in biological applications, such as mimicking natural dynamic systems in vivo.

1.5 Goal of the Dissertation

Differ from past efforts that mainly focused on preparing RNA-DNA hybrid nano-complexes by using extensive strand hybridization between the two types of nucleic acids, this dissertation lays out a new research direction in nucleic acid nanotechnology that seeks to prepare diverse RNA-DNA nano-complexes incorporated structural diversified RNA as architectural joints and chemically robust DNA as connectors and functional sites. The new direction that partitions the structural diversity of RNA modules and chemical flexibility of DNA modules gives rise to nanoparticle units enriched with structural varieties and functional potentials in sub-10 nanometer scale. This dissertation starts from describing a simple screening and a mix-and-match screening method for the construction of RNA-DNA hybrid nano-complexes, laying out general robust methods to identify and prepare RNA-DNA hybrid nanoshapes from diverse libraries of discrete nucleic acid building blocks. Further, the superb modularity of RNA-DNA hybrid nano-complexes assembled from small RNA and DNA modules is exploited by transforming hybrid nucleic acid nanoparticles through replacements of nucleic acid components. Finally, RNA-DNA hybrid nano-complexes are explored as platforms for hierarchical composite materials by conjugating small molecules and proteins to DNA modules that serve as the functional and binding sites.

Chapter 2: A Simple Screening Strategy for RNA-DNA Hybrid Nano-Complexes

2.1 Abstract

The design of nucleic acid hybrid nanomaterials capitalizes on the partitioning of architectural and functional roles between structurally diverse RNA modules and chemically robust DNA components. Selecting optimal combinations of RNA and DNA building blocks is the key to preparing stable polygonal RNA-DNA hybrid nanoshapes. Here, we outline a simple screening strategy by gel electrophoresis under native folding conditions to identify combinations of RNA and DNA modules that self-assemble to robust polygonal hybrid nanoshapes. As a proof of concept, we outline the preparation of RNA-DNA hybrid nanoshapes containing a set of different RNA architectural joints, including internal loop motifs and three-way junction (3WJ) folds. For each hybrid nanoshape, we demonstrate the selection process used to identify optimal DNA modules from a library of DNA connectors. The simple screening strategy outlined here provides a general robust method to identify and prepare RNA-DNA hybrid nanoshapes from diverse libraries of discrete nucleic acid building blocks.

2.2 Introduction

Nucleic acid nanotechnology pursues the construction of nano-scale particles and materials through the predictable architecture and assembly of folding motifs as well as Watson-Crick base paring between complementary oligonucleotide strands. RNA and DNA as the two natural chemotypes of nucleic acids have been used largely separately as building blocks to create diverse architectures that vary from simple two-dimensional nano-shapes to complex three-dimensional dynamic devices(16,49,58–60). After well-established DNA nanotechnology and developing RNA nanotechnology, RNA-DNA hybrid assemblies have recently emerged as promising new materials for reversible nano-material(55–57,61,62). Distinct from past efforts to construct hybrid nano-assemblies by extensive hybridization of RNA and DNA strands, our group has developed

RNA-DNA hybrid nanoshapes that self-assemble from discrete RNA and DNA modules(63–65). In these robust hybrid nanoshapes, RNA components with various tertiary folds serve as architectural joints, while DNA connector modules allow for straightforward modification, including chemical conjugation and introduction of binding sites for ligands and proteins which add diverse functionalities to RNA-DNA hybrid nano-assemblies.

Assembly of stable polygonal nanoshapes from discrete nucleic acid modules critically depends on the selection of optimal combinations of RNA joints and DNA connectors. Previously, circularly closed nanostructures containing interconnected RNA motifs have been rationally designed based on model building from crystal structures(31,33) and through computational methods(37,66,67). The inclusion of DNA modules in hybrid nano-architectures introduces multiple transitions between A-form RNA duplexes and B-form DNA helices(65) which complicates the reliable modeling of optimal nucleic acid modules. Our lab developed a simple screening strategy to experimentally select from libraries of modules such combinations of RNA joints and DNA connectors that assemble into stable hybrid nanoshapes. We designed RNA and DNA building blocks that interact through short single-stranded sequences of 4-7 nucleotides as marginally stable hybridization sites. Arrangement of multiple nucleic acid motifs interacting through labile hybridization sites within a circularly closed architecture leads to synergistic stabilization of the resulting polygonal nanoshapes. The increased stability of circularly closed nanoshapes provides a selection criterion for the optimal combination of RNA and DNA modules analyzed by native polyacrylamide gel electrophoresis (PAGE).

Here, we describe a robust design and screening strategy for the discovery of stable RNADNA hybrid nanoshapes containing multiple nucleic acid modules. We outline the selection process of optimal module combinations for the assembly of several distinct RNA-DNA hybrid

nanoshapes with different programmed module compositions. The design, screening and selection approach to identify stably assembling RNA and DNA building blocks provides a general blueprint for the preparation of modular nucleic acid nanomaterials.

2.3 Materials and Methods

2.3.1 Preparation of nucleic acid stock solutions for screening

RNA and DNA oligonucleotides were purchased from Integrated DNA Technologies. Lyophilized oligonucleotides were rehydrated to 500 μM concentration in 10 mM sodium cacodylate buffer, pH=6.5, as stock solutions. For screening experiments, oligonucleotide stock solutions were diluted in buffer to 100 μM concentration. Sequences of oligonucleotides used in this work are listed in Tables 2.1, 2.2 and 2.3.

Table 2.1. Oligonucleotide sequences for RNA corner modules

Strand	Sequence
i-Loop-In	5’ - rCrCrG rArGrG rUrCrA rGrCrC rUrG - 3’
i-Loop-Out	5’ - rCrGrA rGrArC rCrArG rGrArA rCrUrA rCrUrGrA - 3’
3WJ-RNA-1	5’ - rGrArA rGrGrC rUrGrA rCrArA rUrCrA rUrGrC rU - 3’
3WJ-RNA-2	5’ - rCrCrG rArGrG rArGrC rArUrG rUrGrU rArCrC rU -3’
3WJ-RNA-3	5’ - rCrGrA rGrArC rArGrG rUrArC rUrUrU rGrUrU rGrUrC rA -3’

Table 2.2. Oligonucleotide sequences for double-stranded DNA connectors

Strand	Sequence
DNA-5-In	5’ - GTC TCG TAC GT -3’
DNA-5-Out	5’ - CCT CGG ACG TA - 3’
DNA-6-In	5’ - GTC TCG GTA CGT - 3’
DNA-6-Out	5’ - CCT CGG ACG TAC - 3’
DNA-7-In	5’ - GTC TCG ACG ACG T - 3’
DNA-7-Out	5’ - CCT CGG ACG TCG T - 3’
DNA-8-In	5’ - GTC TCG ACG TAC GT - 3’
DNA-8-Out	5’ - CCT CGG ACG TAC GT - 3’
DNA-9-In	5’ - GTC TCG CAC GTA CGT - 3’
DNA-9-Out	5’ - CCT CGG ACG TAC GTG - 3’
DNA-10-In	5’ - GTC TCG ACG TAT ACG T - 3’
DNA-10-Out	5’ - CCT CGG ACG TAT ACG T - 3’
DNA-11-In	5’ - GTC TCG CGT ACG TAC GT - 3’
DNA-11-Out	5’ - CCT CGG ACG TAC GTA CG - 3’
DNA-12-In	5’ - GTC TCG CCA TGA GCA AAT - 3’
DNA-12-Out	5’ - CCT CGG ATT TGC TCA TGG - 3’
DNA-13-In	5’ - GTC TCG CCA TGA TGC AAA T - 3’
DNA-13-Out	5’ - CCT CGG ATT TGC ATC ATG G - 3’
DNA-14-In	5’ - GTC TCG CCA TGA TTG CAA AT - 3’
DNA-14-Out	5’ - CCT CGG ATT TGC AAT CAT GG - 3’
DNA-15-In	5’ - GTC TCG CCA TGA TTG TCA AAT - 3’
DNA-15-Out	5’ - CCT CGG ATT TGA CAA TCA TGG - 3’
DNA-Connector-8_{in}	5’ - GCC TTC CGT GAC TA -3’
DNA-Connector-8_{out}	5’ - GCC TTC TAG TCA CG -3’

Table 2.3. Oligonucleotide sequences for DNA guide strands.

Strand	Sequences
i-Loop-DNAguide-3	5’ - GTC TCG TAT CGC TAC GTT TTC TCT CTC TCT TTT GTC TCG TAT CGC TAC GTT TTC TCT CTC TCT TTT GTC TCG TAT CGC TAC GT - 3’
i-Loop-DNAguide-4	5’ - GTC TCG TAT CGC TAC GTT TTC TCT CTC TCT TTT GTC TCG TAT CGC TAC GTT TTC TCT CTC TCT TTT GTC TCG TAT CGC TAC GTT TTC TCT CTC TCT TTT GTC TCG TAT CGC TAC GT - 3’
3WJ-DNAguide-3	5’ - GTC TCG ACG ACG TTT TCT CTC TTT T GTC TCG ACG ACG TTT TCT CTC TTT T GTC TCG ACG ACG T - 3’
3WJ-DNAguide-4	5’ - GTC TCG ACG ACG TTT TCT CTC TTT T GTC TCG ACG ACG TTT TCT CTC TTT T GTC TCG ACG ACG TTT TCT CTC TTT T GTC TCG ACG ACG T - 3’
DNAguide-3a	5’ - GTC TCG CAC GTA CGT TTT CTC TCT TTT GTC TCG ACG ACG TTT TCT CTC TTT TGT CTC GCA CGT ACG T - 3’
DNAguide-3b	5’ - GTC TCG CAC GTA CGT TTT CTC TCT TTT GTC TCG CGT ACG TAC GTT TTC TCT CTT TTG TCT CGC ACG TAC GT - 3’
DNAguide-2	5’ - GTC TCG CAC GTA CGT TTC TCT CTT TGT CTC GCA CGT ACG T - 3’
DNAguide-4	5’ - GTC TCG CAC GTA CGT TTC TCT CTT TGT CTC GCA CGT ACG TTT CTC TCT TTG TCT CGC ACG TAC GTT TCT CTC TTT GTC TCG CAC GTA CGT - 3’

2.3.2 Preparation of RNA and DNA combinations for screening

Combinations of RNA and DNA oligonucleotides were prepared by mixing 1 μL of each constituent oligonucleotide at equimolar concentration (100 μM) in the presence of 2 mM or 5 mM magnesium chloride, as indicated for each experiment. Nucleic acid mixtures were annealed by heating at 65°C for 5 min followed by incubation at 37°C for 2 h on a thermocycler. After annealing, mixtures were cooled on water ice for 5 min.

2.3.3 Gel electrophoretic screening

Screening experiments were performed on 5% native polyacrylamide gels (10 cm x 10 cm), polymerized from 15 mL 19:1 acrylamide/bis-acrylamide gel solution in the presence of 2 mM or

5 mM magnesium chloride, 100 µL 10% ammonium persulfate (APS) and 10 µL tetramethylethylenediamine (TEMED). Acrylamide/bis-acrylamide gel solution was purchased from Bio-Rad Laboratory. APS, TEMED and MOPS were purchased from Sigma Aldrich. The 10 cm x 10 cm vertical gel box was purchased from Galio Bioscience (model 85-1010).

Gel electrophoresis was conducted at 220 V, 22 mA, in 2X MOPS buffer (40 mM 3-morpholinopropane 1-sulfonic acid, 10 mM sodium acetate) for 1-1.5 h with externally cooled recycling ice water. After the electrophoresis, polyacrylamide gels containing nucleic acids samples were stained with 0.01% (v/v) ethidium bromide solution for 20 min before imaging under UV light (302 nm).

2.3.4 AFM imaging

Freshly cleaved mica was treated by immersing in 50 mM aqueous solution of 1-(3-aminopropyl)-silatrane for 30 min. After rinsing with de-ionized water and drying in an argon stream, nucleic acid samples at a concentration of 0.5-1.5 ng/µL were deposited on the mica surface for 2 min at 4°C. After deposition, mica substrates loaded with nucleic acid samples were rinsed briefly with ice water and dried under a gentle argon flow. AFM images were recorded with a Multi-Mode AFM Nanoscope IV system (Bruker Instruments) in tapping mode with silicon probes RTESPA-300 (Bruker Nano; resonance frequency ~ 300 kHz, spring constant ~ 40 N/m) at a scanning rate of ~ 2.0 Hz. Image processing was performed with the Fem-to-Scan software package (Advanced Technologies Center).

2.4. Results and discussion

2.4.1 Design of self-assembling RNA-DNA hybrid nanoshapes

An exemplary RNA-DNA hybrid nanosquare contains four copies of each an RNA corner motif and a DNA duplex connector (Fig. 2.1). The RNA and DNA modules are connected through

base pairing of single-stranded complementary sequences of 4-7 nucleotides (nt) which give rise to marginally stable short hybrid helices. The A-form RNA-DNA hybrid helix gradually transitions into a B-form helix within the double-stranded region of the DNA connector as indicated by electrophoretic mobility comparison of RNA-DNA hybrid nanoshapes and their all-RNA analogues(65). Formation of a robust RNA-DNA hybrid nanosquare relies on synergistic stabilization of the assembly in a circularly closed structure which entails accommodation of eight transitions of helical conformations between nucleic acid modules (four transitions from A-form to B-form and four transitions from B-form to A-form).

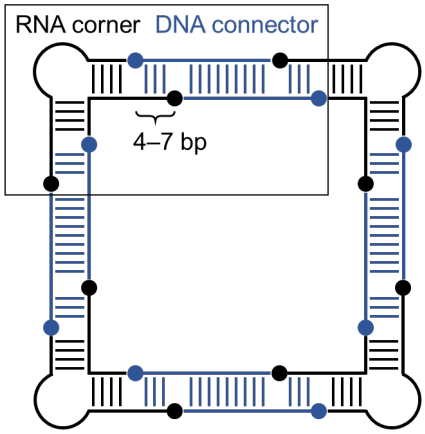

Figure 2.1. RNA-DNA hybrid nanosquare containing a combination of RNA corner modules and DNA connectors. Synergistic module association through marginally stable 4-7 base pair (bp) hybrid regions in a circularly closed structure leads to robust self-assembling nanoshapes.

The design of optimal combinations of RNA and DNA building blocks that assemble to form stable polygons faces a challenge of reliably modeling multiple transitions in helical conformations even for a simple RNA-DNA hybrid nanosquare. On the other hand, the convenient availability of short DNA oligonucleotides as cheap reagents allows the systematic testing of DNA modules containing a wide range of base pairs to identify optimal connectors that participate in the formation of stable nanoshapes with given RNA modules. We developed a simple screening approach that delivers combinations of RNA and DNA building blocks for robust hybrid

nanoshapes by their migration behavior as discrete species on native polyacrylamide gels. PAGE screening is a fast and scalable method for the assessment of nucleic acid module libraries in a combinatorial fashion.

2.4.2 Screening strategy for self-assembling RNA-DNA hybrid nanoshapes

To demonstrate proof of concept for the screening strategy, we designed two RNA corner modules derived from internal loop motifs in noncoding regions of the hepatitis C virus (HCV; RNA-1) and Seneca Valley virus (SVV; RNA-2) genome (Fig. 2.2). While the two viral RNAs both adopt similar overall bent conformations, the strand folding topology of the internal loop motifs is largely dissimilar as revealed by crystal structure determination(32,68). We previously reported the design and preparation of an all-RNA 100-nt nanosquare from four copies of the HCV (RNA-1) motif and an 81-nt nanotriangle from three SVV (RNA-2) corner modules. The polygonal structure was confirmed by X-ray crystallography for the all-RNA nanoshapes which self-assembled from RNA corner motifs that contained 4-nt complementary single-strand overhangs(31)(33). Here, we re-designed the RNA-1 and RNA-2 corner motifs to contain overhang sequences of non-complementary 6 nt to avoid self-hybridization between RNA modules (Fig. 2.2A). Combinations of each RNA corner with a series of DNA connectors carrying 6-nt single-strand extensions complementary to the RNA module overhangs were analyzed by native PAGE (Fig. 2BC). Among a series of DNA connectors ranging between 9-13 base pairs (bp), the 11-bp DNA insert (DNA-11) associated with both RNA-1 and RNA-2 modules to produce clean discrete bands, indicative of stable nanoshape formation. Previously, screening of DNA modules in a range from 6 bp to 15 bp revealed DNA-11 as an optimal connector for the assembly of nanoshapes containing the RNA-1 corner motif(63). AFM imaging of nucleic acid species extracted from individual bands of the RNA-1/DNA-11 mixture demonstrated the formation of

hybrid nanotriangles, nanosquares and nanopentagons (Fig. 2.2B). Perimeter length analysis of particle images obtained by AFM topography was in agreement with the proposed composition of the RNA-1/DNA-11 nanoshapes as regular polygons containing an alternating arrangement of RNA-1 corner and DNA-11 connector motifs(63). PAGE analysis of RNA-2/DNA combinations revealed the DNA-11 module as the optimal connector also for the RNA-2 corner motif, furnishing discrete bands with electrophoretic mobility identical to RNA-1/DNA-11 nanoshapes (Fig. 2.2C), suggesting the formation of hybrid nanotriangles, nanosquares and nanopentagons containing the RNA-2 corner.

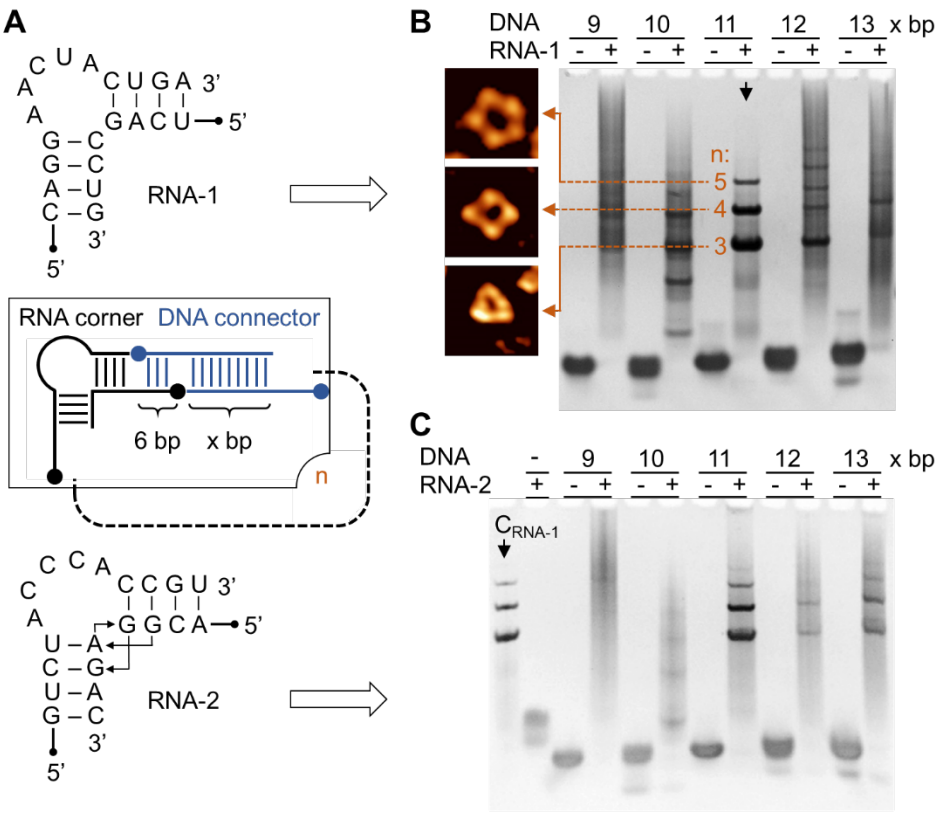

Figure 2.2. Design and screening of RNA-DNA hybrid nanoshapes. (A) RNA corner modules for nanoshape assembly include internal loop motifs derived from structured noncoding regions in the genome of hepatitis C virus (RNA-1) and Seneca Valley virus (RNA-2). Both viral RNA motifs adopt right-angled bent folds as indicated in the secondary structure models shown. RNA modules used for screening carried 6 nucleotide single-strand 5' overhangs. (B) Screening combinations of RNA-1 corner and DNA connectors by native polyacrylamide gel electrophoresis (PAGE) for the formation of stable hybrid nanoshapes. Among a series of DNA modules carrying 9–13 bp in the double stranded region (x), the 11 bp DNA (DNA-11) associating with RNA-1 produced three discrete bands. Representative AFM images of nanoshape species isolated from the three bands are shown. (C) Native PAGE screening RNA-2 corner combinations reveal DNA-11 connectors to furnish stable nanoshapes. C_{RNA-1} is a control containing the mixture of hybrid nanoshapes assembling from RNA-1 and DNA-11 (panel B). PAGE analyses were performed in the presence of 2 mM magnesium chloride.

2.4.3 Self-assembling RNA-DNA hybrid nanoshapes with multiple different RNA corner modules

The success of the PAGE screening strategy in identifying optimal combinations of RNA corner and DNA connector motifs that form stable nanoshapes led us to conceive an iterative mix-

and-match screening approach for assemblies containing multiple different RNA and DNA modules within the same nanoshape(65). To ensure that such complex hybrid nanoshapes could be unambiguously identified by their electrophoretic mobility, we introduced an RNA three-way junction (3WJ) as a corner motif (Fig. 2.3A, RNA-3) which is derived from the genome of the bacteriophage phi29(20). We hypothesized that the larger mass and hydrodynamic volume of the 3WJ corner module would result in nanoshapes with distinct mobility. In a series of DNA modules varying from 5 bp to 9 bp, a DNA module with a core of 7 bp and single-stranded overhangs of 6 nt (DNA-7) was previously identified by PAGE screening as the optimal connector to form polygonal nanoshapes containing 3WJ RNA-3 corner modules (Fig. 2.3C, first gel lane, CRNA-3) (65).

As an example of a hybrid nanoshape with multiple different corner modules, we designed a nanotriangle containing one internal loop RNA-1 corner and two 3WJ RNA-3 motifs connected by a DNA-7 insert (Fig. 2.3B). By PAGE screening for an optimal connector between the RNA-1 and RNA-3 corners, we identified the 9-bp DNA duplex (DNA-9) as a module that furnished a nanoshape whose electrophoretic mobility was consistent with a triangle of the designed complex composition including 4 distinct nucleic acid components (Fig. 2.3C).

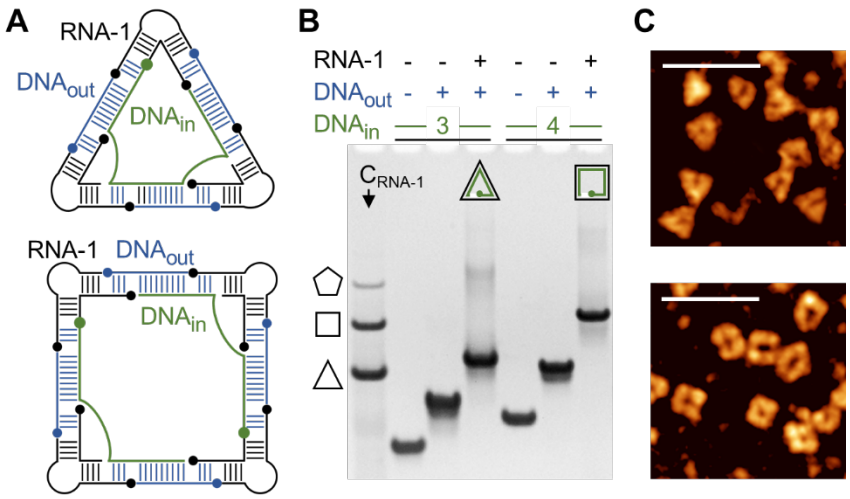

Figure 2.3. Controlled assembly of homogenous RNA-DNA hybrid nanoshapes containing the RNA-1 corner motif. (A) Assembly of homogenous RNA-DNA hybrid nanotriangle and nanosquare is controlled by a DNA guide strand (DNA_{in}) that contains 3 or 4 hybridization sites linked by a single-stranded spacer of 16 nt. (B) PAGE analysis in the presence of 2mM magnesium chloride demonstrated the formation of homogenous nanoshapes. C_{RNA-1} is a control containing the mixture of hybrid nanoshapes assembling from RNA-1 and DNA-11 (Fig. 2.2B). (C) AFM imaging of homogenous nanoshapes obtained through use of DNA guide strand. Scale bars are 50 nm.

Screening of DNA modules of 7-11 bp revealed that formation of a stable nanoshape with the desired structure was remarkably sensitive to the length of connectors as DNA inserts with one less (DNA-8) or more (DNA-10) base pairs did not furnish any stable species. The formation of polygonal nanoshapes depends on the precise end-to-end connection of double-helical nucleic acid components leading to a circularly closed in-plane configuration in which marginally stable hybridization sites are stabilized synergistically in the overall assembly. Deviation of a DNA connector by as little as a single base pair from the optimal insert helix size will lead to out-of-plane dislocation of the nucleic modules and prevent association of stable nanoshapes. This exquisite dependence of complex nanoshape formation on the accurate size of the nucleic acid building blocks highlights the strength of the PAGE screening approach to readily identify optimal RNA and DNA component combinations.

2.4.4 Programmed assembly of homogenous RNA-DNA hybrid nanoshapes

The modular design of the RNA-DNA hybrid nanoshapes accommodates sequence modification and strand extension of the DNA modules permitting to create a wide range of topologies for connectors linking the RNA corner motifs(63). For example, the assembly of homogenous nanotriangles and nanosquares can be programmed by the introduction of a DNA guide strand that contains multiple hybridization sites each replacing one strand of the DNA connectors (Fig. 2.4A). We previously prepared homogenous nanoshapes by including guide DNA strands with hybridization sequences spaced by a linker region of 16 nt and confirmed the formation of clean nanotriangles, nanosquares and nanopentagons by PAGE and AFM topography (Fig. 2.4B)(63).

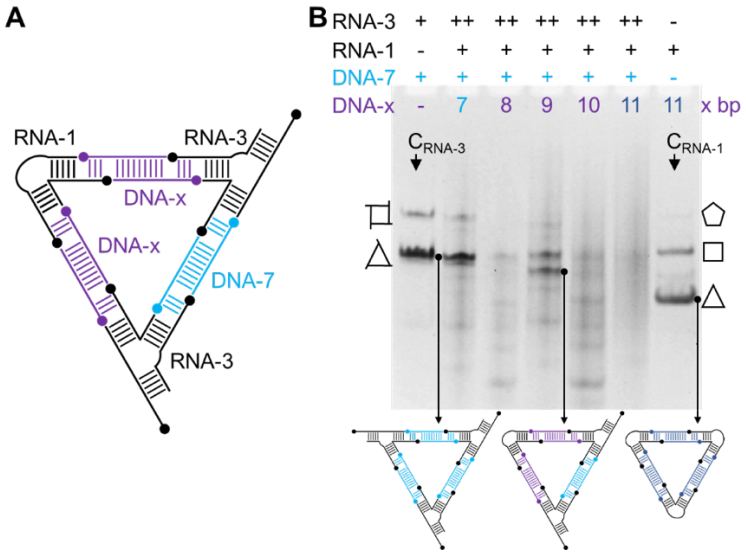

Figure 2.4. Design and screening for RNA-DNA hybrid nanotriangles containing different types of RNA corner modules. (A) Hybrid nanotriangle associating from two RNA three-way junction (3WJ) modules (RNA-3) and one internal loop corner module RNA-1. (B) Iterative PAGE screening in the presence of 5 mM magnesium chloride to select an optimal DNA connector (DNA-x) between RNA-3 and RNA-1 corner modules. C_{RNA-3} and C_{RNA-1} are controls of hybrid nanoshapes assembled from all RNA-3 modules or all RNA-1 modules, respectively. All samples (except for the controls) contained two-fold concentration of the RNA-3 3WJ module over the RNA-1 corner module, and two-fold concentration of the DNA-x over the DNA-7 connector. The sample containing both 7-bp and 9-bp DNA modules generated discrete bands, indicating the formation of stable nanoshapes containing both RNA-3 and RNA-1 modules.

Beyond the preparation of homogenous nanoshapes, DNA guide strands allow the programmed assembly of complex nucleic acid architectures from distinct combinations of RNA corner motifs and DNA connectors. As a proof of concept, we designed homogenous nanotriangles that contained one RNA-1 and two 3WJ RNA-3 corner motifs, or two RNA-1 and one RNA-3 module. Assembly of these architectures was controlled by a DNA-3a guide strand, which contained two hybridization sites for the DNA-9 and one site for the DNA-7, or a DNA-3b guide strand harboring two sites for the DNA-9 and one site for the DNA-11 connector (Fig. 2.5A). Hybridization sequences in the DNA guide strands are connected by a single stranded linker which may contain protein binding sites or serve as hybridization region for other nucleic acids sequences for future applications. Programmed assembly of the two homogenous nanotriangles, guided by DNA-3a and DNA-3b, was supported by their mobility in a native gel (Fig. 2.5B)(65), which was higher than that of a nanotriangle containing three 3WJ RNA-3 corners, but lower than that of the assembly containing three internal loop RNA-1 corners. AFM imaging confirmed the desired composition of the programmed nanotriangles by revealing the presence of the 3WJ RNA-3 module as indicated by extensions visible at the polygon corners (Fig. 2.5B).

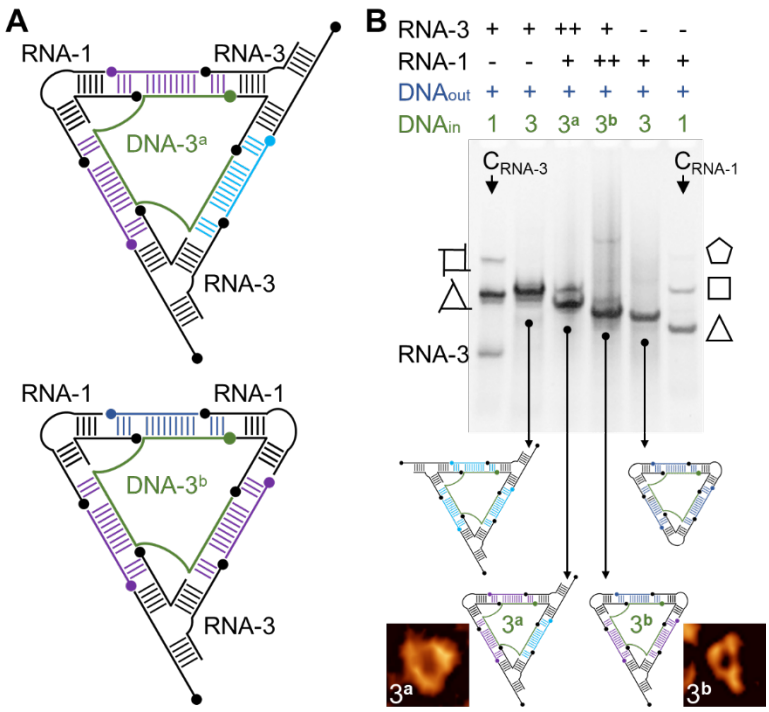

Figure 2.5. Controlled assembly of homogenous RNA-DNA hybrid nanotriangles containing combinations of RNA-1 corner and RNA-3 3WJ modules. (A) Homogeneous hybrid nanotriangles made from two different combinations of RNA-1 and RNA-3 modules. DNA guide strands with distinct hybridization sites (3^a and 3^b) spaced by a 12-nt linker were used to program the formation of the two different types of homogenous nanotriangles. (B) PAGE analysis in the presence of 5 mM magnesium chloride of homogenous triangles containing different RNA corner modules. C_{RNA-3} and C_{RNA-1} are controls of hybrid nanoshapes assembled from all RNA-3 modules or all RNA-1 modules, respectively. Homogenous nanotriangles shows increasing mobility with decreasing number of RNA-3 3WJ modules. Representative AFM images are shown of nanotriangles formed under the control of 3^a and 3^b DNA guide strands.

2.5 Conclusion

We describe a simple yet efficient screening strategy for the discovery of complex RNADNA hybrid nanoshapes that assemble from discrete nucleic acid modules through marginally stable Watson-Crick base paring interactions. The screening assessment carried out by native PAGE provides a robust and scalable method to unambiguously identify optimal combinations of RNA architectural joints and DNA connectors that associate to produce stable RNA-DNA hybrid nanoshapes. To demonstrate proof of concept, we designed three distinct RNA

corner modules (internal loops RNA-1 and RNA-2, and 3WJ RNA-3) and screened sets of DNA connectors for the formation of several unique hybrid nanotriangles with designed composition and arrangement of RNA and DNA components. We further outlined the programmed assembly of homogenous nanoshapes guided by extended DNA strands containing a defined number of hybridization sites that capitalize on the modular design of the hybrid nucleic acid architectures. The design and screening method provide a reliable approach for the scalable preparation of complex polygonal nucleic acid nanoshapes.

2.6 Acknowledgment

The material in Chapter 2, in full, is a reprint of material as it appears in Methods (2021) titled "A simple screening strategy for complex RNA-DNA hybrid nanoshapes" with Alba Monferrer and Thomas Herman as co-authors. The dissertation author was the primary investigator and author of this material. Prof. Hermann was the corresponding author.

The author thanks A. J. Lushnikov for help with AFM imaging.

Chapter 3: Complex RNA-DNA hybrid nanoshapes from iterative mix-and-match screening

3.1 Abstract

Hybrid nucleic acid nanostructures partition architectural and functional roles between RNA joints and DNA connectors. Nanoshapes self-assemble from nucleic acid modules through synergistic stabilization of marginally stable base pairing interactions within circularly closed polygons. Herein, we report the development of hybrid nanoshapes that include multiple different RNA modules such as internal loop and three-way junction (3WJ) motifs. An iterative mix-and-match screening approach was used to identify suitable DNA connectors that furnished stable nanoshapes for combinations of different RNA modules. The resulting complex multicomponent RNA-DNA hybrid nanoshapes were characterized by AFM imaging. Our research provides proof of concept for modular design, assembly and screening of RNA-DNA hybrid nanoshapes as building blocks for complex extended nucleic acid materials with features at the sub-10 nm scale.

3.2 Introduction

Applications of nucleic acids in soft materials nanotechnology exploit the predictable folding and self-assembly of the biopolymer through predominantly base pair formation between sequence-complementary oligonucleotide segments. Designing nanostructures that include predetermined folds of RNA or DNA modules is in many cases reduced to defining the overall topology of the desired architecture which, in turn, establishes connection of the building blocks(16,49,58,59). While RNA and DNA had been used largely separately to create nucleic acid nano-materials, RNA-DNA hybrid assemblies have recently emerged as a promising carrier material for functional biomolecules and the dynamic construction of reversible nano-objects(55–57,61,62). We have previously introduced a versatile kit of hybrid nanoshapes that assemble from both RNA architectural joints derived from a single type of RNA motif and double-helical DNA modules as functional connector modules(63). Hybrid nucleic acid architectures combine RNA

modules that introduce structural complexity with DNA components that allow for straightforward chemical modification and inclusion of diverse protein binding sites as a toolkit for the creation of composite soft materials. Robust hybrid nanoshapes self-assemble from RNA and DNA building blocks that interact through synergistic combination of marginally stable base pairing sites within a circularly closed arrangement. The robust increase of stabilization arising from the combination of individually weak hybridization sites within closed polygonal shapes provides a selection criterion for stable hybrid nanoshapes identified by size- and shape-selective methods. Specifically, systematic screening of mixtures containing selected RNA motifs as architectural joints and diverse DNA connectors of a range of base pairs by native polyacrylamide gel electrophoresis (PAGE) provides a powerful tool for selecting optimal combinations of nucleic acid building blocks that assemble to circularly closed hybrid nanoshapes. To further realize the potential of the hybrid nanoshape design as a blueprint for the creation of responsive materials from versatile nucleic acid modules, we recently prepared RNA-DNA hybrid nanoshapes that conditionally assemble under the control of a small molecule ligand(64).

Here, we describe the design and development of hybrid nanoshapes that incorporate combinations of multiple different RNA and DNA modules. While the previously established PAGE screening strategy sought to identify an optimal DNA connector for a single RNA module, an iterative mix-and-match approach is outlined here, which was used to screen for stable combinations of multi-component nanoshapes self-assembling from up to four different RNA and DNA modules. Several diverse nucleic acid nano-objects with a precisely defined composition were prepared and imaged by atomic force microscopy (AFM), and the dynamic process of self-assembly studied by time-resolved PAGE.

3.3 Results and Discussion

3.3.1 Design and screening for 3WJ RNA-DNA nanoshapes

For the discovery of robust RNA-DNA hybrid nanoshapes we had previously systematically assessed mixtures of a corner motif derived from an internal loop (i-loop) RNA and DNA duplex connector modules for the formation of stable complexes that migrate as discrete bands during electrophoresis on native polyacrylamide gels (PAGE)(63). Both, RNA and DNA building blocks carried short (4-8 nt) single stranded terminal extensions ("toehold"(66)) that enable assembly of modules through marginally stable hybridization of complementary sequences. We previously demonstrated that length adjustment of the unpaired single strands that connect RNA and DNA modules allows modulating the stability of the nanoshapes, with longer extensions resulting in nanoshapes of higher stability(63).

The formation of robust nanoshapes requires synergistic contributions of base pairs between multiple nucleic acid building blocks connected in a circularly closed topology (Fig. 3.1A). The objective of the current study was to apply the same concept for the discovery of nanoshapes that contain an RNA corner motif derived from a three-way junction (3WJ) RNA in the bacteriophage phi29 DNA packaging motor (pRNA) (Fig. 3.1B)(20). The pRNA 3WJ that was originally introduced by Peixuan Guo as a versatile nucleic acid building block of RNA nanoparticles has been instrumental for the development of the RNA nanotechnology field(22,25,74,27,28,66,69–73). For example, extended two-dimensional (2D) RNA materials were obtained by connecting triangular complexes of the 3WJ corner motif through its helical extension as a coupling(25).

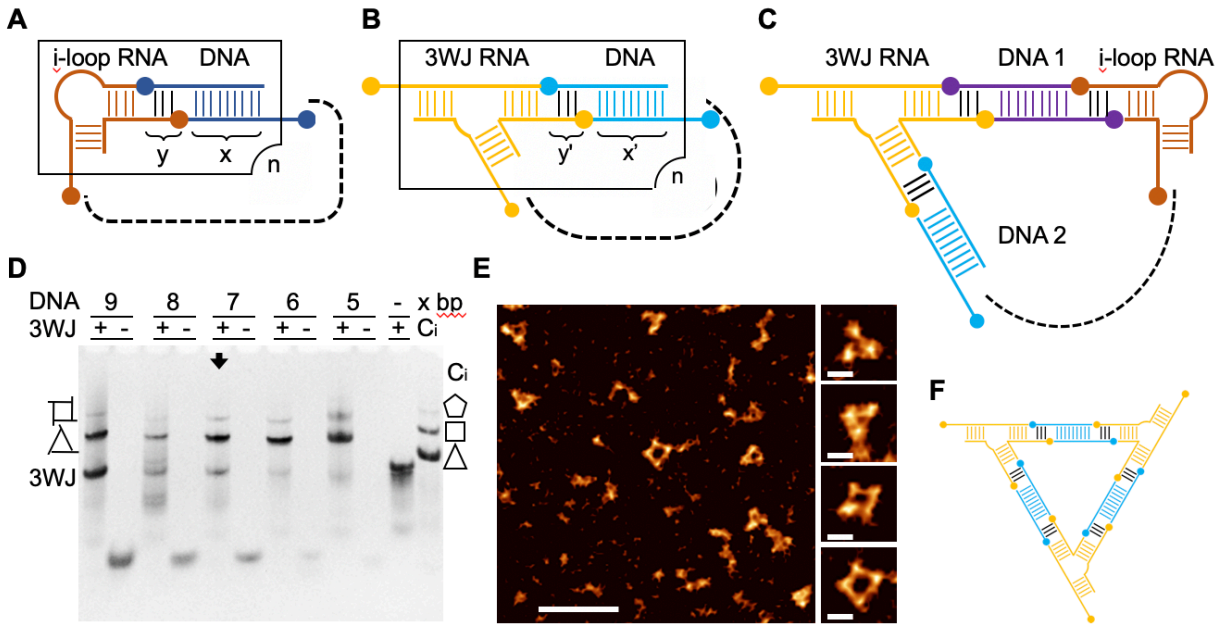

Figure 3.1. Design and screening of RNA-DNA hybrid nanoshapes. (A) Design of RNA-DNA hybrid nanoshapes that assemble from multiple copies of an internal loop (i-loop) RNA motif that serves as architectural joint and a straight DNA module as connector. Variable parameters for nanoshapes include the length of single stranded regions (y) for interaction between the building blocks and the number of base pairs (bp) in the double stranded core (x) of the DNA module. (B) Design of RNA-DNA hybrid nanoshapes that contain a three-way junction (3WJ) RNA as architectural joint. (C) Complex RNA-DNA hybrid nanoshapes that contain multiple different RNA and DNA modules. (D) Screening for stable RNA-DNA hybrid nanoshapes by native polyacrylamide gel electrophoresis (PAGE). Stable polygonal nanostructures that self-assemble from a combination of 3WJ RNA and DNA modules produce discrete bands. The 3WJ RNA with single stranded overhangs of 6 nucleotides (y) was combined with different DNA modules carrying 5-9 bp in the double stranded core (x). For each combination, the DNA module alone (right lane) and together with the 3WJ RNA (left lane) is shown. Ci is a control containing a mixture of previously developed hybrid nanoshapes that contain i-loop RNA and a DNA module with 11 bp in the double stranded region. (E) Atomic force microscopy (AFM) imaging of hybrid nanoshapes obtained from 3WJ RNA modules and DNA connectors with 7 bp (see panel d, arrow). Scale bar represents 50 nm. Images showing individual nanoshapes are 30 nm wide. (F) Composition of 3WJ RNA-DNA nanotriangle shown as an example of hybrid nanoshapes.

Here, we used native PAGE analysis to identify DNA modules for the assembly of stable hybrid nanoshapes that contain the 3WJ RNA corner motif. With distinct DNA connectors specific for the i-loop and 3WJ RNA in hand, we devised nanoshapes that incorporate combinations of multiple different modules (Fig. 3.1C). DNA duplexes with a core of 7 bp flanked by 6 nt single

stranded overhangs were identified by PAGE screening as suitable connectors to form 3WJ hybrid nanoshapes (Fig. 3.1(D, E, F)). Similar to the previously developed i-loop RNA hybrid nanoshapes, a mixture of polygon complexes was obtained for the 3WJ RNA, albeit favouring the assembly of triangles and squares as demonstrated by AFM imaging (Fig. 3.1E). AFM images of individual nanoshapes clearly revealed bulky 3WJ corner motifs connected by less expansive DNA modules. With DNA connectors of 7 bp identified in PAGE screening for 3WJ corner motifs, we designed guide strands to direct formation of a single type of polygons, analogous to homogenous RNA-DNA nanoshapes that we previously developed. DNA guide strands with three or four hybridization sites were used to prepare RNA-DNA hybrid triangles or squares, respectively, containing 3WJ as corner motifs whose structure was confirmed by AFM imaging (Fig. 3.2).

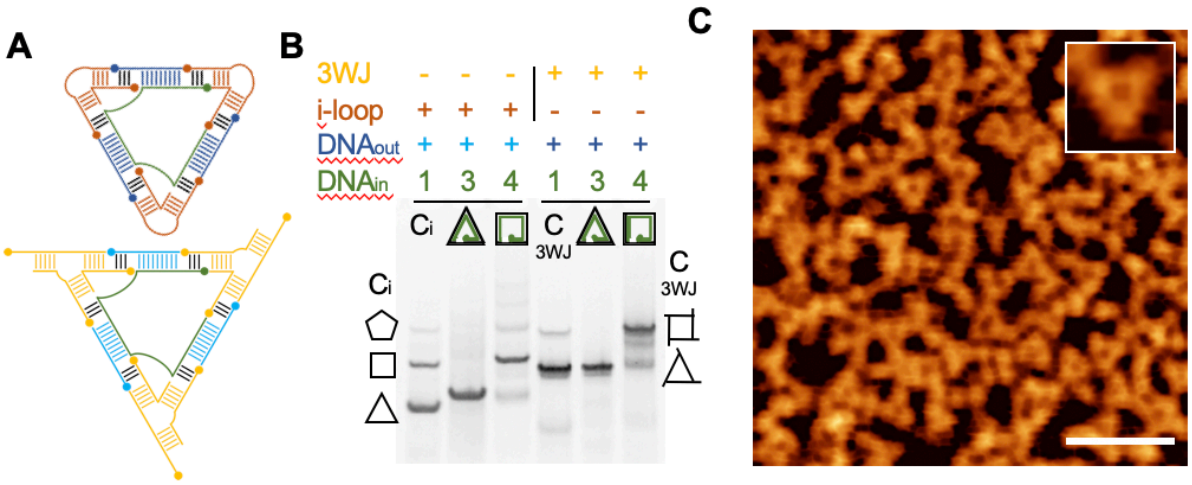

Figure 3.2. Design and characterization of homogenous hybrid nanoshapes. (A) Inclusion of a DNA guide strand (green) that contains a defined number of hybridization sites, spaced by a linker sequence, allows assembly of homogenous hybrid nanoshapes such as the triangles shown here. (B) Native PAGE analysis reveals homogenous nanotriangles and nanosquares containing i-loop or 3WJ RNA modules in combination with appropriate guide DNA. Homogenous nanoshapes migrate slightly slower than the same species in the nanoshape mixture shown as control in lane Ci which contains previously developed hybrid nanoshapes that contain i-loop RNA and a DNA module with 11 bp in the double stranded region. (C) AFM topography image of homogenous nanotriangles containing 3WJ RNA module. Scale bar represents 50 nm. Insert showing individual nanotriangle is 25 nm wide.

3.3.2 Mix-and-match screening for multi-component nanoshapes

The establishment of RNA-DNA nanoshapes containing either the i-loop RNA (Fig. 3.1A) or the pRNA 3WJ (Fig. 3.1B) as corner motifs set the stage for identifying assemblies that incorporate multiple different RNA corner modules (Fig. 3.1C). Design parameters for the selection of optimal nucleic acid building blocks that self-assemble to the desired architectures include the length of base-paired duplexes in the RNA motifs and DNA connectors as well as the length of single-stranded regions for hybridization of modules. With a set of robust RNA corner motifs in hand, we devised an iterative mix-and-match PAGE screening method to discover combinations of DNA connectors that assembled stable hybrid nanoshapes containing multiple different RNA and DNA modules. Advantages of the screening approach include the convenient availability of inexpensive short DNA oligonucleotides that allow the systematic testing of connector modules, and the ability to rapidly and unambiguously identify optimal combinations of building blocks that result in the highest stability assemblies. Previously, Shapiro's group had developed and applied computational methods to design in silico circularly closed self-assembling RNA nanostructures based on the known 3D structures of RNA motifs(37,66,67). Nanostructures that connect both RNA and DNA building blocks through hybridization of the two nucleic acid types pose additional challenges to the precise prediction of module properties, including the length of DNA connectors. While RNA and RNA-DNA hybrid helices adopt the A-form conformation, there is less certainty about the extent to which base pairs in adjacent helices undergo a transition to the B-conformation preferred by DNA. Experimentally confirmed combinations of RNA and DNA building blocks that assemble to robust nanoshapes may inform computational approaches for the in-silico design of complex RNA-DNA hybrid nanoshapes in the future.

Here, stable nano-assemblies containing multiple different RNA and DNA modules were identified by an iterative mix-and-match screening approach from combinations of corner modules and 7 bp DNA connectors identified as components of 3WJ nanoshapes with a selection of 8-11 bp DNA duplexes (Fig. 3.3). Native gel analysis revealed that a mixture of DNA connectors with 7 and 9 bp was required to furnish complex nanoshapes containing one i-loop and two 3WJ corners. Formation of the nanoshapes relies on cooperative stabilization of marginally stable 6 bp RNA-DNA hybrid regions in a circularly closed structure. It appears that only 9 bp DNA afford a stable closed structure including i-loop and 3WJ RNA corners while shorter or longer connectors cannot. Thus, formation of stable multi-component assemblies was exquisitely sensitive to the DNA connector length, as we had previously observed in the discovery of hybrid nanoshapes with all i-loop corners. Systematic analysis of component mixtures demonstrated that all four distinct building blocks, the two different DNA connectors of 7 and 9 bp as well as the two distinct corner modules of i-loop and 3WJ RNA, were required to assemble stable multi-component nanoshapes (Fig. 3.3B & C). Specifically, the DNA connector of 9 bp by itself, in the absence of 7 bp DNA, did not yield a single stable product when combined with i-loop and 3WJ RNA (Fig. 3.3B), and neither did the individual RNA corner motifs in combination with both DNA connectors (Fig. 3.3C).

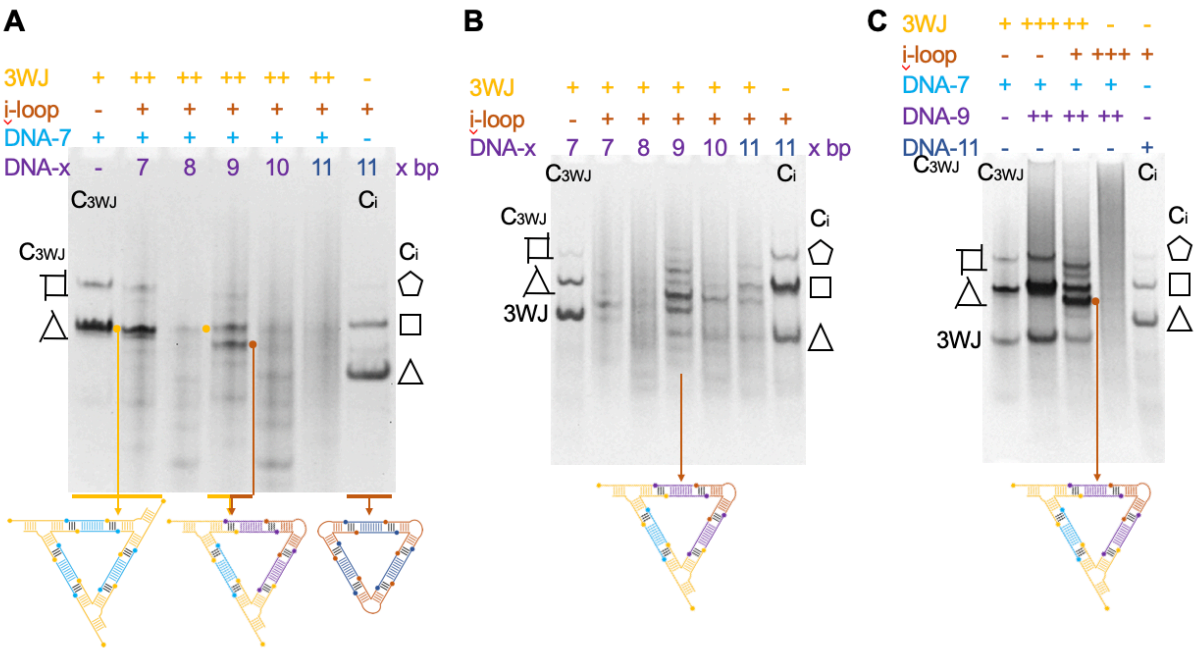

Figure 3.3. Mix-and-match screening for multicomponent RNA-DNA hybrid nanoshapes. Mixtures of two types each of RNA corner modules (3WJ and i-loop) and DNA connectors containing different numbers of base pairs (DNA-7 and DNA-x) were analyzed by PAGE for the formation of stable assemblies indicated by distinct bands on the gel. C3WJ is a control lane of nanoshapes formed from 3WJ RNA modules and DNA connectors with 7 bp (see Fig. 1D). Ci is a control lane of previously developed hybrid nanoshapes that contain i-loop RNA and a DNA module with 11 bp. Except for the controls, 3WJ RNA was used at 2-fold concentration over i-loop RNA to promote incorporation of two 3WJ corners. The concentration of DNA-x was equimolar to i-loop RNA. A mixture containing two types of DNA connectors with 7 and 9 bp results in formation of complex nanoshapes that contain both 3WJ and i-loop RNA. (B-C) Analysis of component essentiality for assembly of multi-component RNA-DNA hybrid nanoshapes. Mixtures of two types each of RNA modules (3WJ and i-loop) and DNA connectors containing different numbers of base pairs (DNA-x) were analyzed by PAGE for the formation of stable assemblies indicated by distinct bands on the gel. C3WJ is a control lane of nanoshapes formed from 3WJ RNA modules and DNA connectors with 7 bp (see Fig. 3.1D). Ci is a control lane of previously developed hybrid nanoshapes that contain i-loop RNA and a DNA module with 11 bp. (B) Connector DNA-9 by itself is not sufficient to produce a single stable product. (C) Corner motifs i-loop or 3WJ each by themselves are not sufficient to produce a single stable product.

3.3.3 Controlled assembly of homogenous multi-component nanoshapes

With a set of RNA corners and DNA connectors for the construction of multi-component nanoshapes in hand, we went on to design homogenous multi-component nanotriangles and -squares. DNA guide strands with three unique hybridization sites afforded control over the

assembly of multi-component nanotriangles containing programmed combinations of 3WJ and i-loop RNA corner modules (Fig. 3.4). Guide strands whose function resembles the role of staple strands in nucleic acid origami architectures(12) were designed by connecting a defined number of DNA module sequences with single-stranded linkers, as we previously devised for homogenous nanoshapes containing i-loop RNA corner motifs. Beyond determining the composition of multi-component nanoshapes, DNA guide strands can add functionality within the singled-stranded linker regions, for example recognition sequences for other nucleic acid components or proteins in composite nanomaterials.

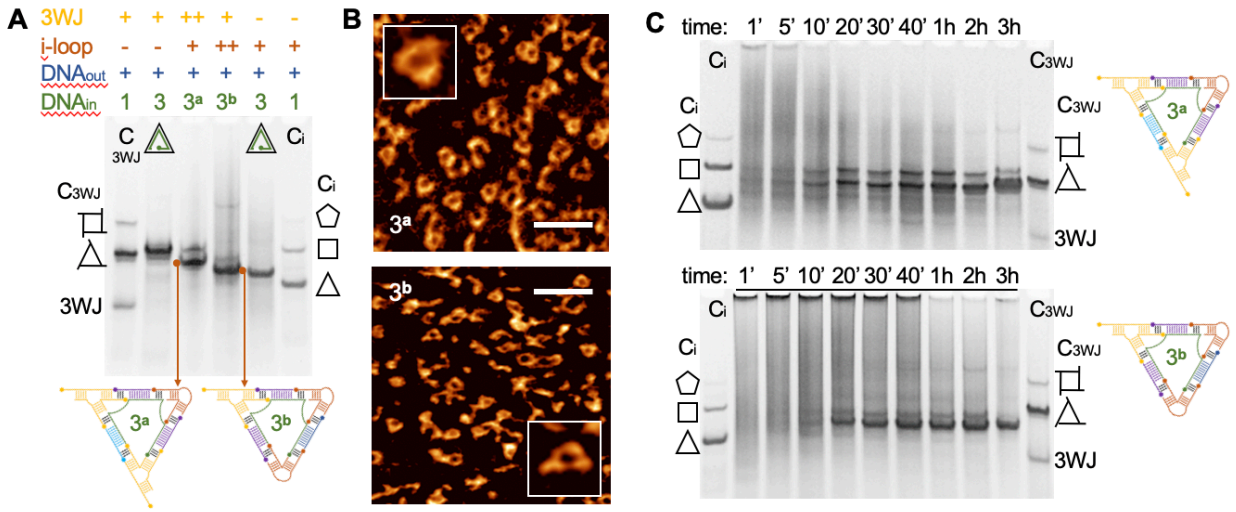

Figure 3.4. Controlled assembly of homogenous multi-component nanotriangles. (A) PAGE analysis of homogenous nanotriangles. Inclusion of a DNA guide strand (green) that contains three hybridization sites for connection of defined RNA corner modules (i-loop or 3WJ), spaced by a linker sequence, directs the formation of homogenous nanoshapes of pre-determined composition, as shown here for nanotriangles with two different DNA guide strands for inclusion of one or two 3WJ modules, respectively (3^a and 3^b). C3WJ is a control lane of nanoshapes formed from 3WJ RNA modules and DNA connectors with 7 bp (see Figure 3.1D). Ci is a control lane of hybrid nanoshapes that contain i-loop RNA and a DNA module with 11 bp. (B) AFM topography images of homogenous nanotriangles containing one or two 3WJ modules, respectively (3^a and 3^b). Scale bar represents 50 nm. (C) Kinetics of the formation of homogenous multi-component nanotriangles containing one or two 3WJ modules (3^a and 3^b), monitored at 37°C. PAGE analysis of samples collected at different time points reveals a slow annealing process that converges to the desired nanoshapes.

Two variants of nanotriangles were created, including assemblies 3^a and 3^b which contained one or two 3WJ corners, respectively (Fig. 3.4A). Formation of the multi-component nanotriangles was confirmed by their mobility on native PAGE, which was distinct from either of the single-component nanotriangles, and by AFM imaging (Fig. 3.4B). Association of the modules to the homogenous multi-component nanotriangles followed a slow kinetics which required 20-60 minutes to complete self-assembly at 37°C (Figure 3.4C). Observation of aggregated material by PAGE at early time points suggest that the formation of nanotriangles converged through resolution of sub-optimal associations between modules to the correct programmed connections by an equilibrium annealing process. In contrast, previously established homogenous nanoshapes, which included a single type of RNA corner module and DNA guide, associated rapidly likely because these involved the same hybridization sequence for all connections between building blocks.

Symmetrical multi-component nanosquares that contained a programmed combination of diagonally opposed corner modules of each 3WJ and i-loop RNA were prepared by including two different designs of DNA guide strands (Fig. 3.5). In one approach, a single DNA guide with four distinct hybridization sites was used (DNAin-4). A second design relied on the combination of DNA guides with two hybridization sites each (DNAin-2), which had previously been shown to direct the association of nanosquares containing two copies of the DNA guide. While both approaches afforded homogenous nanosquares as demonstrated by PAGE analysis, the DNAin-2 design furnished cleaner assemblies (Fig. 3.5A) whose constitution was confirmed by AFM imaging (Fig. 3.5B).

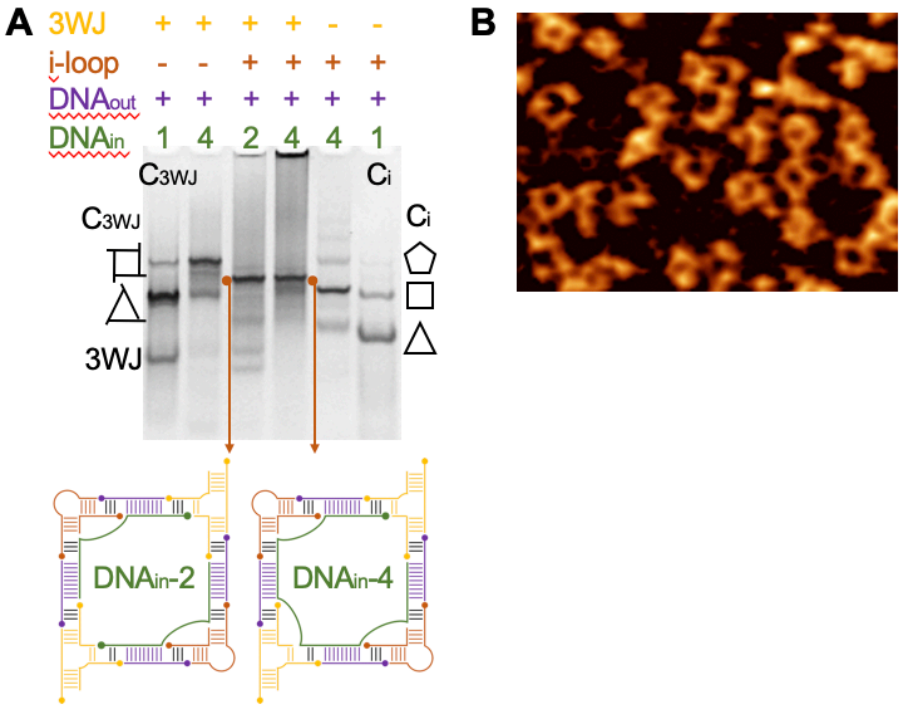

Figure 3.5. Controlled assembly of homogenous multi-component nanosquares. (A) PAGE analysis of homogenous nanosquares. Inclusion of DNA guide strands (green) that contain two or four hybridization sites (DNAin-2 or DNAin-4) for connection of defined RNA corner modules (i-loop or 3WJ) directs the formation of homogenous nanosquares of pre-determined composition. C3WJ is a control lane of nanoshapes formed from 3WJ RNA modules and DNA connectors with 7 bp (see Figure 3.1D). Ci is a control lane of hybrid nanoshapes that contain i-loop RNA and a DNA module with 11 bp. (B) AFM topography images of homogenous nanosquares containing two of each, i-loop and 3WJ RNA modules assembled with DNAin-2 guides. Scale bar represents 50 nm.

3.4 Conclusion and Outlook

Here, we describe an iterative mix-and-match screening approach that identifies synergistic stabilization of marginally stable base pairing interactions between nucleic acid components as a powerful tool to discover self-assembling stable nanoshapes containing multiple different RNA and DNA modules. Sets of optimal DNA connectors were identified by screening that associate with 3WJ RNA corner modules and combinations with i-loop RNA corners to furnish complex hybrid nanoshapes following a programmed stoichiometry of different RNA and DNA building blocks. The mix-and-match screening method allows to rapidly and unambiguously identify

optimal combinations of nucleic acid components from a diverse set of candidate modules that result in the highest stability nanostructures. The screening approach is also amenable to include nucleic acid aptamer motifs in the presence of their cognate ligands, as we demonstrated in preliminary proof-of-concept studies on the design and discovery of RNA-DNA hybrid nanoshapes containing an AMP aptamer RNA corner motif (Fig. 3.6).

We further demonstrated that DNA guide strands containing a defined number of hybridization sites allow the precise assembly of homogenous nanoshape polygons with a precisely defined composition and arrangement of RNA and DNA modules. By choosing from a set of autonomously folding RNA corner motifs, and application of the screening approach to identify appropriate DNA connectors, total control is achieved over assembly and composition of complex hybrid nanoshapes.

Self-assembling nanoshapes containing the 3WJ corner motif, through its helical extension as a coupling, provide versatile tiles for the design and construction of extended RNA-DNA composite 2D materials. As a proof of concept, we demonstrated the connection of multi-component RNA-DNA nanotriangles to form dimers of a precisely defined composition (Fig. 3.7). The dimers self-assemble from 2 different RNA modules (3WJ and i-loop) as well as 3 distinct DNA connectors of 7, 8 and 9 base pairs in a programmed fashion. Hybrid nanoshapes are ideally suited as building blocks that expand the repertoire of nucleic acid composite materials by including multiple RNA, DNA, protein and other chemically diverse components in the controlled noncovalent synthesis of complex supramolecular systems(75).

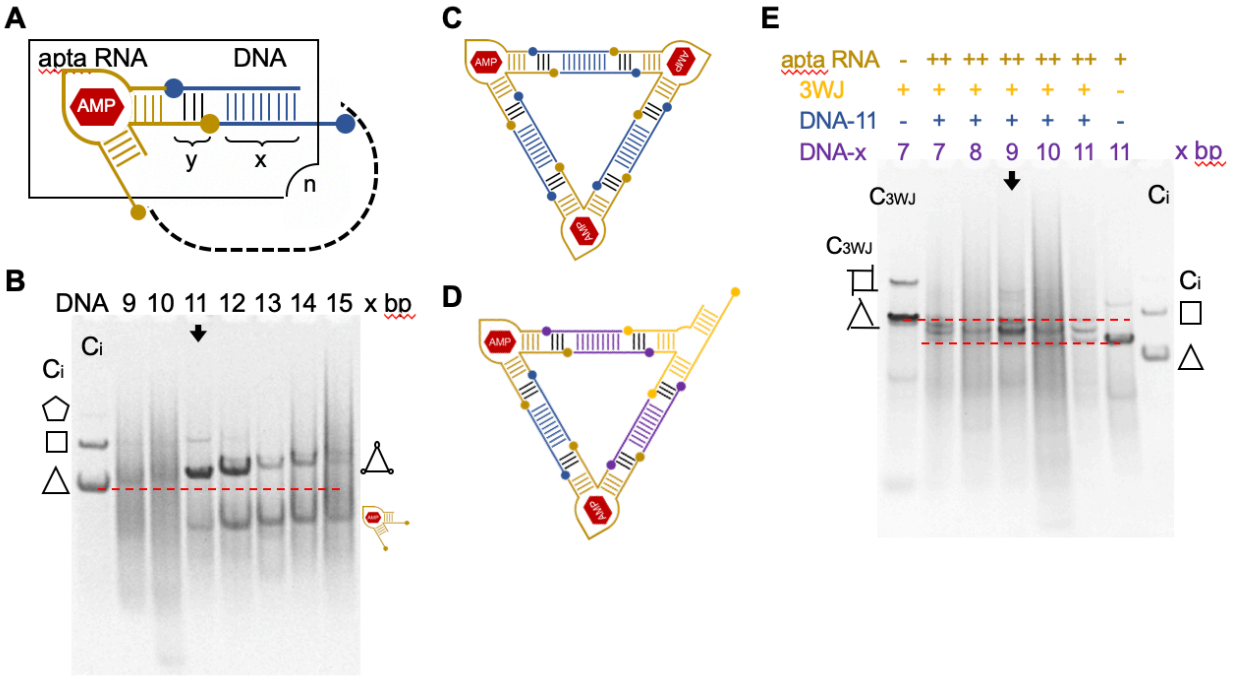

Figure 3.6. Design and screening of RNA-DNA hybrid nanoshapes containing an AMP aptamer RNA corner motif (apta RNA). (A) Design nanoshapes that assemble from multiple copies of the apta RNA motif that serves as architectural joint and a straight DNA module as connector. Variable parameters x and y are described in Fig. 3.1. (B). PAGE screening for stable RNA-DNA hybrid nanoshapes which give rise to discrete bands. The apta RNA with single stranded overhangs of 6 nucleotides (y) was combined with different DNA modules carrying 9-15 bp in the double stranded core (x). Ci is a control containing a mixture of previously developed hybrid nanoshapes that contain i-loop RNA and a DNA module with 11 bp in the double stranded region. The 11 bp DNA connector results in the highest yield of mostly apta RNA-DNA triangle and a faint band indicating nanosquare (arrow). (C) Composition of apta RNA-DNA nanotriangle shown as an example. (D) Multicomponent nanotriangle containing apta RNA and 3WJ RNA corner motifs. (E) Mix-and-match screening for multicomponent RNA-DNA hybrid nanoshapes. Mixtures of two types each of RNA corner modules (3WJ and apta) and DNA connectors containing different numbers of base pairs (DNA-11 and DNA-x) were analyzed by PAGE for the formation of stable assemblies indicated by distinct bands on the gel. C3WJ is a control lane of nanoshapes formed from 3WJ RNA modules and DNA connectors with 7 bp (see Fig. 1(D)). Ci is the control explained in panel (B). The second to last lane, next to Ci, lacks 3WJ RNA as well as DNA-x and results in formation of nanoshapes containing only apta RNA corner modules connected by DNA-11, as shown in panels (B) and (C). The 9 bp DNA connector (arrow) results in the highest yield of mostly nanotriangles whose electrophoretic mobility in between triangles containing all-3WJ and all-apta RNA corners is consistent with assemblies containing a mixture of both RNA corner motifs. Since the apta RNA was used in 2-fold excess over 3WJ RNA corner, the resulting nanotriangles likely have the composition shown in panel (D).

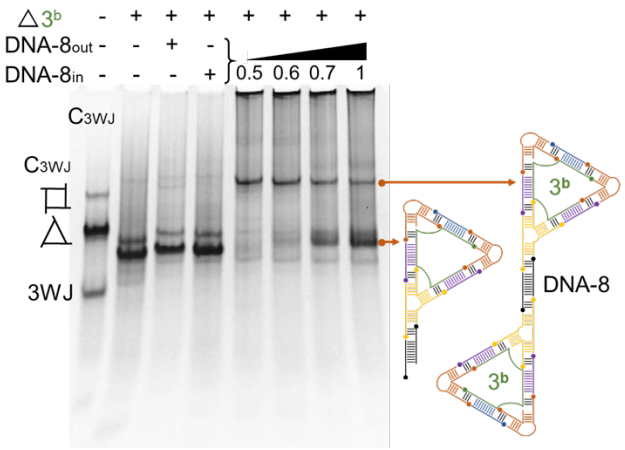

Figure 3.7. Connection of multi-component nanotriangles as proof of concept for the creation of extended 2D materials from hybrid nucleic acid nanoshapes. PAGE analysis of homogenous 3^b nanotriangle constructs that contain i-loop and 3WJ RNA modules (Fig. 3.4), connected by a DNA duplex of 8 bp (DNA-8). The 3WJ module provides an anchor to bind the DNA-8 connector in 3^b nanotriangle dimers. Increasing concentration of the DNA-8 connector led to preferential association with a single nanotriangle as indicated by occurrence of the corresponding complex bands.

3.5 Experimental

3.5.1 Materials

DNA and RNA oligonucleotides were purchased from Integrated DNA Technologies. Lyophilized oligonucleotides were rehydrated by dissolving in 10 mM sodium cacodylate buffer, pH 6.5. Sequences of oligonucleotides are provided in the Table 3.1, 3.2 and 3.3.

Table 3.1. Oligonucleotide sequences for RNA corner modules

Strand	Sequence
i-Loop-In	5’ - rCrCrG rArGrG rUrCrA rGrCrC rUrG - 3’
i-Loop-Out	5’ - rCrGrA rGrArC rCrArG rGrArA rCrUrA rCrUrGrA - 3’
3WJ-RNA-1	5’ - rGrArA rGrGrC rUrGrA rCrArA rUrCrA rUrGrC rU - 3’
3WJ-RNA-2	5’ - rCrCrG rArGrG rArGrC rArUrG rUrGrU rArCrC rU -3’
3WJ-RNA-3	5’ - rCrGrA rGrArC rArGrG rUrArC rUrUrU rGrUrU rGrUrC rA -3’

Table 3.2. Oligonucleotide sequences for double-stranded DNA connectors.

Strand	Sequence
DNA-5-In	5’ - GTC TCG TAC GT -3’
DNA-5-Out	5’ - CCT CGG ACG TA - 3’
DNA-6-In	5’ - GTC TCG GTA CGT - 3’
DNA-6-Out	5’ - CCT CGG ACG TAC - 3’
DNA-7-In	5’ - GTC TCG ACG ACG T - 3’
DNA-7-Out	5’ - CCT CGG ACG TCG T - 3’
DNA-8-In	5’ - GTC TCG ACG TAC GT - 3’
DNA-8-Out	5’ - CCT CGG ACG TAC GT - 3’
DNA-9-In	5’ - GTC TCG CAC GTA CGT - 3’
DNA-9-Out	5’ - CCT CGG ACG TAC GTG - 3’
DNA-10-In	5’ - GTC TCG ACG TAT ACG T - 3’
DNA-10-Out	5’ - CCT CGG ACG TAT ACG T - 3’
DNA-11-In	5’ - GTC TCG CGT ACG TAC GT - 3’
DNA-11-Out	5’ - CCT CGG ACG TAC GTA CG - 3’
DNA-12-In	5’ - GTC TCG CCA TGA GCA AAT - 3’
DNA-12-Out	5’ - CCT CGG ATT TGC TCA TGG - 3’
DNA-13-In	5’ - GTC TCG CCA TGA TGC AAA T - 3’
DNA-13-Out	5’ - CCT CGG ATT TGC ATC ATG G - 3’
DNA-14-In	5’ - GTC TCG CCA TGA TTG CAA AT - 3’
DNA-14-Out	5’ - CCT CGG ATT TGC AAT CAT GG - 3’
DNA-15-In	5’ - GTC TCG CCA TGA TTG TCA AAT - 3’
DNA-15-Out	5’ - CCT CGG ATT TGA CAA TCA TGG - 3’
DNA-Connector-8_{in}	5’ - GCC TTC CGT GAC TA -3’
DNA-Connector-8_{out}	5’ - GCC TTC TAG TCA CG -3’

Table 3.3. Oligonucleotide sequences for DNA guide strands

Strand	Sequences
i-Loop-DNAguide-3	5’ - GTC TCG TAT CGC TAC GTT TTC TCT CTC TCT TTT GTC TCG TAT CGC TAC GTT TTC TCT CTC TCT TTT GTC TCG TAT CGC TAC GT - 3’
i-Loop-DNAguide-4	5’ - GTC TCG TAT CGC TAC GTT TTC TCT CTC TCT TTT GTC TCG TAT CGC TAC GTT TTC TCT CTC TCT TTT GTC TCG TAT CGC TAC GTT TTC TCT CTC TCT TTT GTC TCG TAT CGC TAC GT - 3’
3WJ-DNAguide-3	5’ - GTC TCG ACG ACG TTT TCT CTC TTT T GTC TCG ACG ACG TTT TCT CTC TTT T GTC TCG ACG ACG T - 3’
3WJ-DNAguide-4	5’ - GTC TCG ACG ACG TTT TCT CTC TTT T GTC TCG ACG ACG TTT TCT CTC TTT T GTC TCG ACG ACG TTT TCT CTC TTT T GTC TCG ACG ACG T - 3’
DNAguide-3a	5’ - GTC TCG CAC GTA CGT TTT CTC TCT TTT GTC TCG ACG ACG TTT TCT CTC TTT TGT CTC GCA CGT ACG T - 3’
DNAguide-3b	5’ - GTC TCG CAC GTA CGT TTT CTC TCT TTT GTC TCG CGT ACG TAC GTT TTC TCT CTT TTG TCT CGC ACG TAC GT - 3’
DNAguide-2	5’ - GTC TCG CAC GTA CGT TTC TCT CTT TGT CTC GCA CGT ACG T - 3’
DNAguide-4	5’ - GTC TCG CAC GTA CGT TTC TCT CTT TGT CTC GCA CGT ACG TTT CTC TCT TTG TCT CGC ACG TAC GTT TCT CTC TTT GTC TCG CAC GTA CGT - 3’

3.5.2 RNA-DNA hybrid nanostructure preparation

RNA-DNA hybrid structures were prepared by mixing constituent oligonucleotides at equimolar concentration (100 μM) in the presence of 5 mM magnesium chloride. Unless indicated otherwise, samples were annealed by heating at 65°C for 5 minutes followed by incubation at 37°C for 10 minutes before cooling on ice for 5 minutes.

3.5.3 Gel electrophoresis

Polyacrylamide gel electrophoresis was performed on 5% acrylamide/bisacrylamide (19:1) native gel matrix at 220 V, 22 mA in 2X MOPS buffer (40 mM 3-morpholinopropane 1-sulfonic acid, 10 mM sodium acetate and 5 mM magnesium chloride. For detection of nucleic acid complexes, gels were stained with ethidium bromide and imaged under UV light.

3.5.4 AFM imaging

AFM imaging of nucleic acid samples was performed on surface-modified mica carrier. Freshly cleaved mica was immersed in 50 mM aqueous solution of 1-(3-aminopropyl)-silatrane (APS) for 30 min, rinsed with deionized water and dryed in an argon stream. Imaging samples were diluted in buffer containing 10 mM HEPES, pH 7, and 2 mM magnesium chloride to 0.5-1.5 ng/μL concentration, and applied on APS-modified mica carrier for 2 min. Sample preparation was performed at 4°C. After deposition, mica strips were rinsed briefly with ice cold water and dried under a gentle argon flow. AFM images were recorded with a MultiMode AFM Nanoscope IV system (Bruker Instruments) in Tapping Mode with silicon probes RTESPA-300 (Bruker Nano Inc.; resonance frequency ~300 kHz, spring constant ~40 N/m) at a scanning rate of ~2.0 Hz. Image processing was performed with the FemtoScan software package (Advanced Technologies Center).

3.6 Acknowledgement

The material in Chapter 3, in full, is a reprint of material as it appears in Nano Research (2021, 14(1), 46-51) titled “Complex RNA-DNA hybrid nanoshapes from iterative mix-and-match screening” with Zhiyuan Zhang, Eugene Alforque and Thomas Hermann as co-authors. The dissertation author was the primary investigator and author of this material. Prof. Hermann was the corresponding author.

The author thanks A. J. Lushnikov for help with AFM imaging.

Chapter 4: Transform RNA-DNA Hybrid Nano-Complexes Through Swift Replacements of Nucleic Acid Modules

4.1 Abstract

Hybrid nucleic acid nanotechnology seeks to construct nano-complexes with defined topologies from small structural diversified RNA motifs serving as architectural joints and chemically robust DNA duplexes as functional sites. Nanoshapes self-assembling from discrete RNA and DNA modules through synergistic stabilization of marginally stable base pairing interactions within circularly closed polygons possess outstanding modularity which allows for dynamic switch of all components and thereby conformations. Herein, we report a simple strand-replacement strategy based on a single unpaired nucleotide or a single mismatched base pair to substitute RNA and DNA modules in hybrid nucleic acid nano-complexes swiftly and consecutively. By switching DNA modules that direct the formation of homogeneous nanoshapes, hybrid nucleic acid nano-complexes transformed between different conformations. Our research demonstrated and exploited the superb modularity of RNA-DNA hybrid nano-complexes, outlining a simple strategy for switching every component in a circularly closed nanostructure and opening a door for designing and preparing dynamic devices with switchable nucleic acid components.

4.2 Introduction

Nucleic acid nanotechnology has been established as an important and promising field in nanoscience owing to its remarkable ability and accuracy to control materials assembly(76,77). Between largely separated DNA and RNA nanotechnology, RNA nanotechnology seeks to assemble diverse nanoparticles with superb modularity by connecting small structural diversified RNA motifs in a defined and controlled manner through a dominant bottom-up assembling strategy(59,78). This building game was named as RNA tectonics(19,58,79) and frequently compared as RNA-Lego game(80). Recent emerging RNA-DNA hybrid nanotechnology that uses

RNA modules with intrinsic structural diversities to define the topology of the overall hybrid nucleic acid assemblies can be largely seen as an expansion of the game as it adds DNA modules as building bricks to the Lego game(63). The new direction in the nucleic acid nanotechnology that marries the structural diversified RNA motifs and chemically robust DNA modules gives rise to nanoparticle units enriched with structural varieties and functional potentials in sub-10 nanometer (nm) scale. Previously, we have proposed a simple screening method, as well as an iterative mix-and-match screening strategy, to rapidly select the optimal combinations of multiple different RNA and DNA modules to prepare circularly closed hybrid nucleic acid nano-assemblies(64,65). As proof-of-concept, we developed a series of polygonal nanoshapes from multiple DNA duplexes with different lengths and functions and various RNA structural motifs, including RNA corners derived from viral RNA1213, a 3-way junction motif in the bacteriophage phi29 DNA packaging motor promoter–associated RNAs (pRNAs)(20) and RNA aptamers stabilized upon the binding of ligands(81).

In the nucleic acid Lego game, assembling nucleic acid nanoparticles from a set of bricks made of small RNA and DNA pieces has widely succeed as a number of various nucleic acid nano-assemblies made from different nucleic acid components have been reported(22,27,42,45–47,71). However, superb modularity of those Lego constructs that allows for swift replacements of every nucleic acid Lego brick and thereby transformation of conformations have rarely been studied.

Here, we proposed a simple strand-replacement method to transform nucleic acid nanoshapes by swiftly replacing nucleic acid components in RNA-DNA hybrid nano-assemblies. While the strand-replacement was based on a single unpaired nucleotide or a single mismatched base pair, it can be done swiftly and consecutively at 37 degrees in a short time (20mins). Modular nucleic acid nanoparticles were able to transform between heterogeneous nanoshapes and

homogeneous nanoshapes, as well as from one homogenous nanoshape to another homogenous nanoshape, by switching DNA components that directed homogeneous assembly of nano-complexes. The substitution of nucleic acid components and transformation of RNA-DNA hybrid nanoshapes were analysed by native polyacrylamide gel electrophoresis (PAGE), fluorescent experiments and atomic force microscopy (AFM).

4.3 Results and Discussion

4.3.1 Swift Replacements of DNA Modules in RNA-DNA Hybrid Nanoshapes

Our lab has prepared a number of RNA-DNA hybrid nanoshapes incorporated discrete RNA and DNA modules with diverse structural and chemical properties and various functions91011. An exemplary RNA-DNA hybrid nanosquare contained four copies of each an RNA corner motif and a DNA duplex connector (Fig. 4.1A) which were hybridized through marginally stable 4-7 Watson-Crick hybrid base pairs. Formation of a robust RNA-DNA hybrid nanosquare relies on synergistic stabilization of the assembly in a circularly closed structure. Modular design of hybrid nucleic acid nano-assemblies had both RNA and DNA modules available to switch to modules for nano-complexes with higher stability. Previous experiments have concluded that adjustment of the unpaired single strands that connect RNA and DNA modules allowed for modulating the stability of the nanoshapes(63). Therefore, among variations of 5-13, 6-11 and 7-9 RNA-DNA hybrid nanoshapes that gave rise to three separate bands with identical electrophoretic mobilities, nanoshapes' stability increased with increasing number of base pairs in the connection area (y) (Fig. 4.1B). AFM imaging of nucleic acid species extracted from individual bands of the 6-11 mixture demonstrated the formation of hybrid nanotriangles, nanosquares and nanopentagons.

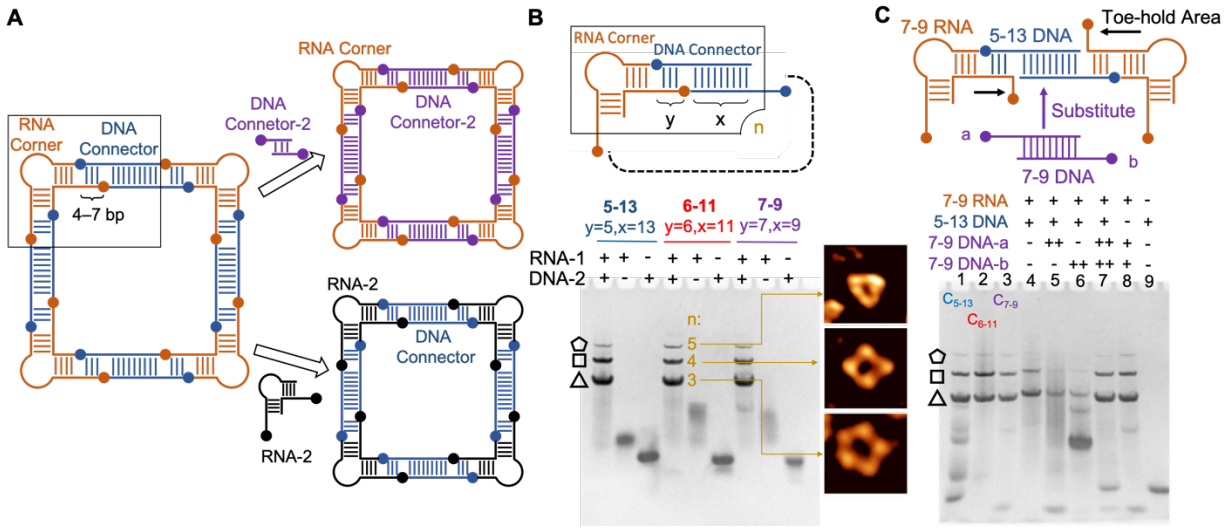

Figure 4.1. Modular RNA-DNA hybrid nanoshapes with fully switchable components. (A) Exemplary RNA-DNA hybrid nanosquare assembled from RNA corner modules and DNA connectors through marginally stable hybrid regions containing 4-7 base pairs (bp). Modular design of the hybrid nano-assembly allows for the replacement of both RNA and DNA motifs with new types of nucleic acid components. (B) Three variations of RNA-DNA hybrid nanoshapes with different length of RNA-DNA hybrid areas. Inserted AFM images (with a size of 20nm) showed the isolated species of nucleic acid nano-assemblies. Nanoshapes' stability increases with increasing number of base pairs in the hybridization area (y). (B) A strand-replacement method to substitute DNA modules in the nanoshapes. 7-9 RNA corners associated with 5-13 DNA modules to form nanoshapes at a low-stable state (lane 4) with two unpaired nucleotides serving as the toe-hold area at the end of each RNA corner. 7-9 DNA duplexes that associated with the 7-9 RNA to form fully base paired hybridization region (7 base pairs) substituted the 5-13 DNA to form nanoshapes at a high-stable state (lane 7) with the 7-9 RNA. $C_{5\text{-}13}$, $C_{6\text{-}11}$ and $C_{7\text{-}9}$ are controlled nanoshapes which had no unpaired.

Based on the variations' differences in thermal stability, we conceived a strand-replacement strategy to convert RNA-DNA hybrid nanoshapes from a low-stable state to a high-stable state. The 7-9 RNA carrying single-stranded overhang sequences of 7 nucleotides (nt) reacted with 5-13 DNA with a 5-nt overhang and a core of 13 base pairs (bp) to form a mixture of nanoshapes at a relatively low-stable state (Fig. 4.1C, lane 4). At the end of each RNA corner in the circularly closed nanoshapes, there were 2 unpaired nucleotides that can start a toe-hold reaction. Invading 7-9 DNA with a 7-nt single stranded region can replace the 5-13 DNA and fully base pair with the 7-9 RNA's overhang to form nanoshapes at a more stable state (Fig. 4.1C, lane

8). The substitution was confirmed by native PAGE analysis as the nanoshapes at the high-stable state exhibited higher electrophoretic mobility than that of the nanoshapes at the low-stable state which had 8 additional unpaired nucleotides.

The substitution's kinetics was further analysed on PAGE (Fig. 4.2). Although the strand replacement from the 5-13 DNA to the 7-9 DNA relied on differences in thermal stabilities introduced by only 2 unpaired nucleotides, the replacement was completed gradually but swiftly after incubating the mixture at 37 degrees for 20 minutes. This was consistent with previous re-equilibration test showing a purified RNA-DNA hybrid nanotriangle assembled from 6-11 RNA and DNA modules re-equilibrated to a mixture of nanoshapes in 20 minutes at 37 degrees. The co-existence of nanoshapes at both low- and high-stable states was observed at early time points, further confirming the substitution of the DNA module.

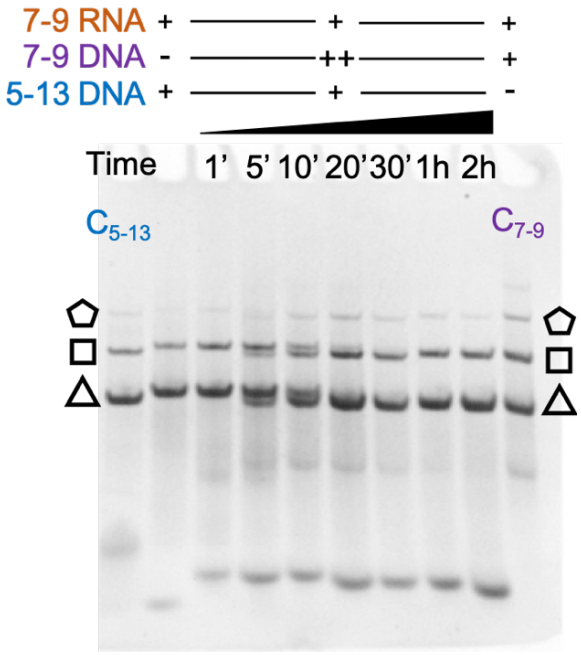

Figure 4.2. Kinetics of the substitution of DNA modules from 5-13 DNA to 7-9 DNA duplexes. The substitution was completed gradually in 20 minutes after incubating at 37 degrees. At 5' and 10' time points, two variations of nanoshapes (7-9 RNA + 5-13 DNA and 7-9 RNA + 7-9 DNA) were co-existed, confirming the strand-replacement from 5-13 DNA to 7-9 DNA duplexes. $C_{5\text{-}13}$ and $C_{7\text{-}9}$ are controlled nanoshapes with no unpaired nucleotides in the hybridization region. "++" indicated the components were added secondly.

Based on the same strategy, the replacement of the DNA modules in RNA-DNA hybrid nanoshapes was tested with a single unpaired nucleotide in the hybridization region. As shown in supplementary Fig.1A, 6-11 DNA duplexes successfully replaced 5-13 DNA modules in the nanoshapes made from 6-11 RNA and 5-13 DNA modules which had only one unpaired nucleotide at the end of each RNA corner. Therefore, with two or more unpaired nucleotides in the toe-hold region, swift strand-replacements of components in nucleic acid nano-assemblies can be done consecutively with a single base pair difference in each step. For example, nanoshapes that had 7-9 RNA corners as architectural joints were transformed from a low-stable state with 5-13 DNA modules to a medium-stable state with 6-11 DNA modules and then to a high-stable state containing 7-9 DNA modules (Fig. 4.3). Increasing electrophoretic mobilities of nanoshapes in different steps confirmed the sequential substitution of DNA duplexes.

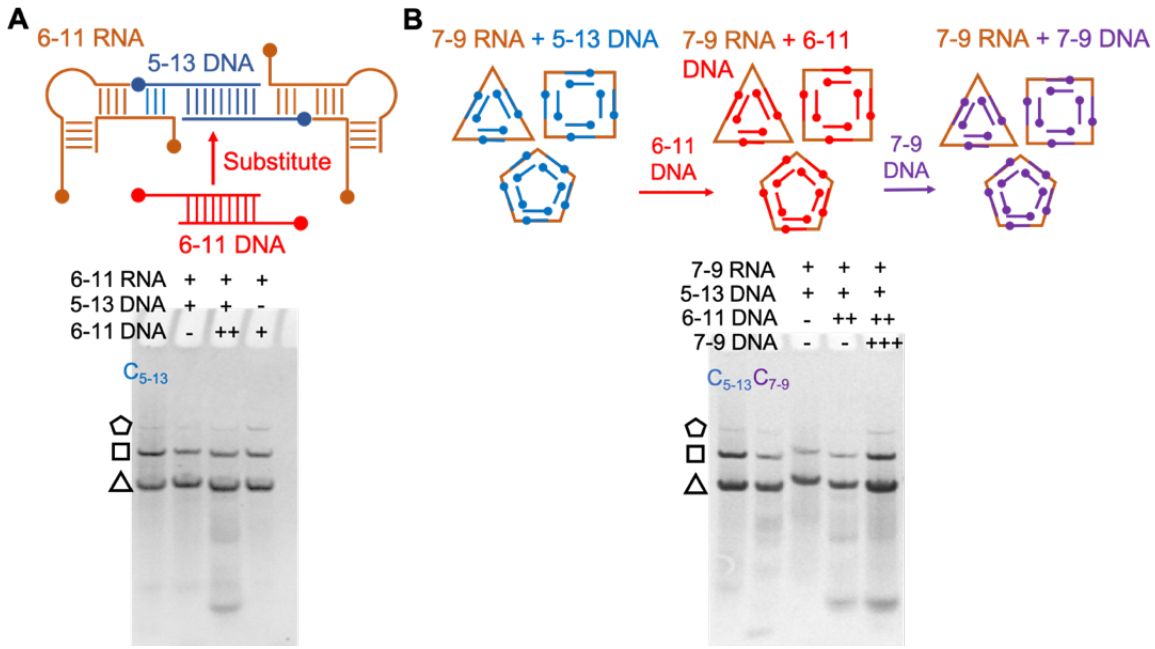

Figure 4.3. Consecutive replacements of DNA modules in RNA-DNA hybrid nanoshapes. (A) Replacement of DNA modules based on a single unpaired nucleotide. 6-11 RNA and 5-13 DNA assembled into hybrid nano-assemblies containing a single unpaired nucleotide at the end of each RNA corner. Invading 6-11 DNA replaced 5-13 DNA dimers to form nano-assemblies with fully base paired hybridization regions. $C_{5\text{-}13}$ was the controlled assembly formed by 5-13 RNA and DNA modules. (B) Sequential replacements of DNA modules from 5-13 DNA to 6-11 DNA and then to 7-9 DNA duplexes. Two unpaired nucleotides in the nanoparticles assembled from 7-9 RNA and 5-13 DNA allowed 6-11 DNA modules to replace 5-13 DNA duplexes in RNA-DNA hybrid nanoshapes and left one nucleotide unpaired in the hybridization regions. The single unpaired nucleotide facilitated the switch from 6-11 DNA to 7-9 DNA dimers. $C_{5\text{-}13}$ and $C_{7\text{-}9}$ are controls assembled from 5-13 modules and 7-9 modules. "++" indicated the components were added in the second place, and "+++" indicated the components were added thirdly.

4.3.2 Reshape RNA-DNA Hybrid Nanoshapes by Strand-Replacements

Modular RNA-DNA hybrid nanoshapes allow for modifications of DNA modules that enable controlled assembly of homogenous polygon populations without touching RNA modules. By introducing a long DNA guide strand with different number of hybridization sites linked by a short single-stranded region, homogeneous nanoshapes were assembled in a selective manner, which were confirmed by both PAGE and AFM analysis (Fig. 4.4A and 4.4B). Therefore, introducing and switching DNA guide strands that direct the formation of homogeneous nanoshapes can result in transformation of conformations of RNA-DNA hybrid nanoshapes. As

shown in Fig. 4.4C, switching regular 5-13 DNA duplexes to the 6-11 guide strand for nanotriangles transformed heterogeneous nano-assemblies to a homogeneous nanotriangle. Further substitution of the 6-11 guide strand with regular 7-9 DNA duplexes transformed the homogeneous nanoparticle back to a mixture of nanoshapes. Applying the same concept, RNA-DNA hybrid nano-assemblies can be sequentially transformed from heterogeneous nanoshapes to homogeneous nanoshapes and then from one type of homogeneous nanoshape to another type of homogeneous nanoshape (Fig. 4.5).

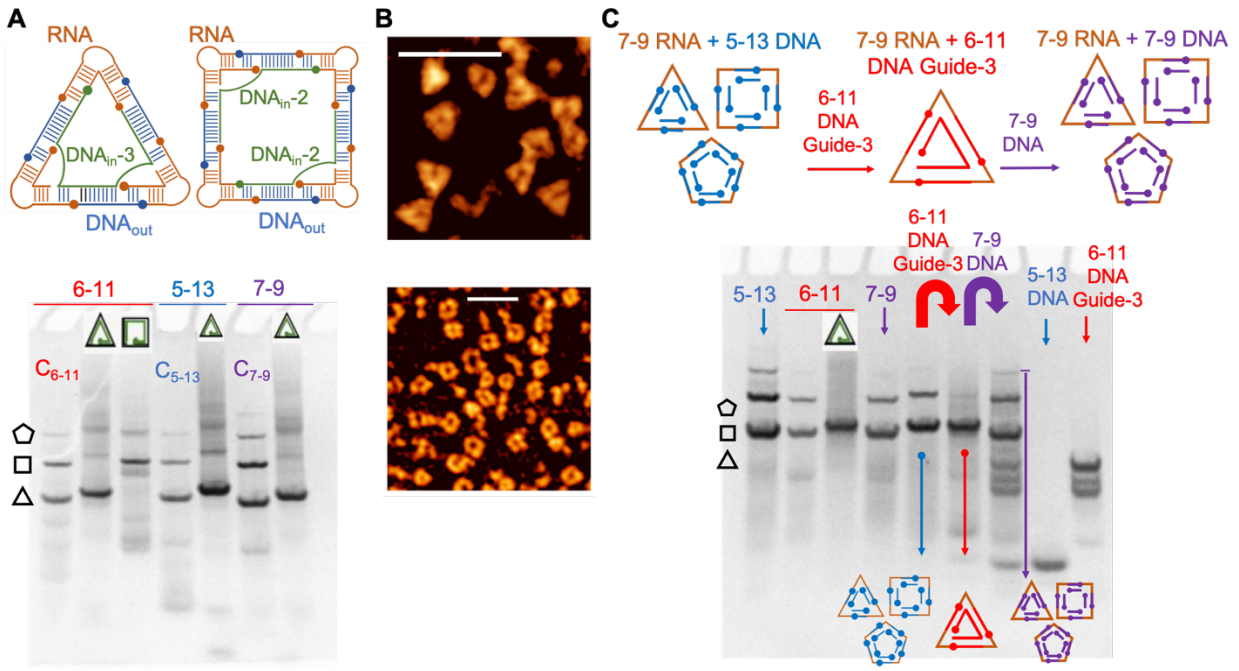

Figure 4.4. Controlled assembly of homogeneous nanoshapes and transformation of nanoshapes through strand-replacement reactions. (A) Controlled assembly of homogeneous nanoshapes under the direction of DNA guide strands. A long DNA guide strand with 3 hybridization sites spaced a short single-stranded linker directed the formation of homogenous nanotriangles, while two DNA guide strands with 2 hybridization sites on each directed forming single square species. (B) AFM images of homogenous nanoparticles assembled from 6-11 RNA and DNA modules. Scale bar is 50nm. (C) Transformation of nucleic acid hybrid nanoshapes by introducing and replacing DNA guide strands. By switching regular 5-13 DNA duplexes to the 6-11 DNA guide that directed the formation of homogeneous nanotriangles, a mixture of nanoshapes were transformed into homogeneous nanotriangles. Following this, regular 7-9 DNA duplexes replaced the 6-11 DNA guide grand to transform nanoparticles back to heterogeneous nanoshapes containing 7-9 RNA and DNA modules.

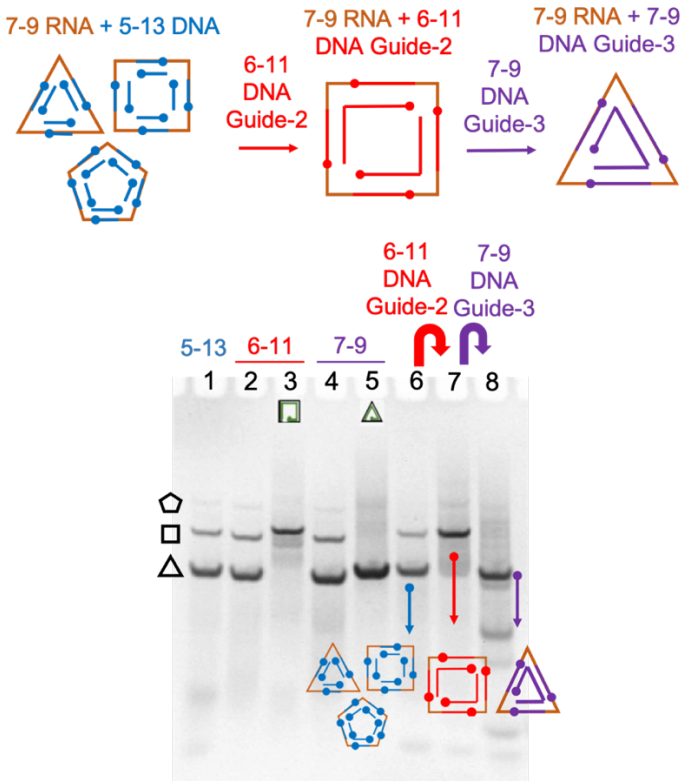

Figure 4.5. Transformation of RNA-DNA hybrid nanoparticles from heterogeneous nanoshapes to homogeneous nanosquares and then to homogeneous nanotriangles.

4.3.3 Replace RNA and DNA Modules Based on a Single Mismatched Base Pair

Strand replacements through a toe-hold reaction outlined above provided an efficient method to substitute DNA modules in RNA-DNA hybrid nanoshapes with the same RNA architectural joints. To switch RNA modules, we further developed a strand-replacement method based on a single mismatched base pair (mbp). As a proof-of-concept, we designed a new type of RNA corner motif (RNA-2) derived from internal loop motifs in noncoding regions of the Seneca Valley virus (SVV) with a 6-nt single stranded region used to connect DNA modules(32) (Fig. 4.6A). A screening experiment carried on PAGE identified a DNA module with a core of 11 base pairs (DNA-2-11) as the best connector between RNA-2 motifs to give rise to three discrete bands whose electrophoretic mobility was identical to 6-11 nanoshapes (Figure 4.6C), indicating the

formation of a new type of hybrid nanotriangles, nanosquares and nanopentagons containing RNA-2 corner motifs.

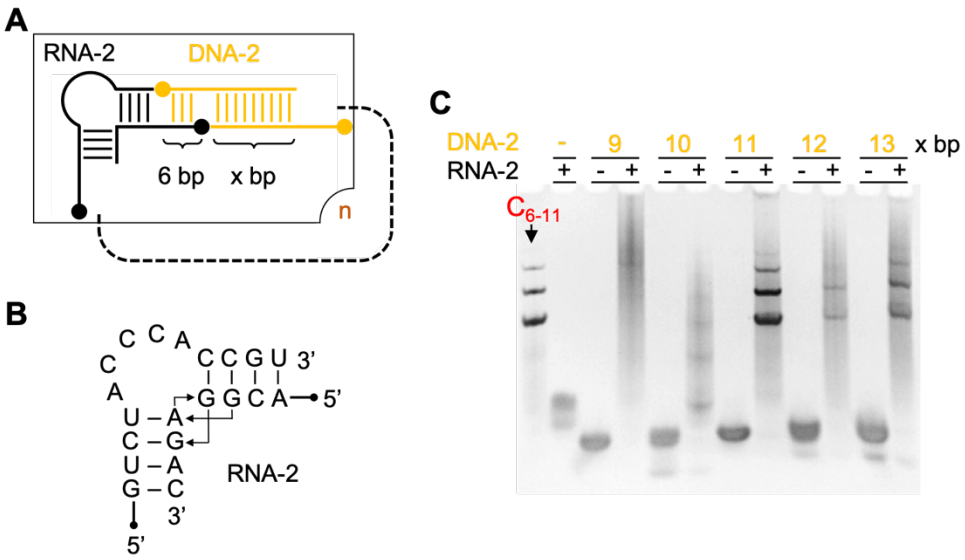

Figure 4.6. Design and screening of RNA-DNA hybrid nanoshapes containing RNA-2 modules. (A) Design of RNA-DNA hybrid nanoshapes that were associated from discrete RNA and DNA modules connected by 6 hybrid base pairs. (B) The RNA-2 corner module for nanoshape assembly derived from structured noncoding regions in the genome of Seneca Valley virus (SVV). It adopted a unique right angle bent overall structure that was previously resolved by crystallization(32). (C) Screening combinations of RNA-2 corner and DNA connectors by native polyacrylamide gel electrophoresis (PAGE) for stable hybrid nanoshapes. Among a series of DNA modules carrying 9–13 bp in the double stranded region (x), the 11 bp DNA (DNA-2-11) associating with RNA-2 produced three discrete bands. C_{6-11} is the controlled sample assembled from 6-11 RNA and DNA modules.

Nanoshapes assembled from RNA-2 and 6-11 DNA modules had a single G and U mbp in hybrid areas that have only 5 hybrid Watson-Crick base pairs (Fig. 4.7). The single GU mbp lowered the stability of the overall RNA-DNA hybrid nanoshapes (Fig. 4.7, lane 2), showing fewer stable bands in the native gel. This allowed for the invasion from 6-11 RNA corners to substitute the RNA-2 modules and form a more stable circularly closed nano-assemblies with RNA and DNA modules connected by 6 hybrid Watson-Crick base pairs (Fig. 4.7, lane 3). The differences in the nanoparticles' mobilities in the native gel indicated the transition from low stable nanoshapes

(RNA-2 and 6-11 DNA) to high stable ones (6-11 RNA and 6-11 DNA). The increasing Cy3 fluorophore's signal from low stable to high stable nanoshapes also confirmed the replacement of the RNA-2 module by the Cy3 labeled 6-11 RNA module.

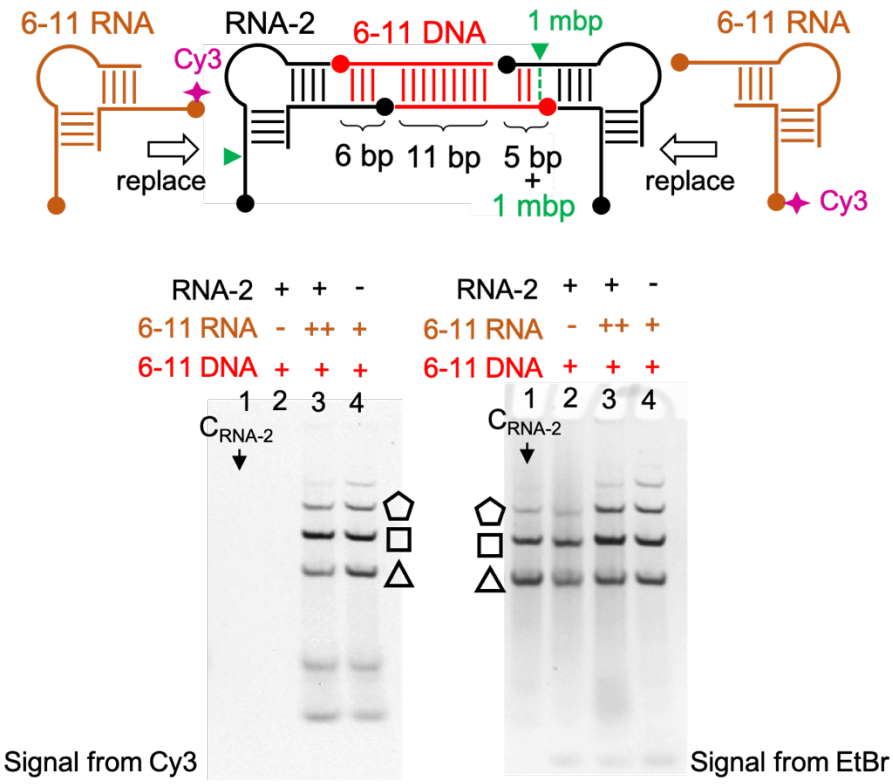

Figure 4.7. Substitution of RNA corner motifs based on a single mismatched base pair (mbp) in the hybridization region. Nanoparticles assembled from RNA-2 corners and 6-11 DNA duplexes formed less stable nanoshapes (lane 2) with hybridization regions containing 5 hybrid base pairs and 1 mbp. The 6-11 RNA replaced the RNA-2 to form more stabled nanoshapes (lane 3) with 6-11 DNA whose mobility was lower than that of nanoshapes containing RNA-2. The Cy3 signal difference between nanoshapes in lane 2 and 3 also confirmed the switch from the RNA-2 corner modules to the 6-11 RNA which was attached with a Cy3 fluorophore. C_{RNA-2} is the control assembled from RNA-2 and DNA-2-11 modules. "++" indicated the components were added secondly.

Moreover, with a single mismatched base pair in the marginally stable hybrid region, every nucleic acid component in RNA-DNA hybrid nanoshapes was switchable. For example, a single mbp in hybrid regions of nanoparticles assembled from 6-11 RNA and DNA-2-11 made both RNA and DNA modules available for substitution: 6-11 RNA and DNA-2-11 components were replaced

by RNA-2 and 6-11 DNA modules respectively to form stable nanoshapes with no mbp. As shown in Fig. 5A, RNA-2 corners replaced the 6-11 RNA to form more stable nanoshapes with DNA-2-11 duplexes, giving rise to three discrete bands with slightly higher mobility in the native gel (Fig. 4.8A, lane 3) than that of the nanoshapes containing the 6-11 RNA (Fig. 4.8A, lane 2). The Cy3 signal in the newly formed nanoshapes decreased dramatically as Cy3-modified 6-11 RNA corners were replaced by RNA-2 modules. It is worth noting there was faint Cy3 signal remaining in these nanoshapes, indicating the possibility of co-existence of 6-11 RNA and RNA-2 corner motifs in nano-assemblies and relatively slow kinetics of the replacing process from the 6-11 RNA to the RNA-2. Taking advantage of the mbp in the same design, DNA-2-11 modules was also substituted by 6-11 DNA duplexes which assembled to more stable nanoshapes with 6-11 RNA corners. Difference in the electrophoretic mobility between two different configurations and fluorescent signals coming from TAMRA fluorophores attached to the 6-11 DNA modules confirmed the strand placements (Fig. 4.8B).

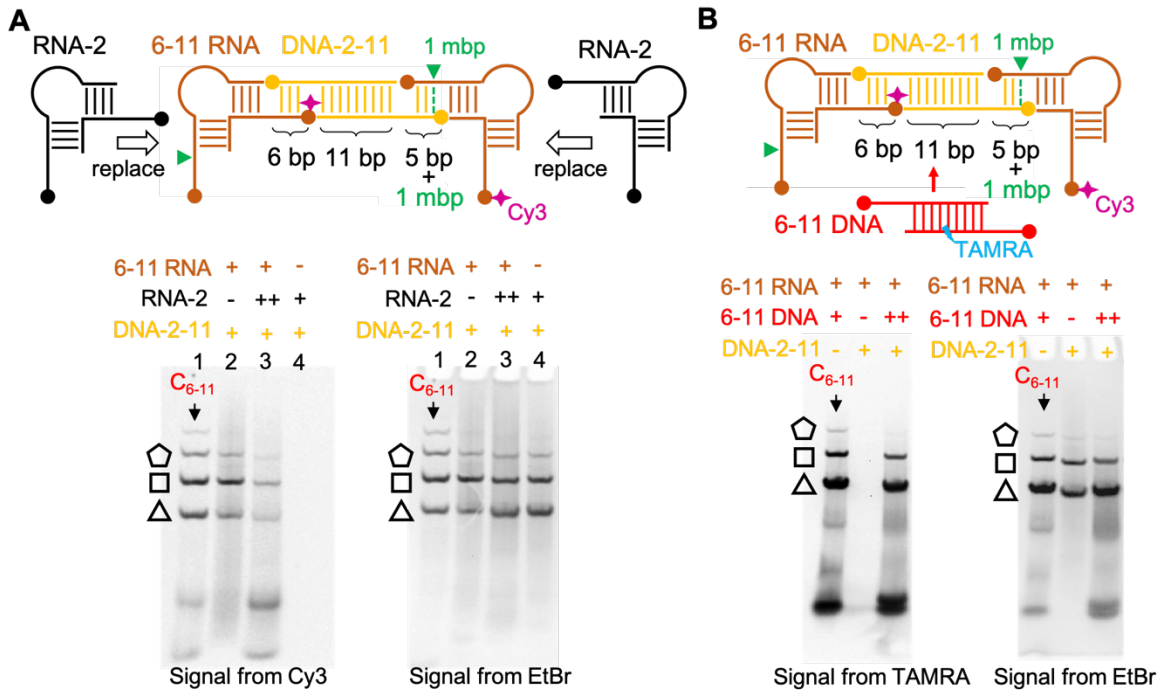

Figure 4.8. Swift replacements of RNA and DNA modules in hybrid nanoshapes based on a single mismatched base pair. (A) Substitution of RNA corners. The RNA-2 corners replaced the 6-11 RNA to form nanoshapes with fully based paired hybridization regions. The difference in Cy3 signal and electrophoretic mobility in native gels between nanoshapes containing the 6-11 RNA (lane 2) and the RNA-2 (lane 3) confirmed the switch between RNA corners. (B) Substitution of DNA modules from DNA-2-11 to 6-11 DNA. TAMRA-modified 6-11 DNA replaced DNA-2-11 duplexes to form nanoshapes showing strong fluorescent signals. $C_{6\text{-}11}$ is the controlled sample assembled from 6-11 RNA and DNA modules. "++" indicated the components were added secondly.

4.4 Conclusion

Here, we exploited the superb modularity of RNA-DNA hybrid nano-complexes assembled from discrete RNA and DNA modules and outlined a simple but efficient strand-replacement strategy to replace every nucleic acid component and transform the nucleic acid nanoparticles. The substitution that can be completed based on a single unpaired nucleotide in the hybridization region of nucleic acid nano-assemblies allowed for sequential substitutions of DNA modules and thereby transformation of RNA-DNA hybrid nanoshapes for multiple times. A single mismatched base pair in the hybridization region had both RNA and DNA modules available for replacements. The highly modular nucleic acid nano-assemblies with fully switchable components

provide versatile nano-platforms with transformable structural and chemical properties. Preparation of nucleic acid nano-assemblies with superb modularity and strand-replacement strategy outlined here open a door for the design and preparation of static and dynamic devices with wide applications, such as nanomachines and drug delivery and release.

4.5 Experimental

4.5.1 Materials

DNA and RNA oligonucleotides were purchased from Integrated DNA Technologies. Lyophilized oligonucleotides were rehydrated by dissolving in 10 mM sodium cacodylate buffer, pH 6.5. Sequences of oligonucleotides are provided in the Table 4.1 and 4.2.

Table 4.1. RNA oligonucleotides sequences.

Name	**Sequence**
5-13 RNA-In	5’ - rCrGrA rGrGrU rCrArG rCrCrU rG - 3’
5-13 RNA-Out	5’ - rGrArG rArCrC rArGrG rArArC rUrArC rUrGrA - 3’
6-11 RNA-In	5’ - rCrCrG rArGrG rUrCrA rGrCrC rUrG - 3’
6-11 RNA-Out	5’ - rCrGrA rGrArC rCrArG rGrArA rCrUrA rCrUrG rA - 3’
7-9 RNA-In	5’ - rUrCrC rGrArG rGrUrC rArGrC rCrUrG - 3’
7-9 RNA-Out	5’ - rArCrG rArGrA rCrCrA rGrGrA rArCrU rArCrU rGrA - 3’
RNA-2-In	5’ - rCrCrG rArGrG rArCrG rGrArG rArC - 3’
RNA-2-Out	5’ - rCrGrA rGrArU rGrUrC rUrArC rCrCrA rCrCrG rU - 3’
6-11 RNA-In-Cy3	5’ - rCrCrG rArGrG rUrCrA rGrCrC rUrG /Cy3/ - 3’

Table 4.2. DNA oligonucleotides sequences.

Name	Sequence
5-13 DNA-a	5’ - GTC TCT AAT CGC TAC CAA - 3’
5-13 DNA-b	5’ - CCT CGT TGG TAG CGA TTA - 3’
6-11 DNA-a	5’ - GTC TCG ATG CAA GGA CA - 3’
6-11 DNA-b	5’ - CCT CGG TGT CCT TGC AT - 3’
7-9 DNA-a	5’ - GTC TCG TAT CGC TAC G - 3’
7-9 DNA-b	5’ - CCTCGGACGTAGCGAT - 3’
DNAin-3	5’ - GTC TCG TATCGCTACGT TTTCTCTCTCTCTTTT GTC TCG TATCGCTACGT TTTCTCTCTCTCTTTT GTC TCG TATCGCTACGT - 3’
DNAin-2	5’ - GTCTCG TATCGCTACGT TTTCTCTCTCTCTTTT GTCTCG TATCGCTACGT - 3’
6-11 DNA Guide-3	5’ - GTC TCG ATG CAA GGA CA TTTCTCTCTCTTTT GTC TCG ATG CAA GGA CA TTTCTCTCTCTTTT GTC TCG ATG CAA GGA CA - 3’
6-11 DNA Guide-2	5’ - GTCTCG ATGCAAGGACA TTTCTCTTTT GTCTCG ATGCAAGGACA - 3’
7-9 DNA Guide-3	5’ - GTC TCGT ATC GCT ACG TTTCTCTCTCTTTT GTC TCGT ATC GCT ACG TTTCTCTCTCTTTT GTC TCGT ATC GCT ACG - 3’
DNA-2-9-a	5’ - ATC TCG CAC GTA CGT - 3’
DNA-2-9-b	5’ - CCT CGG ACG TAC GTG - 3’
DNA-2-10-a	5’ - ATC TCG ACG TAT ACG T - 3’
DNA-2-10-b	5’ - CCT CGG ACG TAT ACG T - 3’
DNA-2-11-a	5’ - ATC TCG TAT CGC TAC GT - 3’
DNA-2-11-b	5’ - CCT CGG ACG TAG CGA TA - 3’
DNA-2-12-a	5’ - ATC TCG ACG TAC GTA CGT - 3’
DNA-2-12-b	5’ - CCT CGG ACG TAC GTA CGT - 3’
DNA-2-13-a	5’ - ATC TCG CAC GTA CGT ACG T - 3’
DNA-2-13-b	5’ - CCT CGG ACG TAC GTA CGT G - 3’
6-11 DNA-a-TAMRA	5’ - CCTCGGACG/i5-TAMK/AGCGATA - 3’

4.5.2 RNA-DNA hybrid nanostructure preparation and strand-replacement reaction

RNA-DNA hybrid structures were prepared by mixing constituent oligonucleotides at equimolar concentration (100 μM) in the presence of 2 mM magnesium chloride. Samples were annealed by heating at 65°C for 5 minutes followed by incubation at 37°C for 10 minutes before cooling on ice for 5 minutes.

Strand-replacement reaction was taken place at 37 degrees for 2 hours in the presence of 2mM magnesium chloride before cooling on ice for 5mins.

4.5.3 Gel electrophoresis

Polyacrylamide gel electrophoresis was performed on 5% acrylamide/bisacrylamide (19:1) native gel matrix at 220 V, 22 mA in 2X MOPS buffer (40 mM 3-morpholinopropane 1-sulfonic acid, 10 mM sodium acetate) and 2 mM magnesium chloride. For detection of nucleic acid complexes, gels were stained with ethidium bromide and imaged under UV light.

4.5.4 AFM imaging

AFM imaging of nucleic acid samples was performed on surface-modified mica carrier. Freshly cleaved mica was immersed in 50 mM aqueous solution of 1-(3-aminopropyl)-silatrane (APS) for 30 min, rinsed with deionized water and dryed in an argon stream. Imaging samples were diluted in buffer containing 10 mM HEPES, pH 7, and 2 mM magnesium chloride to 0.5-1.5 ng/μL concentration, and applied on APS-modified mica carrier for 2 min. Sample preparation was performed at 4°C. After deposition, mica strips were rinsed briefly with ice cold water and dried under a gentle argon flow. AFM images were recorded with a MultiMode AFM Nanoscope IV system (Bruker Instruments) in Tapping Mode with silicon probes RTESPA-300 (Bruker Nano Inc.; resonance frequency ~300 kHz, spring constant ~40 N/m) at a scanning rate of ~2.0 Hz. Image processing was performed with the FemtoScan software package (Advanced Technologies Center).

4.6 Acknowledgement

The material in Chapter 4, in part, is currently prepared for submission with Thomas Hermann as co-author. The dissertation author was the primary investigator and author of this material. Prof. Hermann was the corresponding author. The author thanks A. J. Lushnikov for help with AFM imaging.

Chapter 5: RNA-DNA Hybrid Nanoshapes that Self-Assemble Dependent on Ligand Binding

5.1 Abstract

Self-assembly of nucleic acid nanostructures is driven by selective association of oligonucleotide modules through base pairing between complementary sequences. Herein, we report the development of RNA-DNA hybrid nanoshapes that conditionally assemble under the control of an adenosine ligand. The design concept for the nanoshapes relies on ligand-dependent stabilization of DNA aptamers that serve as connectors between marginally stable RNA corner modules. Ligand-dependent RNA-DNA nanoshapes self-assemble in an all-or-nothing process by coupling adenosine binding to the formation of circularly closed structures which are stabilized through extensive continuous base stacking in the resulting polygons. By screening combinations of various DNA aptamer constructs with RNA corner modules for the formation of stable complexes, we identified adenosine-dependent nanosquares whose shape was confirmed by atomic force microscopy. As a proof-of-concept for sensor applications, adenosine-responsive FRET-active nanosquares were obtained by dye conjugation of the DNA aptamer components.

5.2 Introduction

Nucleic acid nanotechnology aims at designing and building functional architectures from oligonucleotides which fold and self-assemble through base pairing between complementary sequence segments(59,82,83). Nanostructures that assemble or respond dependent on the presence of a ligand have been obtained by incorporating aptamer motifs for adaptive recognition. Nucleic acid aptamers fold concurrently with ligand association and provide a conformational transduction mechanism that couples molecular recognition with structure change(84). Ligand-responsive molecular devices for cellular delivery and sensing applications have been obtained by adding aptamers to self-assembling DNA and RNA nanostructures(21,27,47,85–88). In these systems, ligand-dependent functionality is achieved by aptamers serving as a decoration rather than as

intrinsic building blocks of the nanostructures(37,89,90). Alternative approaches seek to incorporate aptamers as architectural motifs into origami folds or complex nano-assemblies(50,51,91–94). In few instances, synthetic aptaswitches or natural riboswitches have been used directly as discrete modules for self-assembling nanostructures(95,96). While the use of nucleic acid components for nanotechnology applications has been pursued for DNA or RNA largely separately(59,82), we have recently introduced hybrid nanoshapes that self-assemble from combinations of RNA motifs as architectural joints and DNA building blocks as functional modules(63). The modular architecture of the hybrid nanoshapes lends itself to the incorporation of aptamer building blocks that allow for ligand control over nanostructure assembly and function. Here, we describe the design and development of RNA-DNA hybrid nanoshapes that conditionally assemble under the control of adenosine and its derivatives.

5.3 Results and Discussion

5.3.1 Design and discovery of ligand-dependent nanoshapes

Hybrid RNA-DNA nanoshapes are circularly closed nucleic acid structures that form by association between single-stranded regions in bent RNA modules and straight DNA. For the design blueprint of ligand-dependent nanoshapes, we combined a previously discovered RNA corner motif(30) with variants of DNA connectors derived from an adenosine/AMP/ATP-binding aptamer whose solution structure in complex with AMP had been determined by NMR spectroscopy (Fig. 5.1)(97,98). Design parameters included the number of base pairs closing the adenosine-binding loop (Figure 1a, variables y and z) as well as the length of the single-stranded region for association between RNA and DNA modules (Fig. 5.1A, variable x).

To identify combinations of the RNA corner motif with DNA aptamer connectors that assemble into stable nanostructures, we intended to use a gel-based screening approach which we

previously developed for the discovery of self-assembling hybrid nanoshapes(63). A small library of DNA building blocks was conceived that contained the adenosine-binding loop flanked by short base-paired regions of 2-4 nucleotides (Figure 5.2). The rationale for these design parameters was that such intrinsically labile aptamer duplexes were to depend on concurrent ligand binding and hybridization with RNA corner modules for robust strand association which, in turn, furnished circularly closed nanoshapes. For connection of the RNA and DNA modules by hybridization, complementary single-stranded sequences of 6 nucleotides were added. In previous studies that established the hybrid RNA–DNA nanoshapes, we found that among a range of 5–8 nucleotide overhangs tested, 6 residues provide an optimal compromise between stability and sensitivity towards geometry changes in the nanoshapes(63).

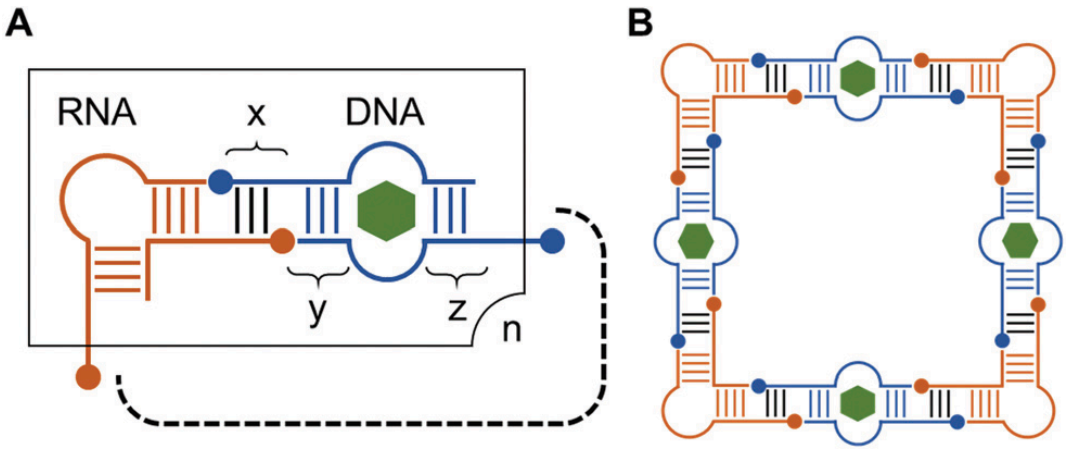

Figure 5.1. Design of ligand-dependent RNA-DNA hybrid nanoshapes. (A) A bent RNA motif as architectural joint and a ligand-bound DNA aptamer module connect to form closed RNA-DNA hybrid nanoshapes. A screening library of RNA and DNA components is obtained by choice of the DNA aptamer and length variation of the flanking double-stranded regions (y, z) as well as the single-stranded overhang (x) for hybridization between the building blocks. Ligand is shown as hexagon. (B) Example of an RNA-DNA hybrid nanosquare.

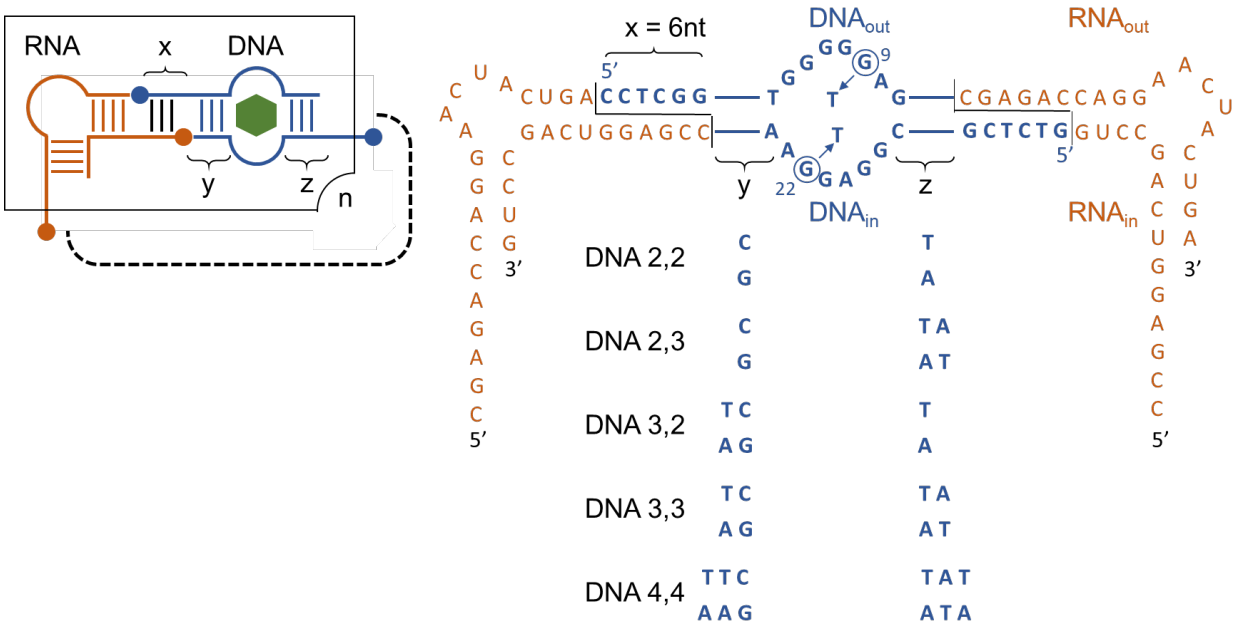

Figure 5.2. Design of ligand-dependent RNA-DNA hybrid nanoshapes. RNA corner modules (orange) are derived from the subdomain IIa internal loop of the hepatitis C virus (HCV) internal ribosome entry site (IRES), which was previously used to construct a self-assembling all-RNA nanosquare. A series of DNA module inserts (blue) was designed that carried an internal loop sequence of an AMP aptamer flanked by double-stranded regions (y, z) of 2-4 base pairs (bp). RNA corner modules and DNA inserts each contain complementary 5' single-stranded overhangs (x) of 6 nucleotides (nt) which allow for self-assembly through inter-strand base pairing. Single-stranded overhangs within modules have distinct sequences (indicated by green and blue color) to prevent formation of homomeric assemblies. Base changes introduced at positions G9 and G22 in some of the constructs are indicated (see also Figure 5.3B). See Table 5.1 for a complete list of all oligonucleotides used in this research.

Combinations of the RNA corner motif and variants of the DNA aptamer module were screened by native polyacrylamide gel electrophoresis (PAGE) to detect formation of stable nanostructures in the presence of AMP and 2 mM magnesium salt (Fig. 5.3A). DNA connectors which had the ligand-binding loop bracketed between 3 base pairs on the left (y = 3) and 2 or 3 base pairs on the right side (z = 2-3), (DNA 3,3 and DNA 3,2), gave rise to a single species of RNA-DNA hybrid complex in the presence of 100 µM AMP ligand. In the absence of AMP, none of the tested RNA-DNA combinations produced stable assemblies. At a higher magnesium concentration of 5 mM, a slightly increased occurrence of DNA 3,3 and DNA 3,2 assemblies was

observed in the absence of AMP, perhaps attributable to stabilization of the RNA corner modules by the divalent ions (Fig. 5.4); however, the clear distinction of fully stable complexes requiring the ligand remained. Stable nanostructures were also obtained for the combinations of RNA corner and DNA 3,3 or 3,2 aptamer modules in the presence of adenine instead of AMP (Fig. 5.5), as was expected due to the base-selectivity of the DNA aptamer for adenine and its glycoside derivatives(97). The uncharged nature of the adenine ligand led to complexes migrating slower on native polyacrylamide gel compared to AMP-bound nanostructures (Fig. 5.5).

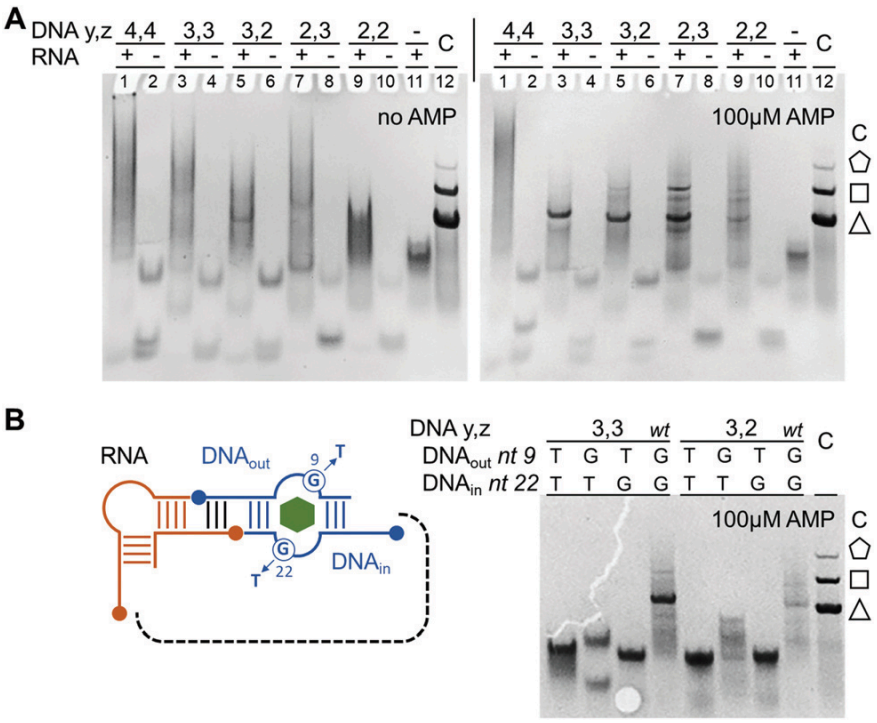

Figure 5.3. Discovery of ligand-dependent RNA-DNA hybrid nanoshapes. (A) Screening by native polyacrylamide gel electrophoresis (PAGE) for stable nanoshapes that assemble from an RNA corner motif and variants of an AMP-binding DNA aptamer module in the presence of 2 mM magnesium ions. Stable RNA-DNA hybrid nanoshapes give rise to discrete bands without leaving nucleic acid material retained in the gel pocket. DNA aptamer modules were tested that contain single-stranded overhangs (x) of 6 nucleotides and different lengths of the double stranded regions (y, z) flanking the AMP-binding loop (see Fig. 5.2 for sequences). PAGE analysis of the RNA-DNA module combinations was performed on two separate gels, respectively, in the absence and presence of 100 μM AMP ligand. For each aptamer variant, the DNA module was tested by itself and in combination with the RNA corner motif (lanes 1-10). Control lanes show the RNA corner by itself (lane 11) and, as similarly-shaped size markers, hybrid nanoshapes (C, lane 12) that contain the same RNA corner motif connected by a simple double-stranded DNA module of 11 base pairs flanked by 6-nucleotide single-stranded overhangs. Nanoshapes used for the control (C, lane 12) assemble as a mixture of polygons as previously confirmed by atomic force microscopy (AFM). (B) PAGE analysis of nanoshapes that contain mutated DNA aptamer modules carrying single or double base changes (G→T) at positions 9 and 22 of the AMP binding loop which ablate ligand recognition. Mutation at either position prevent formation of the nanoshapes in the presence of AMP. Numbering was adapted from a construct that had been used to determine the solution structure of the aptamer. For reference, a control lane is included showing a mixture of polygonal nanoshapes containing a simple DNA helix module as described in panel A.

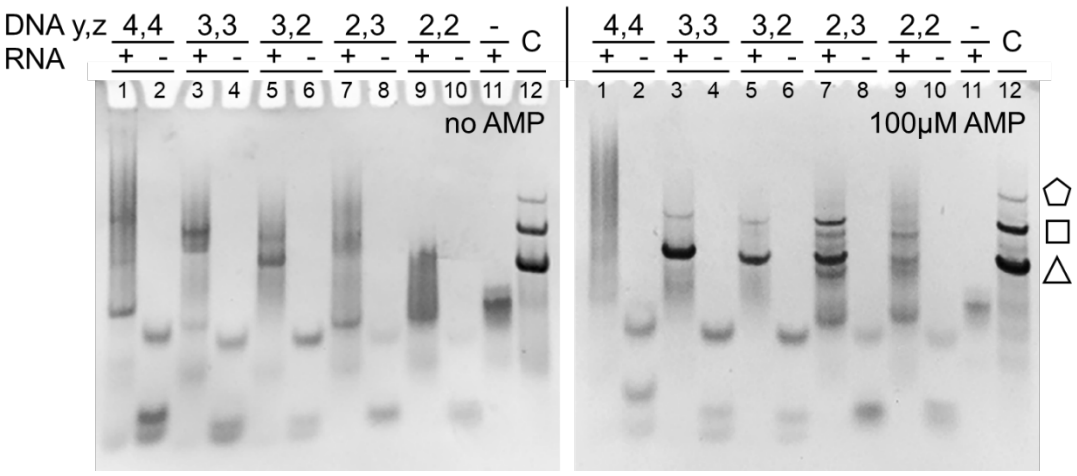

Figure 5.4. PAGE analysis of combinations of an RNA corner motif and variants of an AMP-binding DNA aptamer module in the presence of 5 mM magnesium ions. Gel execution and sample arrangement are identical to the gels shown in Figure 5.3A, except for the higher magnesium concentration. Stable RNA-DNA hybrid nanoshapes give rise to discrete bands without leaving nucleic acid material retained in the gel pocket. DNA aptamer modules were tested that contain single-stranded overhangs (x) of 6 nucleotides and different lengths of the double stranded regions (y, z) flanking the AMP-binding loop (see Figure 5.2 for sequences). PAGE analysis of the RNA-DNA module combinations was performed on two separate gels, respectively, in the absence and presence of 100 µM AMP ligand. For each aptamer variant, the DNA module was tested by itself and in combination with the RNA corner motif (lanes 1-10). Control lanes show the RNA corner by itself (lane 11) and hybrid nanoshapes (C, lane 12) that contain the same RNA corner motif connected by a simple double-stranded DNA module of 11 base pairs flanked by 6-nucleotide single-stranded overhangs. Nanoshapes used for the control (C, lane 12) assemble as a mixture of polygons as previously confirmed by AFM.

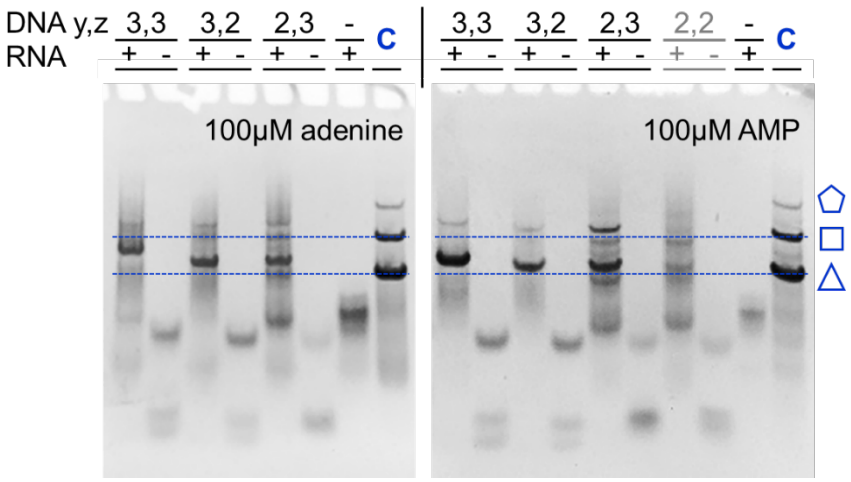

Figure 5.5. PAGE analysis of hybrid nanoshapes containing aptamer DNA variants in the presence of 100 μM adenine (left gel) compared to the same nanoshape preparations in the presence of 100 μM AMP (right gel). Sample preparation and PAGE analysis were performed on samples containing 5 mM magnesium ions for both gels. The analysis in the presence of AMP is shown for comparison (right gel) and is part of the gel image reproduced in Figure 5.3. Lanes marked by C show hybrid nanoshapes that contain the RNA corner motif connected by a simple double-stranded DNA module of 11 base pairs flanked by 6-nucleotide single-stranded overhangs.

5.3.2 Design and discovery of ligand-dependent nanoshapes

Surprisingly, monovalent cations inhibited the formation of the RNA-DNA aptamer nanostructures at 100 mM concentration, with potassium exerting a stronger inhibitory effect than sodium, and affecting the complex including the DNA 3,2 module more significantly than the assembly containing DNA 3,3 (Fig. 5.6). Inhibition of nanostructure formation by potassium and sodium may be related to their stabilizing effect on an alternative G-quartet structure perhaps involving the guanine-rich DNA aptamer outer strand (Fig. 5.2)(97,99). While the architecture of the AMP-bound aptamer does not contain a G-quartet(98), high concentrations of monovalent ions may sequester such an alternative configuration within one or both of the component DNA strands and thereby prevent their availability to participate in the aptamer-ligand complex.

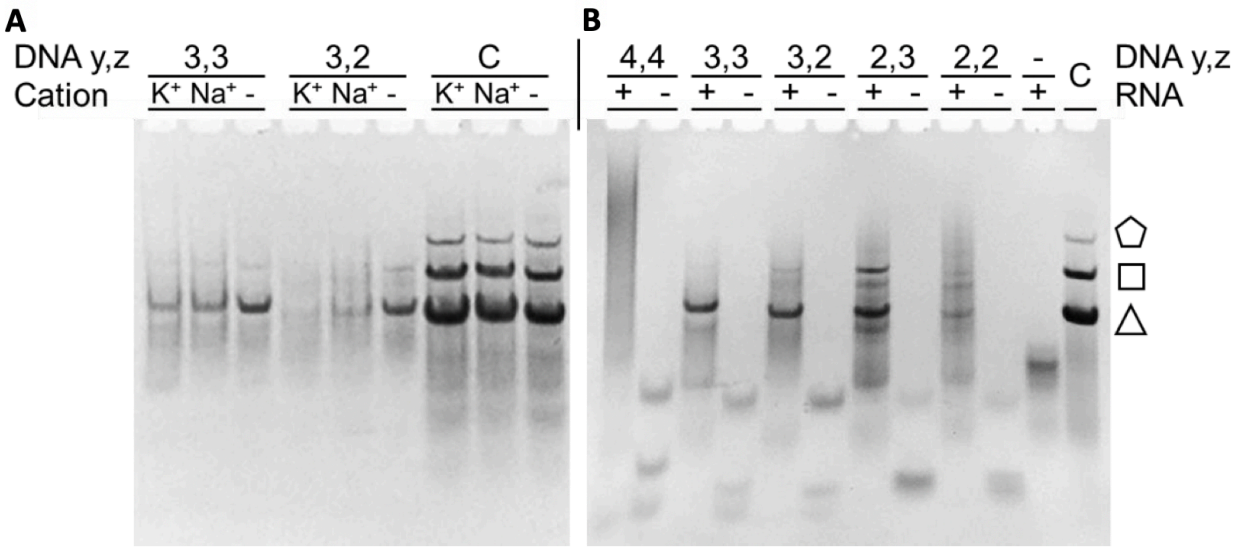

Figure 5.6. Impact of monovalent cations on the formation of hybrid nanoshapes containing aptamer DNA variants in the presence of 100 μM AMP and 2 mM magnesium ions. (A) PAGE analysis of samples containing combinations of the RNA corner motif and AMP-binding DNA aptamer variants in the presence of 100 mM potassium or sodium ions. Monovalent ions were present in the sample preparation but not added to the gel or electrophoresis buffer. Lanes without monovalent ions indicated contain magnesium only. Lanes marked by C show hybrid nanoshapes that contain the RNA corner motif connected by a simple double-stranded DNA module of 11 base pairs flanked by 6-nucleotide single-stranded overhangs. (B) For comparison, a gel image from Fig. 5.3A is reproduced which shows PAGE analysis of hybrid nanoshapes containing DNA aptamer variants in the presence of 100 μM AMP ligand and 2 mM magnesium ions.

The design premise for the DNA aptamer modules to gain duplex stability through concurrent association with both AMP ligand and RNA corners was tested by PAGE analysis of the constitutive oligonucleotides (Figure 5.7). DNA aptamer duplexes did not form in the presence of 100 μM AMP ligand, suggesting that the nanostructures identified by screening (Fig. 5.3A) self-assemble in an all-or-nothing process that requires the presence of all components, including RNA corners, DNA aptamer strands and ligand. To unequivocally prove that AMP binding at the aptamer loop is essential for nanoshape formation, DNA connector constructs derived from DNA 3,3 and DNA 3,2 were tested which carried single or double base changes at two key bases involved in ligand binding (Fig. 5.3B)(97). Mutation at any of these positions ablated nanoshape assembly, thus demonstrating the obligatory requirement for AMP binding at the aptamer loop.

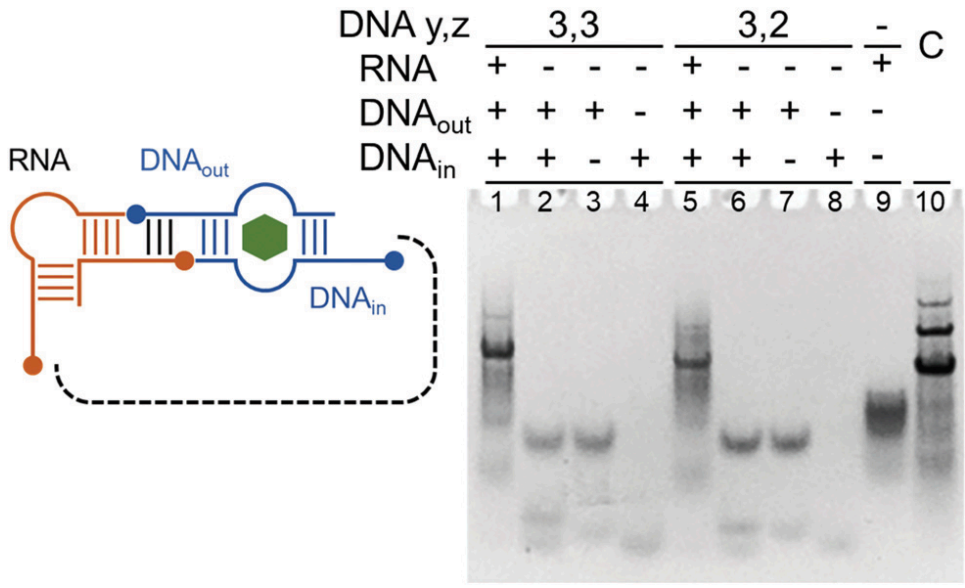

Figure 5.7. PAGE analysis of the nucleic acid components that were used to assemble RNA–DNA hybrid nanoshapes containing DNA aptamer modules in the presence of 100 μM AMP ligand. Aptamer DNA insert variants were tested as individual strands (lanes 3, 4, 7, 8) and as DNA duplex (lanes 2, 6) in comparison with the combination with the RNA corner motif (lanes 1, 5). Analysis of individual DNA strands in combination with the RNA corner motif is shown in Fig. 5.8. RNA corner by itself is applied in lane 9. Lane 10 (C) shows hybrid nanoshapes that contain the same RNA corner motif connected by a simple double stranded DNA module of 11 base pairs flanked by 6-nucleotide single stranded overhangs.

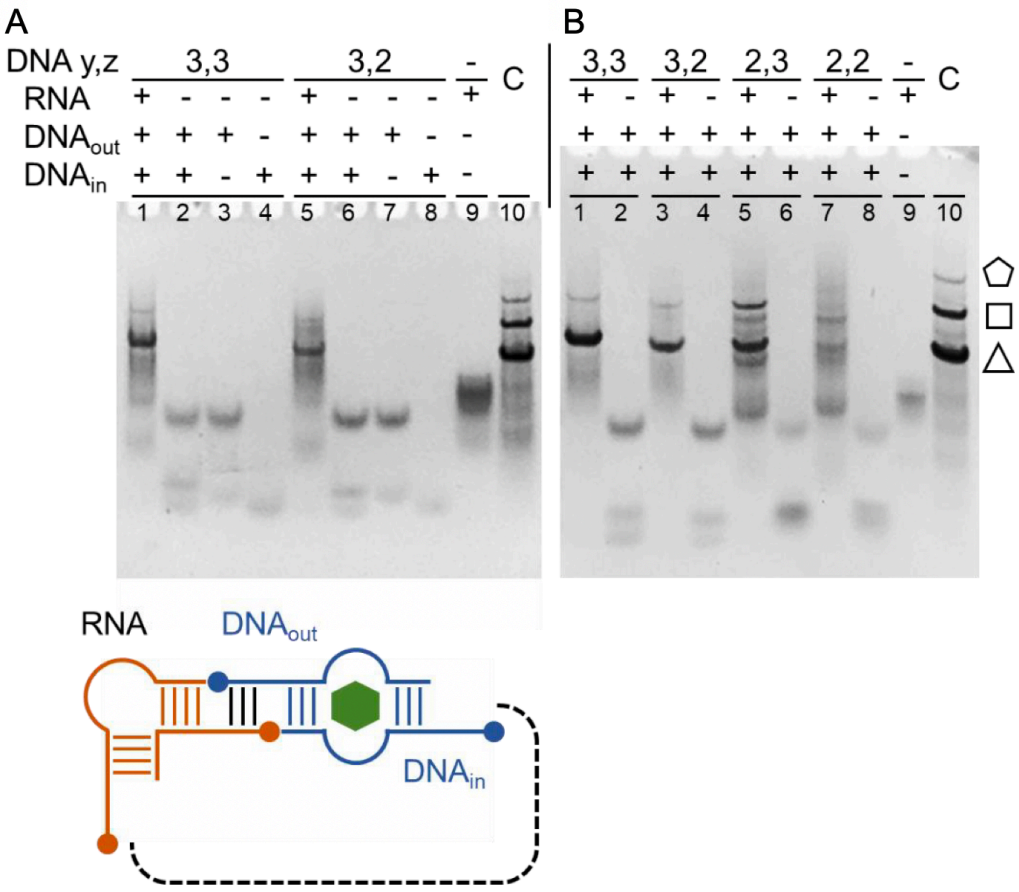

Figure 5.8. PAGE analysis of the nucleic acid components that were used to assemble RNA-DNA hybrid nanoshapes containing DNA aptamer modules in the presence of 100 μM AMP ligand. (A) Analysis of aptamer DNA insert variants as individual strands (lanes 3, 4, 7, 8) and as DNA duplex (lanes 2, 6) in comparison with the combination with the RNA corner motif (lanes 1, 5). RNA corner by itself is applied in lane 9. Lane 10 (C) shows hybrid nanoshapes that contain the same RNA corner motif connected by a simple double-stranded DNA module of 11 base pairs flanked by 6-nucleotide single-stranded overhangs. (B) For comparison, part of a gel image from Figure S2 is reproduced which shows PAGE analysis of hybrid nanoshapes containing aptamer DNA variants in the presence of 100 μM AMP ligand. Lanes 1 and 3 in panel b correspond to the same combinations of DNA and RNA modules in, respectively, lanes 1 and 5 in panel a. Lanes 2 and 4 in panel b correspond to the same combinations of DNA and RNA modules in, respectively, lanes 2 and 6 in panel a.

Electrophoretic mobility of the complex assemblies formed with the DNA 3,3 and DNA 3,2 aptamer inserts in the presence of AMP was similar to that of previously developed triangle nanoshapes which carried the same RNA corner motif connected by a simple double-stranded DNA module of 11 base pairs (Fig. 5.3A)(63). Since gel mobility at native conditions depends on

both the charge to mass ratio and hydrodynamic radius of the migrating species, PAGE analysis cannot conclusively reveal the composition of the DNA aptamer-containing nucleic acid complexes. To investigate the shape and constitution of the aptamer hybrid nanostructures, atomic force microscopy (AFM) imaging was performed (Fig. 5.9 and Figure 5.10). AFM analysis of the complexes formed between RNA corner and DNA 3,3 aptamer modules revealed square-shaped nanostructures as the dominant species (Fig. 5.10) which were comparable in size to previously described simple RNA-DNA hybrid nanosquares (Fig. 5.9B)(63) but migrated on gel more similar to simple hybrid nanotriangles (Fig. 5.3A). For the complexes of DNA 3,3 aptamer modules, nanotriangles and larger circularly closed structures were observed with fewer occurrences (Figure 5.11) corresponding to considerably weaker bands for these species on polyacrylamide gel (Fig. 5.3A).

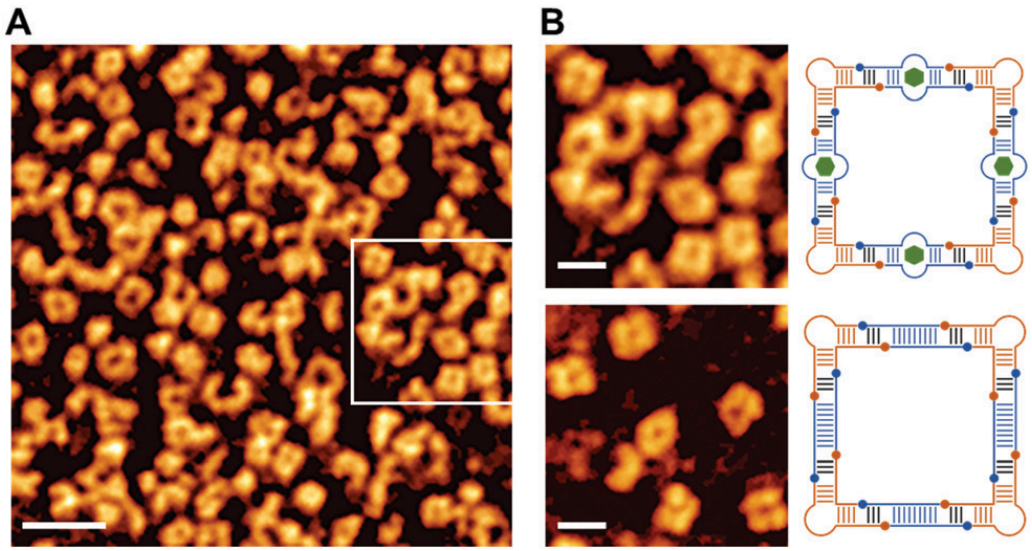

Figure 5.9. Atomic force microscopy (AFM) imaging of RNA-DNA hybrid nanoshapes. (A) AFM image of nanoshapes obtained from combination of the RNA corner motif and DNA 3,3 aptamer module in the presence of 100 μM AMP ligand and 2 mM magnesium salt. Scale bar represents 50 nm. See also Figure 5.10, 5.11). (B) Detail view (boxed area in panel a) of square nanoshapes from RNA corner motif and DNA 3,3 aptamer with AMP (top) in comparison to purified nanosquares (bottom) obtained from a nanoshape mixture that assembled from the same RNA corner and a simple double-stranded DNA module. Scale bar represents 20 nm.

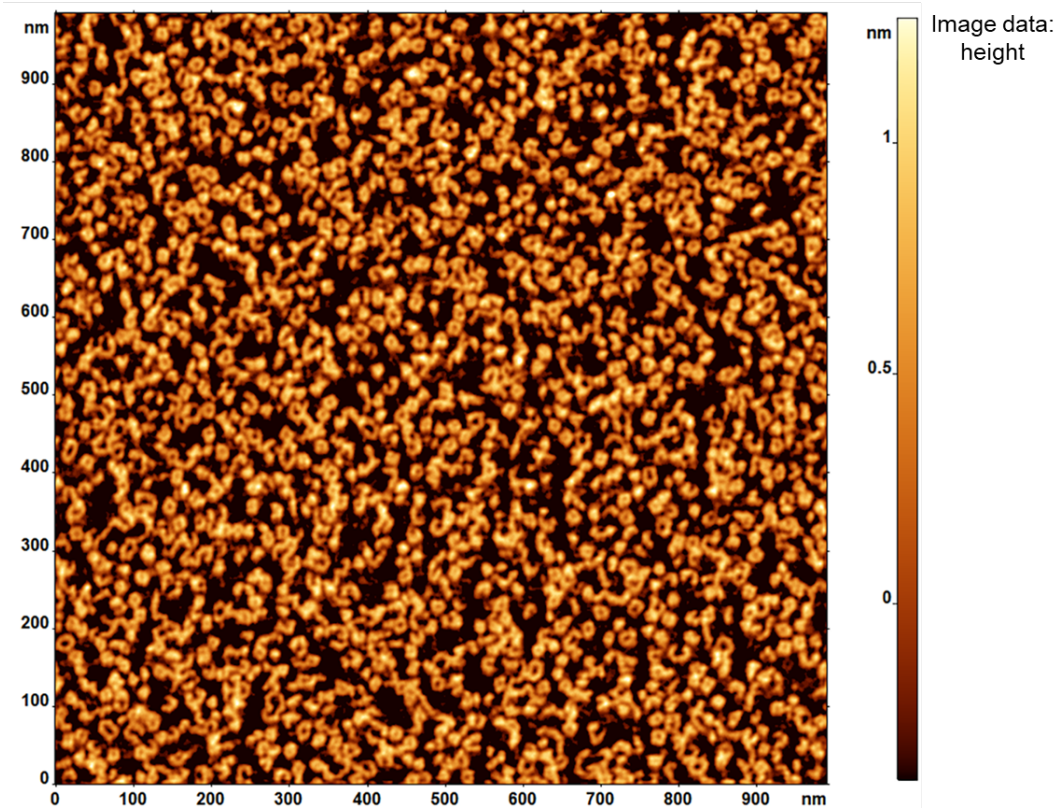

Figure 5.10. AFM imaging field of ligand-dependent RNA-DNA hybrid nanoshapes. Imaging was performed on nanoshapes obtained from combination of the RNA corner motif and DNA 3,3 aptamer module in the presence of 100 μM AMP ligand and 2 mM magnesium salt (Fig. 5.7, lane 3). See also Figure 5.7.

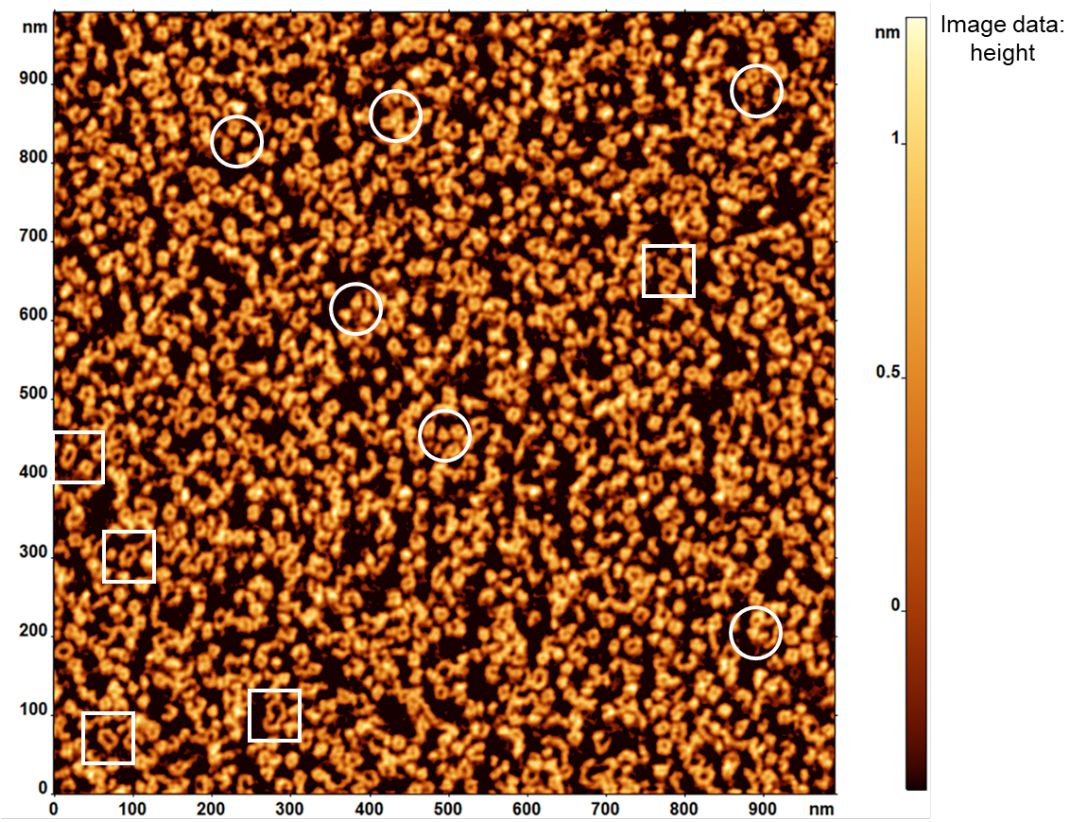

Figure 5.11. AFM imaging field of ligand-dependent RNA-DNA hybrid nanoshapes as shown also in Figure 5.10. Here, nanotriangles are highlighted with circles and larger polygons marked by squares.

5.3.3 Nanoshapes as sensors: FRET experiments

To demonstrate proof of concept for the application of ligand-dependent RNA-DNA hybrid nanoshapes as a platform for sensor development, we designed dye-labeled DNA aptamer constructs that create a fluorescent readout upon nanosquare self-assembly (Fig. 5.12). FRET pair dyes Cy3 and Cy5 were attached at the 3' terminus of the two DNA strands that constitute the aptamer module. Duplex formation during ligand-driven assembly would co-locate the dye pair in close proximity and generate a FRET signal upon excitation of the Cy3 donor dye. To discriminate stabilizing effects of divalent cations from duplex stabilization through ligand binding, we first performed titrations of the fluorescently labeled DNA aptamer strands with magnesium salt in the absence of AMP ligand (Fig. 5.12A). The pair of DNA strands did not give rise to FRET at

magnesium concentrations tested up to 10 mM, which suggests that duplex did not form. However, when RNA corner oligonucleotides were present in the mixture with the DNA strands, a dose-dependent increase of FRET was observed between 2-10 mM magnesium concentration, which suggests that metal-induced folding of RNA corner modules provide a framework to stabilize ligand-free DNA aptamer inserts within RNA-DNA hybrid structures. This hypothesis is consistent with the structure-supporting role identified for magnesium ions that were present at two high-affinity coordination sites in the crystal structure of the RNA corner motif(30). The range of FRET signal increase was nearly identical for the two variants of DNA aptamer inserts tested (DNA 3,2 and DNA 3,3, Fig. 5.12A), which further indicates that magnesium cations exert their stabilizing role on the RNA corner exclusively and without differentially affecting the DNA insert variants. At 2 mM magnesium concentration, the residual FRET signal from marginally stable ligand-free RNA-DNA assemblies was significantly higher for the DNA 3,3 insert than for the DNA 3,2 variant, likely due to the stabilizing contribution of an additional base pair in the DNA 3,3 construct. Titration of AMP ligand in the presence of 2 mM magnesium induced the formation of hybrid nanoshapes as attested by the dose-dependent rise in FRET intensity (Fig. 5.12B) and in agreement with PAGE analysis (Fig. 5.3A). The higher background fluorescence observed at 2mM magnesium for ligand-free assemblies containing the DNA 3,3 variant resulted in an overall reduced dynamic range of FRET signal over the course of the AMP titration compared to assemblies including DNA 3,2. In the absence of RNA corner oligonucleotides, AMP ligand alone was not sufficient to stabilize the DNA aptamer.

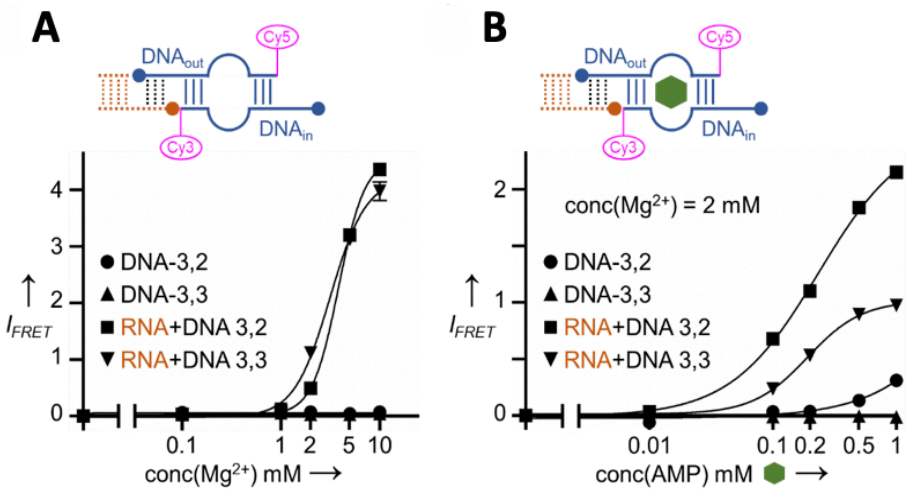

Figure 5.12. FRET response in titrations of fluorescently labeled nanoshape component mixtures with magnesium ions and AMP ligand. Mixtures contained DNA aptamer variant strands with the FRET dye pair Cy3/Cy5 attached at the 3' terminus of, respectively, DNA_{in} and DNA_{out} (DNA 3,2 ● and DNA 3,3 ▲), and the same DNA strands combined with the RNA corner motif (RNA+DNA 3,2 ■ and RNA+DNA 3,3 ▼). (A) Titration of nucleic acid components with $MgCl_2$. FRET intensities are plotted as normalized values obtained by subtraction of intensity at $[Mg^{2+}] = 0$ (first data point) divided by this same number (fractional difference). (B) Titration of nucleic acid components with AMP in the presence of 2 mM magnesium ions. Plotted FRET intensities are normalized as described in panel a. Each data point is an average of triplicates in both titrations, panel a and b. Error bars of ±1σ are obscured by the symbols for most data points.

To discriminate stabilizing effects of divalent cations from duplex stabilization through ligand binding, we first performed titrations of the fluorescently labeled DNA aptamer strands with magnesium salt in the absence of AMP ligand (Fig. 5.13). The pair of DNA strands did not give rise to FRET at magnesium concentrations tested up to 10 mM, which suggests that duplex did not form. However, when RNA corner oligonucleotides were present in the mixture with the DNA strands, a dose-dependent increase of FRET was observed between 2–10 mM magnesium concentration, which suggests that metal-induced folding of RNA corner modules provide a framework to stabilize ligand-free DNA aptamer inserts within RNA–DNA hybrid structures. This hypothesis is consistent with the structure-supporting role identified for magnesium ions that were present at two high-affinity coordination sites in the crystal structure of the RNA corner motif. The

range of FRET signal increase was nearly identical for the two variants of DNA aptamer inserts tested in RNA hybrid assemblies (DNA 3,2 and DNA 3,3, Fig. 5.12), which further indicates that magnesium cations exert their stabilizing role on the RNA corner exclusively and without differentially affecting the DNA insert variants. At 2 mM magnesium concentration, the FRET signal from stabilization of RNA–DNA hybrid assemblies in the absence of AMP ligand was minimal (Fig. 5.13). The small residual FRET signal from marginally stable ligand-free RNA–DNA assemblies was higher for the DNA 3,3 insert than for the DNA 3,2 variant (Fig. 5.12), likely due to the stabilizing contribution of an additional base pair in the DNA 3,3 construct. Titration of AMP ligand in the presence of 2 mM magnesium induced the formation of hybrid nanoshapes as attested by a significant dose-dependent rise in FRET intensity (Fig. 5.12 & Fig. 5.13) and in agreement with PAGE analysis (Fig. 5.3A). The higher background fluorescence observed at 2 mM magnesium for ligand-free assemblies containing the DNA 3,3 variant resulted in an overall reduced dynamic range of FRET signal over the course of the AMP titration compared to assemblies including DNA 3,2. In the absence of RNA corner oligonucleotides, AMP ligand alone was not sufficient to stabilize the DNA aptamer (Fig. 5.12 & Fig. 5.13). Inhibition of the formation of the RNA–DNA aptamer nanostructures by monovalent cations was demonstrated with the fluorescently labeled DNA aptamer inserts in combination with the RNA corner module (Fig. 5.14) consistent with PAGE analysis.

Future applications of the modular RNA–DNA aptamer nanoshapes may exploit the ability to use metal ion concentration for adjusting nanostructure stability coupled to ligand binding. For example, fluorescently labeled nanosquare constructs carrying the DNA 3,2 aptamer inserts were able to discriminate cognate ligands such as AMP and adenine from other nucleobase derivatives such as GMP (Fig. 5.15)

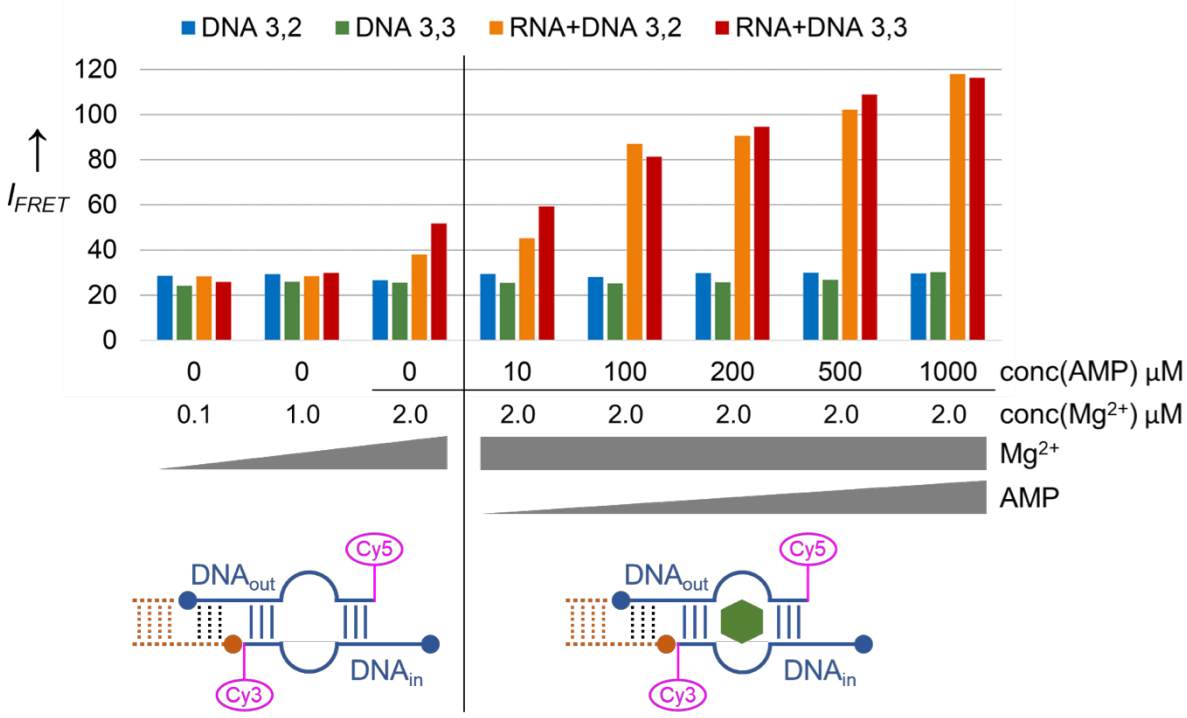

Figure 5.13. FRET response in titration of fluorescently labeled nanoshape component mixtures with MgCl2 and AMP ligand. Measurements are shown in groups of four mixtures which contained DNA aptamer variant strands with the FRET dye pair Cy3/Cy5 attached at the 3' terminus of, respectively, DNAin and DNAout (DNA 3,2, blue, and DNA 3,3, green), and the same DNA strands combined with the RNA corner motif (RNA+DNA 3,2, orange and RNA+DNA 3,3, red). FRET intensities are plotted as absolute measured values. The first three groups show FRET response to increased Mg^{2+} concentration up to 2 mM. The following 5 groups show FRET response to increased AMP concentration on a background of 2 mM Mg^{2+}.

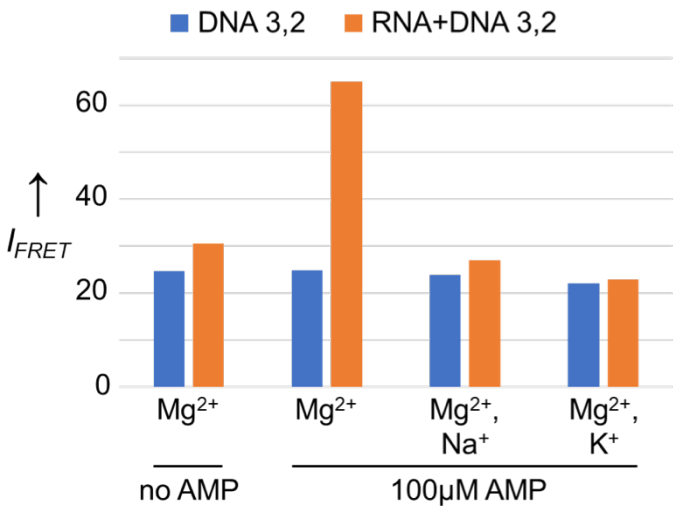

Figure 5.14. Impact of monovalent cations on the formation of hybrid nanoshapes containing fluorescently labeled aptamer DNA as monitored by FRET response. Measurements are shown for the DNA 3,2 aptamer variant strands with the FRET dye pair Cy3/Cy5 attached at the 3' terminus of, respectively, DNA_{in} and DNA_{out} (DNA 3,2, blue), and the same DNA strands combined with the RNA corner motif. All samples contained 2 mM $MgCl_2$. FRET intensities are plotted as absolute measured values. Samples with monovalent cations contained 100 mM sodium or potassium ions. An increased FRET signal that indicated formation of RNA-DNA aptamer nanostructures was observed only for the combination of all nucleic acid components (RNA corner and DNA aptamer insert) in the presence of both Mg^{2+} and AMP. Consistent with PAGE analysis (Fig. 5.6), monovalent cations at 100 mM concentration inhibited the formation of the nanostructures as indicated by low FRET signal.

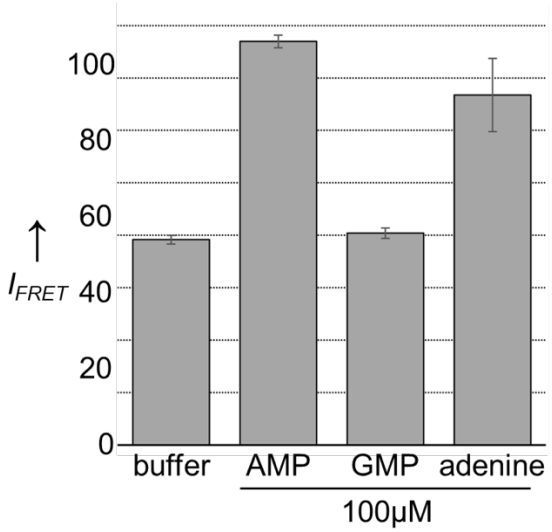

Figure 5.15. FRET response of hybrid nanoshapes containing the DNA 3,2 aptamer to different small molecules at 100 μM concentration in the presence of 2 mM magnesium ions. Error bars indicate ±1σ of triplicates tested for each condition.

5.4 Conclusions

We designed hybrid nanoshapes that self-assemble from RNA corner modules and DNA aptamer inserts dependent on the concurrent presence of both divalent metal cations and aptamer ligand. Robust assembly of nanoshapes requires ligand binding at the DNA aptamer inserts. RNA–DNA hybrid nanoshapes that include aptamer modules provide a novel general blueprint for the design of stimulus-responsive materials. The modular nature of the hybrid nanoshapes, along with their exceptional ability to tolerate a wide range of DNA insert topologies26 will open new avenues for the development of smart materials and sensors for diverse analytes.

5.5 Experimental

5.5.1 Materials

DNA and RNA oligonucleotides, including HPLC purified dyeconjugated oligonucleotides, were purchased from Integrated DNA Technologies. Lyophilized oligonucleotides were rehydrated by dissolving in 10 mM sodium cacodylate buffer, pH 6.5. Adenosine monophosphate disodium salt (CAS 4578-31-8) was purchased from Sigma-Aldrich and adenine hydrochloride (CAS 2922-28-3) from Spectrum Chemical. RNA–DNA hybrid nanostructure preparation RNA–DNA hybrid assemblies were prepared by mixing the constituent oligonucleotides at equimolar concentration (100 μM) with the desired amount of magnesium chloride (to 2 mM or 5 mM final concentration) and adenosine or adenine salt (to 100 μM). Samples were annealed by heating at 65 °C for 5 minutes followed by incubation at 37 °C for 10 minutes before cooling in an ice bath for 5 minutes. DNA and RNA oligonucleotides sequences are listed in the table 5.1.

Table 5.1. Oligonucleotide sequences

Name	MW g/mole	Sequence
RNA		
RNA_{out}	6107	5' – rCrGrA rGrArC rCrArG rGrArA rCrUrA rCrUrG rA – 3'
RNA_{in}	4461	5' – rCrCrG rArGrG rUrCrA rGrCrC rUrG – 3'
DNA		
DNA_{out} Control	5171	5' – CCT CGG ACG TAC GTA CG – 3'
DNA_{in} Control	5177	5' – GTC TCG CGT ACG TAC GT – 3'
DNA_{out} 2,2	4954	5' – CCT CGG CTG GGG GAG T – 3'
DNA_{in} 2,2	4971	5' – GTC TCG ACG GAG GAA G – 3'
DNA_{out} 2,3	5267	5' – CCT CGG CTG GGG GAG TA – 3'
DNA_{in} 2,3	5275	5' – GTC TCG TAC GGA GGA AG – 3'
DNA_{out} 3,2	5258	5' – CCT CGG TCT GGG GGA GT – 3'
DNA_{in} 3,2	5284	5' – GTC TCG ACG GAG GAA GA – 3'
DNA_{out} (G_9→T) 3,2	5233	5' – CCT CGG TCT GGG GTA GT – 3'
DNA_{in} (G_{22}→T) 3,2	5259	5' – GTC TCG ACG GAG TAA GA – 3'
DNA_{out} 3,3	5572	5' – CCT CGG TCT GGG GGA GTA – 3'
DNA_{in} 3,3	5589	5' – GTC TCG TAC GGA GGA AGA – 3'
DNA_{out} (G_9→T) 3,3	5547	5' – CCT CGG TCT GGG GTA GTA – 3'
DNA_{in} (G_{22}→T) 3,3	5564	5' – GTC TCG TAC GGA GTA AGA – 3'
DNA_{out} 4,4	6180	5' – CCT CGG TTC TGG GGG AGT AT – 3'
DNA_{in} 4,4	6215	5' – GTC TCG ATA CGG AGG AAG AA – 3'
DNA-dye conjugated		
DNA_{out} (Cy5) 3,2		5' – CCT CGG TCT GGG GGA GT /Cy5/ – 3'
DNA_{in} (Cy3) 3,2		5' – GTC TCG ACG GAG GAA GA /Cy3/ – 3'
DNA_{out} (Cy5) 3,3		5' – CCT CGG TCT GGG GGA GTA /Cy5/ – 3'
DNA_{in} (Cy3) 3,3		5' – GTC TCG TAC GGA GGA AGA /Cy3/ – 3'

5.5.2 Gel electrophoresis

Polyacrylamide gel electrophoresis was performed on 5% acrylamide/bisacrylamide (19 : 1) native gel. Gels were run at 220 V, 22 mA for about 1 h in 2× MOPS buffer (40 mM 3-morpholinopropane 1-sulfonic acid, 10 mM sodium acetate) and the appropriate magnesium chloride concentration, if desired (2 mM or 5 mM). Visualization of nucleic acid complexes was performed under UV light after ethidium bromide staining.

5.5.3 AFM imaging

Samples for AFM imaging were prepared on freshly cleaved mica which was modified with 50 mM aqueous solution of 1-(3-aminopropyl)-silatrane (APS) by immersing for 30 min followed by rinsing with deionized water and drying in an argon stream.27 Imaging samples were diluted at 4 °C in buffer containing 10 mM HEPES, pH 7, and 2 mM magnesium chloride to 0.5–1.5 ng μL−1 concentration, and deposited onto APSmodified mica for 2 min. After deposition, mica strips were rinsed briefly with ice cold water and dried under flowing argon. AFM images were recorded with a MultiMode AFM Nanoscope IV system (Bruker Instruments) in Tapping Mode with silicon probes RTESPA-300 (Bruker Nano Inc.; resonance frequency ∼300 kHz, spring constant ∼40 N m−1) at a scanning rate of ∼2.0 Hz. Image processing was performed with the FemtoScan software package (Advanced Technologies Center).

5.5.4 FRET experiments

Nucleic acid assemblies containing dye-conjugated oligonucleotides were annealed at 200 nM concentration in 10 mM HEPES (4-(2-hydroxyethyl)-1 piperazineethanesulfonic acid) buffer, pH 7.0, by the same annealing protocol described above. 95 μL of each sample was then transferred to a 96-well plate and incubated in the dark at room temperature for 1–2 h prior to measurement. FRET measurements were performed on a Spectra Max Gemini XS monochromator plate reader

(Molecular Devices) at 22 °C by exciting the Cy3 fluorophore at 520 nm and reading the transferred fluorescence as Cy5 emission at 670 nm. An emission cut-off filter was applied at 665 nm.

5.6 Acknowledgment

The material in Chapter 5, in part, has been published in Nanoscale titled "RNA–DNA hybrid nanoshapes that self-assemble dependent on ligand binding" with Thomas Hermann as co-author. The dissertation author was the primary investigator and author of this material. Prof. Hermann was the corresponding author.

The author thanks A. J. Lushnikov for help with AFM imaging.

Chapter 6: Nano-sandwich composite by kinetic-trapping assembly from protein and nucleic acid

6.1 Abstract

Design and preparation of layered composite materials alternating between nucleic acids and proteins has been elusive due to limitations in occurrence and geometry of interaction sites in natural biomolecules. We report the design and kinetically controlled stepwise synthesis of a nano-sandwich composite by programmed noncovalent association of protein, DNA and RNA modules. The nucleic acid layers form co-parallel RNA-DNA hybrid nanotriangles flanking the protein core of the nano-sandwich composite. The 3D architecture of the complex was confirmed by fluorescence labeling and cryo-electron microscopy studies. The synthesis strategy for the nano-sandwich composite provides a general blueprint for controlled noncovalent assembly of complex supramolecular architectures from protein, DNA and RNA components which expand the design repertoire for bottom-up preparation of layered biomaterials.

6.2 Introduction

Self-assembling soft materials have been obtained from design and synthesis efforts at the interface of supramolecular chemistry and nanotechnology. The association of molecular building blocks through noncovalent interactions orchestrated by self-recognition leads to materials that exhibit patterns and functionality at the nanoscale. Proteins and nucleic acids have unique 3D folding and sequence-encoding properties that render these biopolymers ideal modules for self-assembling soft materials. Proteins provide a diverse repertoire of 3D architectures, chemical functionality and enzymatic activities, while DNA and RNA enable programmable noncovalent assembly through predictable base pair formation. Among nucleic acid components, RNA combines architectural complexity of stable autonomous folds with the ability to assemble in a sequence-dependent fashion(19,58,80). The three types of biopolymers, proteins, DNA, and RNA have been extensively used for nanoscale self-assembly of soft materials with a multitude of

applications, for example, in sensing, catalysis, plasmonic devices, biocompatible coatings, synthetic pores, surface patterning and dynamic nanodevice(16,59,83,100). Combining different biopolymer types enables the design of composite materials with increasingly complex properties and functionality at the nanoscale(101). Composite biopolymer nanomaterials have been created from DNA-protein(102) and RNA-protein(103) complexes as well as RNA-DNA hybrid assemblies(53,55,56,61,63); however, self-assembling materials containing protein and both types of nucleic acid have been elusive to date.

Molecular complexity in such noncovalent supramolecular systems emerges from precisely vectored assembly rather than inherent chemical complexity of the diverse building blocks. Maximizing control over the preparation of composite materials from multiple different types of biopolymers requires multistep noncovalent synthesis that exploits thermodynamics and kinetics of self-assembly pathways to sequentially process information stored in the constituent component architectures towards creation of the desired complex product(75). Base-pair formation of complementary sequences within nucleic acid building blocks often drives assembly to thermodynamically stable structures which may not be kinetically favored over uncontrolled aggregation. One approach to overcome undesirable pathways of nucleic acid folding and assembly is to exploit local interactions that drive fast folding as a kinetic trap(53), thus avoiding unwanted oligomerization of modules.

Here, we describe the design, stepwise synthesis and structure characterization of a nano-sandwich composite that contains three types of biopolymers, protein, DNA and RNA, each playing a distinct role for assembly and architecture. The composite includes a protein core sandwiched between two co-parallel nanotriangles that assemble from RNA-corner and DNA-connector modules (Fig. 6.1). Distinct from previous approaches of locating proteins on pre-

formed nucleic acid frameworks(104,105), we used a protein component to direct self-assembly of nucleic acid nanoshapes in precisely pre-determined positions of a sandwich architecture. As a protein core, we chose streptavidin which is a homo-tetramer of subunits, each containing a high-affinity binding site for a biotin molecule. Association of the nucleic acid nanotriangles with the protein was achieved by connecting DNA oligonucleotide components that carried a biotin ligand.

6.3 Results and Discussion

The nanotriangles were designed to contain modules partitioning architectural and functional roles between RNA and DNA components according to an approach that we recently established for nucleic acid hybrid nanoshapes(63,65). Self-assembling polygonal nanoshapes are obtained by combining autonomously folding RNA corner motifs with linear double-stranded DNA connectors that associate through short single-stranded complementary sequences. Here, a guide DNA with three hybridization sites (DNA_{in}) was used to assemble nanotriangles from RNA corner modules and DNA connectors (DNA_{out}) (Fig. 6.1B). In such nanoshapes, association of nucleic acid modules kinetically favors the rapid formation of circularly closed polygons is over the slower end-to-end oligomerization(63). By introducing unique sequences in the hybridization sites of the DNA guide strand, the three DNA connector sides of a nanotriangle were programmed for successive assembly with biotin-conjugated oligonucleotides to furnish nanoshapes carrying 0–3 biotin ligands. Mobility analysis of the biotin-modified nanotriangles by native polyacrylamide gel electrophoresis (PAGE) confirmed the formation of clean RNA-DNA hybrid complexes (Fig. 6.1C).

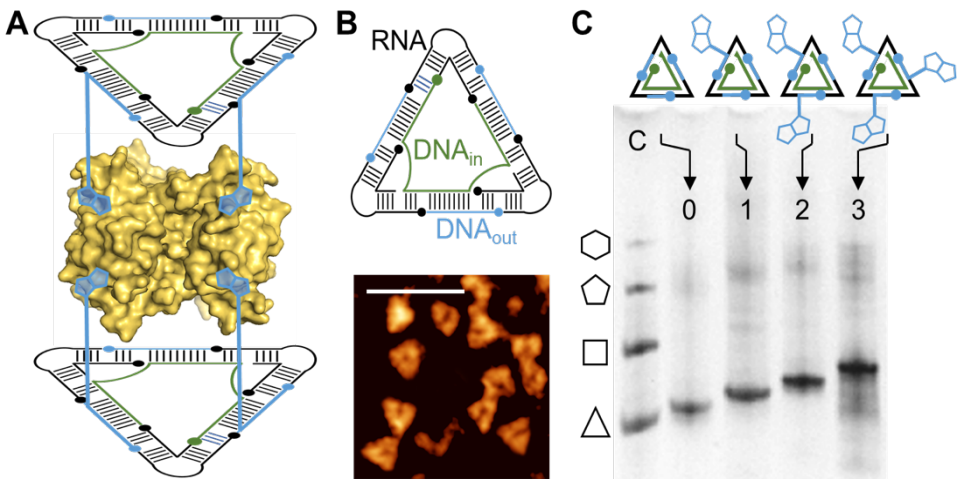

Figure 6.1. Design of nucleic acid-protein nano-sandwich composite. (A) Architecture of the nano-sandwich composite containing a streptavidin protein tetramer (yellow) that associates with two flanking nucleic acid nanotriangles, each bound through two DNA-conjugated biotin ligands (blue). The rotational arrangement of the nanotriangles in this and the following schematics is arbitrarily shown in an eclipsed configuration. The design of the nano-sandwich components allows for eclipsed or staggered arrangement. (B) Nucleic acid hybrid nanotriangles that self-assemble from RNA corner modules and DNA connectors (DNA_{out}) controlled by a DNA guide strand (DNA_{in}) with three hybridization sites for the connector units. AFM imaging confirmed the nanotriangle architecture(63). (C) Programmed assembly of modified nucleic acid nanotriangles that carry 0–3 biotin ligands attached at DNA connectors (DNA_{out}). Increasing number of biotin ligands is revealed by decreasing mobility of modified nanotriangles on native polyacrylamide gel. Lane C is a mobility control sample containing a previously established mixture of unmodified polygonal RNA-DNA hybrid nanoshapes(63).

An initial attempt to prepare nano-sandwich complexes of streptavidin by mixing the protein with pre-assembled biotin-conjugated nanotriangles failed to deliver the desired architecture (Fig. 6.2). Nanotriangles carrying a single biotin modification formed discrete complexes having a gel mobility consistent with 1-3 nucleic acid triangles bound to a streptavidin protein (Fig. 6.2A, lane 2). Addition of a fourth triangle was not observed, possibly prevented by sterical hindrance. Streptavidin binding of nanotriangles that contained two or three biotin ligands led to mostly aggregation in addition to the formation of some equimolar ($SA:T_1$) complex (Fig. 6.2A, lanes 3, 4). Imaging and particle height measurements by atomic force microscopy (AFM) of purified equimolar ($SA:T_1$) complex between streptavidin bound to one nanotriangle with 2 biotin ligands (Fig. 6.2A, lane 3) revealed the triangular shape of the nucleic acid component (Fig.

6.2B) and supported the 1:1 stoichiometry of a streptavidin tetramer positioned on top of a single RNA-DNA hybrid nanotriangle(63).

We hypothesized that the failure of obtaining the nano-sandwich complex from the binding of preformed nanotriangles that carry 2 or 3 biotin ligands to streptavidin is caused by a kinetic effect that favors aggregation through crosslinking of proteins by nanotriangles. Following a fast association of the first biotin nanotriangle ligand with streptavidin, binding of the second conjugated biotin is kinetically disfavored through sterical hindrance which slows the favorable orientation of the nanoshape required for the formation of the second bond. Instead, association of the second biotin ligand with another streptavidin may become a competing reaction which eventually produces heterogeneous protein-nanotriangle aggregates.

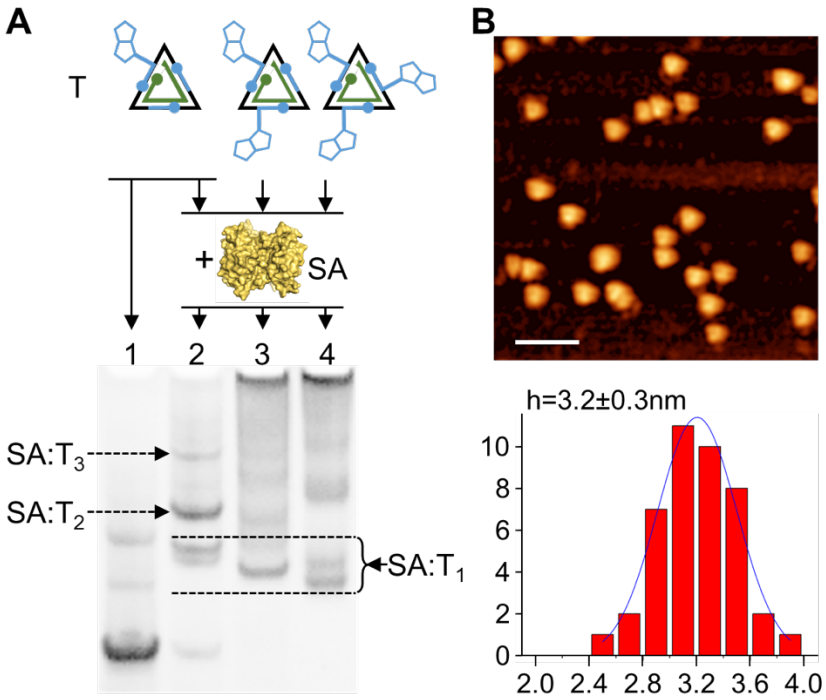

Figure 6.2. Complex formation of streptavidin with preformed nucleic acid nanotriangles. (A) PAGE analysis of mixtures that contained streptavidin tetramer protein (SA) and nucleic acid nanotriangles (T) carrying a defined number of biotin ligands. Nanotriangles with a single biotin modification formed complexes with 1–3 triangles bound to a single streptavidin tetramer ($SA:T_n$, n=1–3). Nanotriangles conjugated with 2 or 3 biotin ligands formed equimolar complexes ($SA:T_1$) in addition to significant aggregation. Compaction of equimolar $SA:T_1$ assemblies by increasing number of biotin ligands that tether nanotriangles to streptavidin increased complex mobility. Double bands for equimolar $SA:T_1$ complexes observed with nanotriangles carrying 1 or 3 biotin ligands suggest formation of two different complex configurations due the non-equivalence of biotin binding sites on the protein tetramer. Lane 1 is a mobility control sample containing an RNA-DNA hybrid nanotriangle with a single biotin ligand. (B) AFM imaging of $SA:T_1$ complexes assembled from streptavidin and nanotriangles with 2 biotin ligands (panel A, lane 3). Scale bar, 50 nm. The histogram shows particle height measured by AFM which was consistent with equimolar complexes of a streptavidin tetramer positioned on top of a single RNA-DNA hybrid nanotriangle(63).

To overcome the uncontrolled association of streptavidin and preformed nanotriangles ending in aggregates, we devised a synthetic route for the nano-sandwich that harnessed the rapid self-assembly of the RNA-DNA hybrid nanoshapes through short-range local interactions as a fast-kinetic trap(106). We had previously demonstrated that RNA corner modules and DNA connectors that associate through hybridization of complementary single-stranded overhang sequences form

exclusively polygonal nanoshapes without oligomerization or aggregate formation(63,65). During the folding and self-assembly of these nucleic acid hybrid architectures, incorporation of bent RNA modules provides precise vectoring of complementary sequences, thereby favoring the rapid formation of circularly closed nanoshapes over runaway oligomerization. To capitalize on the fast self-assembly of nanoshapes as a kinetic trap that prevents aggregation of the nano-sandwich components, we devised a stepwise synthetic route (II) in which the vectoring RNA corner modules are added last to a mixture of pre-formed protein-DNA and DNA precursor complexes (Fig. 6.3A). Binding of biotin-conjugated DNA_{out} connector oligonucleotides to streptavidin furnished a protein-DNA precursor complex for the sandwich core (Fig. 6.3A, II-a) which was mixed with programmed guide DNA_{in} and the complementary unmodified DNA_{out} connector (Fig. 6.3A, II-b). Addition of RNA corner module to the mixture of the protein-DNA and DNA precursors initiated rapid folding and self-assembly of the RNA-DNA hybrid nanoshapes, which kinetically trapped the nucleic acid components in nanotriangles tethered at the protein sandwich core before association with further streptavidin tetramers occurred (Fig. 6.3A, II-c). PAGE analysis of precursors and products of the kinetic-trapping route (II), in comparison with the route (I) of mixing pre-formed nanotriangles and streptavidin, demonstrated the synthesis of predominantly soluble nano-sandwich from route II in contrast to component aggregation in route I (Fig. 6.3B). Clean formation of the nano-sandwich required close matching of the component stoichiometry to the expected 1:4 ratio of streptavidin tetramer to biotin-conjugated DNA_{out} connector (Fig. 6.4). Aggregation at the expense of sandwich formation was observed with increasing concentration of the constituent components above a critical concentration, supporting the concept of kinetic trapping in the self-assembly process (Fig. 6.5).

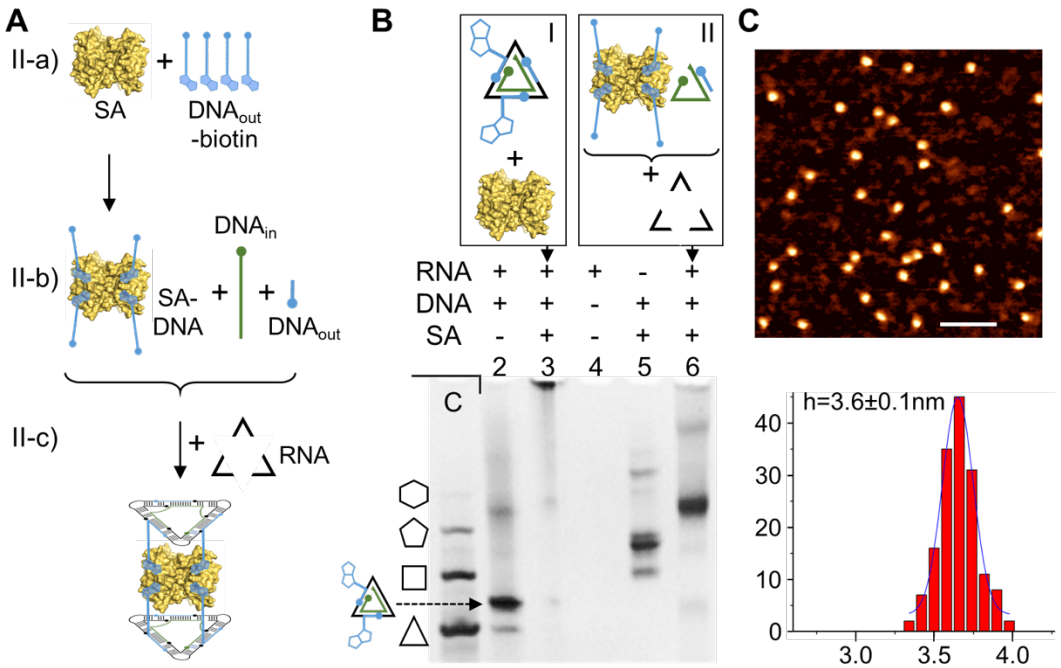

Figure 6.3. Synthesis of nucleic acid-streptavidin nano-sandwich composite. (A) Route II for kinetic-trapping assembly: II-a), binding of biotin-conjugated DNA_{out} connector oligonucleotides to streptavidin (SA) furnishing the protein-DNA sandwich core complex precursor (SA-DNA); II-b), addition of DNA_{in} guide and unmodified DNA_{out} connector to the core complex precursor; II-c) induction of RNA-DNA hybrid nanotriangle self-assembly by addition of RNA corner modules. (B) PAGE analysis of precursors and products in synthetic routes for the nano-sandwich composite. In route I (shown also in Fig. 6.2A, lane3), preformed RNA-DNA hybrid nanotriangles carrying 2 biotin ligands (lane 2) are mixed with streptavidin which resulted in mostly aggregation (lane 3). Lane C is a mobility control sample containing a previously established mixture of polygonal RNA-DNA hybrid nanoshapes. In route II, a mixture containing preformed complex of biotin-conjugated DNA connectors bound to streptavidin (II-a) in addition to unconjugated DNA connector and DNA guide strand (II-b) was prepared first (lane 5). Subsequent addition of RNA corner modules furnished the nano-sandwich composite as a single predominant product (lane 6). (C) AFM imaging of the nano-sandwich composite product from gel lane 6 (scale bar, 50 nm). The histogram shows particle height measured by AFM.

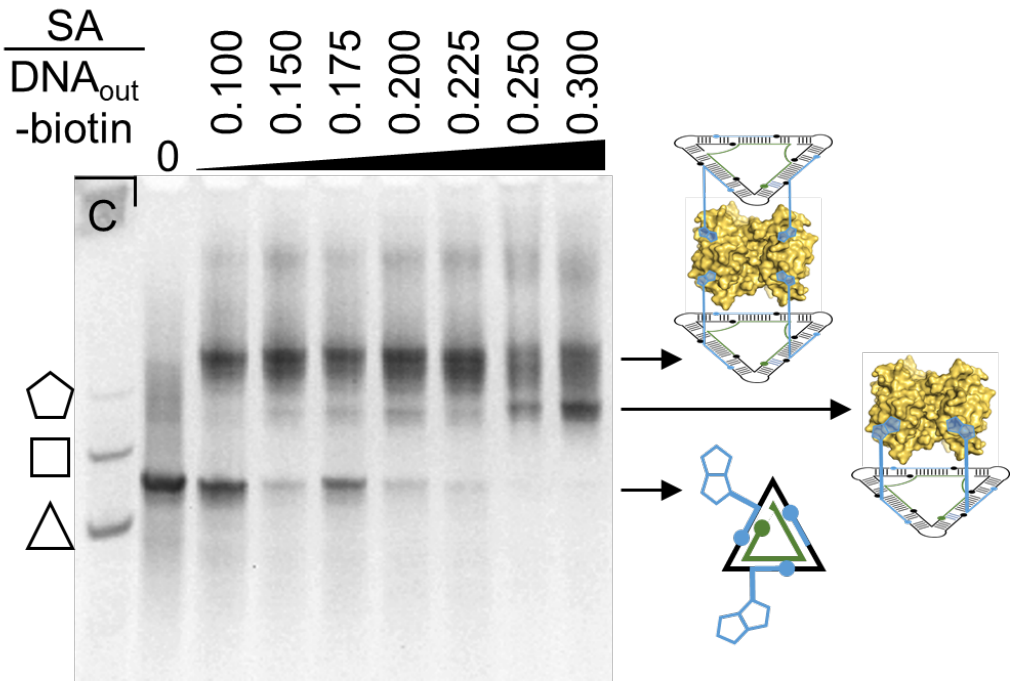

Figure 6.4. Nano-sandwich composite assembly dependent on streptavidin concentration. PAGE analysis of the formation of nano-sandwich composite following route II (Fig. 6.3AB) at increasing concentration of streptavidin. At and above a 1:4 stoichiometric ratio of streptavidin tetramer (SA) relative to biotin-labeled DNA connector (DNA_{out}-biotin), complexes of a single triangle associated with streptavidin are formed at the expense of nano-sandwich composite. Lane C is a mobility control sample containing a previously established mixture of polygonal RNA-DNA hybrid nanoshapes.

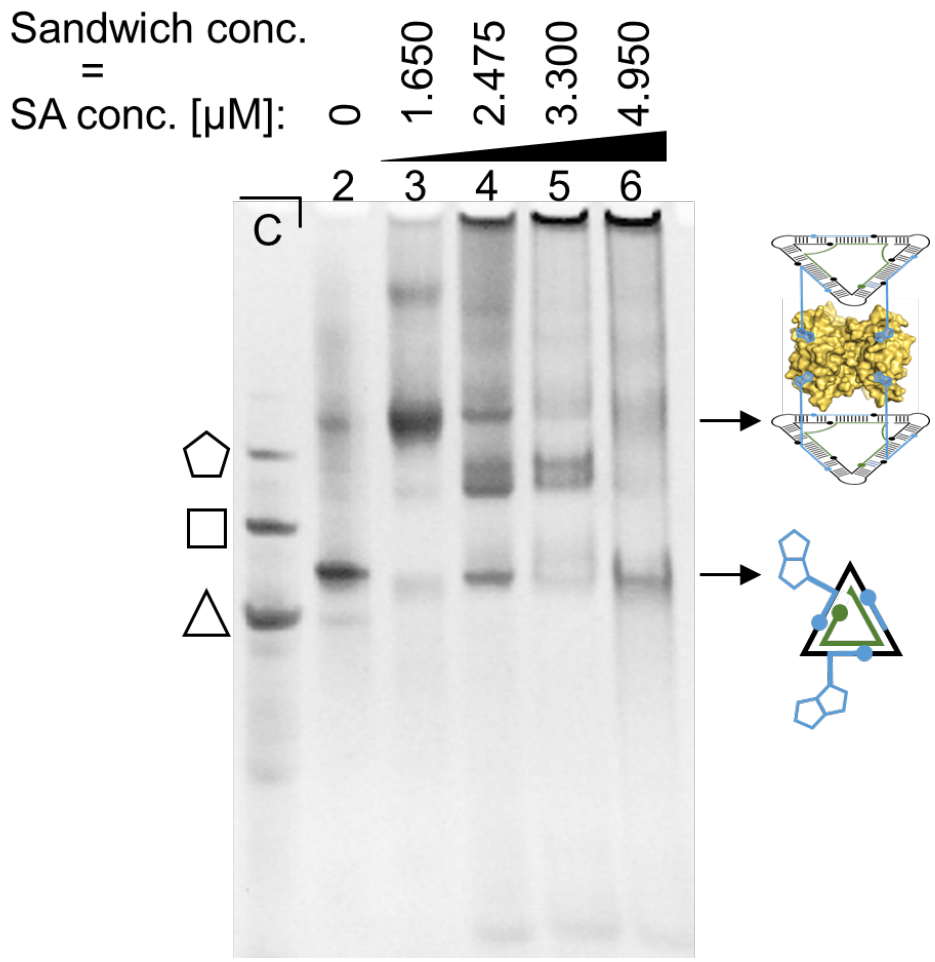

Figure 6.5. Nano-sandwich composite assembly dependent on complex concentration. PAGE analysis of the formation of nano-sandwich composite following route II (Fig. 6.3AB) at increasing concentration of all sandwich components (lanes 3-6). At sandwich concentrations above 1.65 μM, aggregation is competing with sandwich complex formation. Lane 2 is a control sample containing a mixture of all nucleic acid components but no streptavidin, resulting in assembly of biotin-modified nanotriangle as indicated in the schematic. Lane C is a mobility control sample containing a previously established mixture of polygonal RNA-DNA hybrid nanoshapes.

Clean nano-sandwich complexes obtained through synthetic route II presented as discrete nanoparticles in AFM imaging (Fig. 6.3C). To confirm the composition and structure of the nano-sandwich, we analyzed the product from synthetic route II by fluorescence labeling and cryo-EM (Fig. 6.6). Incorporation of Cy5 acceptor dye-conjugated RNA corner module into the sandwich composite was monitored by Förster resonance energy transfer (FRET) with an Alexa 488 donor dye-labeled streptavidin protein. FRET signal was observed only when all components of the

nano-sandwich were present but not when the dye-conjugated RNA and protein were mixed in the absence of DNA (Fig. 6.6A), supporting the essential contribution of all constituents for the assembly of the sandwich architecture. When antisense DNA complementary to the biotin-conjugated DNA_{out} connectors was added to fluorescent dye-labeled sandwich composite, the FRET signal decreased over time, which suggested dissociation of the sandwich architecture (Fig. 6.7).

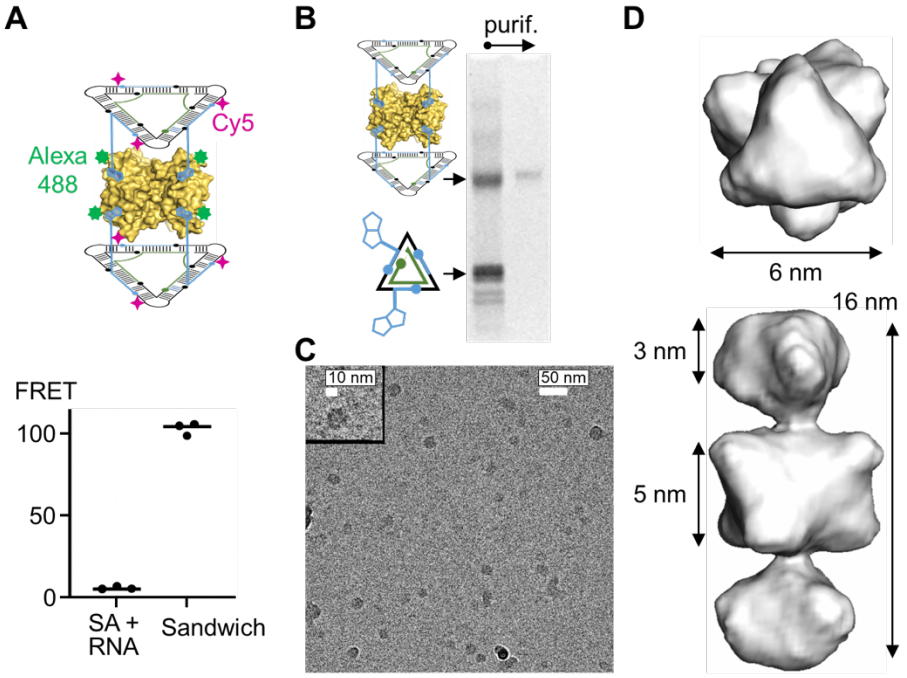

Figure 6.6. Structure characterization of nucleic acid-streptavidin nano-sandwich composite. (A) Nano-sandwich composite formation was demonstrated in solution by observing FRET signal from fluorescently labeled streptavidin (Alexa 488 donor dye) and RNA corner modules (Cy5 acceptor dye). Nano-sandwich composite prepared according to synthetic route II (Fig. 6.3A) produced a robust signal whereas omission of DNA components abolished FRET. (B) Purification of nano-sandwich composite by native PAGE yielded a clean sample for structure determination by cryo-EM. (C) Representative electron micrograph of nano-sandwich composite sample. (D) Two orthogonal views of cryo-EM maps obtained by 3D reconstruction for the nano-sandwich composite, shown as iso-density surface.

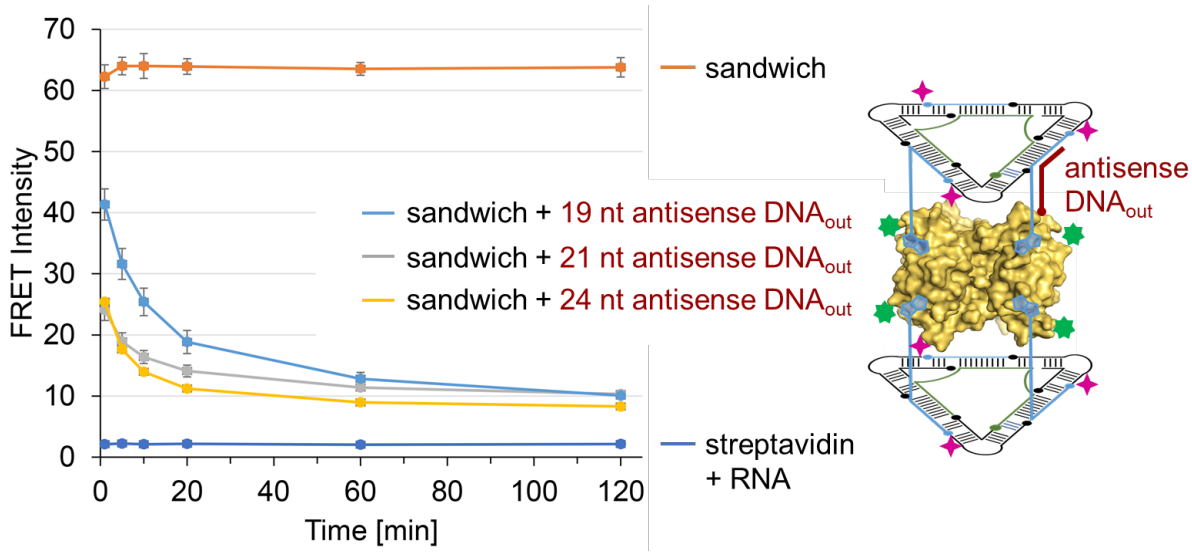

Figure 6.7. Dissociation of nano-sandwich composite by antisense DNA. FRET signal from nano-sandwich composite containing fluorescently labeled streptavidin (Alexa 488 donor dye) and RNA corner modules (Cy5 acceptor dye) (Fig. 6.6) was monitored after addition of antisense DNA that was complementary to the biotin-conjugated DNA_{out} connector oligonucleotides. The antisense DNA was fully complementary to the DNA_{out} connector sequence within the nanotriangle (11 nucleotides) and extending by an additional 8, 10 or 13 nucleotides (19, 21, or 24 nt antisense) into the linker carrying the biotin ligand.

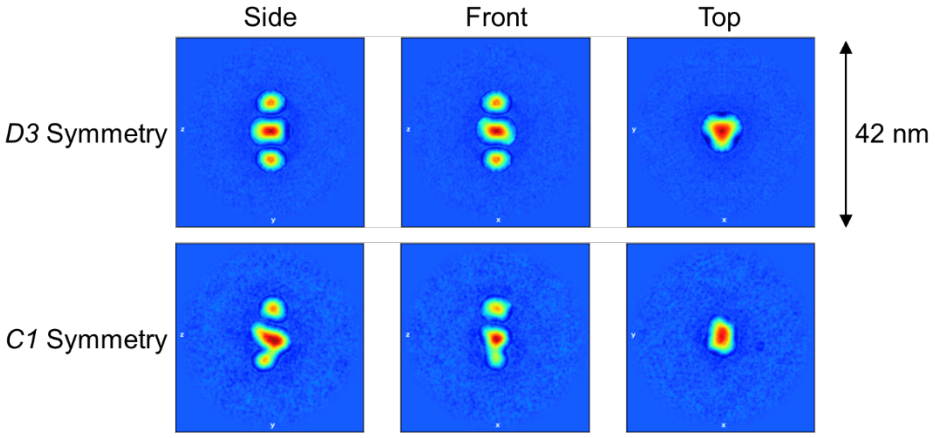

Figure 6.8. Cryo-EM density map slices for nano-sandwich composite. Comparison of slices through cryo-EM density maps obtained from 3D reconstruction of the nano-sandwich 3D structure under superimposed D3 or C1 symmetry.

Gel purification of nano-sandwich product obtained from synthetic route II provided a clean sample for structure analysis by cryo-EM (Fig. 6.6A,B). Reconstruction of the 3D structure from particle imaging by cryo-EM confirmed the nano-sandwich architecture of the composite complex in agreement with the desired design (Fig. 6.6D and Fig. 6.8). The shape and axial

dimensions of the cryo-EM electron density map were consistent with a streptavidin protein core sandwiched between two nucleic acid nanotriangles in a staggered rotational arrangement. Height and diameter of the sandwich core density of 5x6 nm correspond closely to the dimensions of the streptavidin tetramer(107). The lateral width of the flanking triangle density at 6 nm was shorter, and the height at 3 nm larger than expected for the RNA-DNA hybrid nanotriangles(63). We hypothesized that the flexible attachment by two biotin-conjugated DNA strands at the streptavidin core allows for axial tilting mobility of the nanotriangles which led to a laterally compressed and axially extended envelope in the averaged density calculated from cryo-EM imaging (Fig. 6.9).

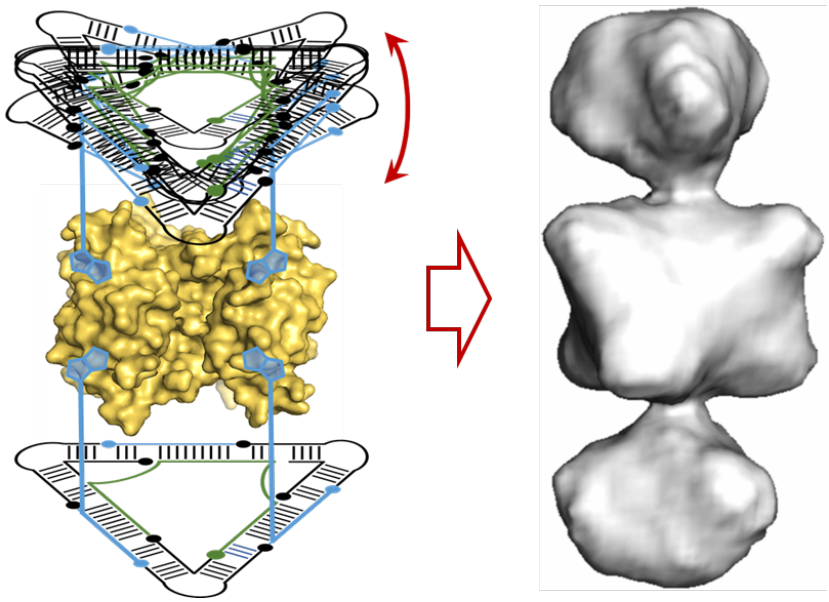

Figure 6.9. Precession conformational flexibility of nucleic acid nanotriangles in the sandwich composite. Flexible attachment by two biotin-conjugated DNA strands at the streptavidin core allows for axial tilting mobility of the nanotriangles which led to a laterally compressed and axially extended envelope in the averaged density from cryo-EM imaging. Precession conformational flexibility affects both nanotriangles in the sandwich composite; bottom nanotriangle is shown in one idealized orientation for comparison.

The unique modular design of the nano-sandwich composite partitions architectural and functional roles between a protein as the central organizing core, RNA building blocks that provide precise vectoring for closed polygon formation, and DNA components that serve as connectors.

We had previously demonstrated that modules of the nucleic acid hybrid nanoshapes are readily interchangeable from a diverse set of RNA and DNA motifs. The DNA connectors in nanoshapes tolerate topological variation by extension, connection and circular permutation of strands as well as insertion of aptamer motifs(63,64). RNA three-way junction (3WJ) folds can substitute for two-stranded internal loop motifs as corner modules and provide extension sites for the lateral connection of nanoshapes(65) as repeating units in layer assemblies(47). The selection of modules in the nanoshape components of a sandwich composite can be programmed individually through sequence-encoding self-assembly of the building blocks. Taken together, the design concept and multistep synthesis strategy for the sandwich composite described here, combined with the versatility of robust nanoshape components, provide a blueprint for the conception and creation of extended composite materials that include alternating layers of proteins and nucleic acids presenting diverse functional features embedded in patterns at the nanoscale. The success of a kinetic-trapping approach for synthesis of the nano-sandwich from precursors at physiological temperature opens a direction for self-assembly strategies of hierarchical nanoparticles in vivo.

6.4 Materials and Methods

6.4.1 Materials

DNA and RNA oligonucleotides were purchased from Integrated DNA Technologies. Unmodified DNA and RNA oligonucleotides and biotin-modified DNA oligonucleotides were rehydrated in 10 mM sodium cacodylate buffer, pH 6.5, to 500 μM stock before further diluting to working concentration with the same buffer. Cy5-modified RNA oligonucleotide was dissolved in 10 mM HEPES buffer, pH 7.0, to stock concentration at 200 μM. Oligonucleotide sequences are listed in Table 6.1. Streptavidin tetramer was purchased from Promega Corporation. Alexa Fluor

488-conjugated streptavidin was purchased from Thermo Fisher Scientific. Proteins were rehydrated and diluted in 10 mM HEPES buffer, pH 7.0.

Table 6.1. Oligonucleotide sequences

Name	**Sequence**
RNA_{in} corner	5’ - CCGAGGUCAGCCUG - 3’
RNA_{out} corner	5’ - CGAGACCAGGAACUACUGA - 3’
DNA_{in} connector for mixture of unmodified nanoshapes control C	5’ - GTCTCGTATCGCTACGT - 3’
DNA_{out} connector for mixture of unmodified nanoshapes control C	5’ - CCTCGGACGTAGCGATA - 3’
DNA_{in} guide	5’ - GTCTCGTATCGCTACGT TTTCTCTCTCTCTTTT GTCTCGTATCGCTACGT TTTCTCTCTCTCTTTT GTCTCGTATCGCTACGT - 3’
DNA_{in} guide with binding site for 1 biotin-conjugated DNA_{out}	5’ - GTCTCGTATCGCTACGT TTTTCCTTTT GTCTCGATGTCCTTGCA TTTTCCTTTT GTCTCGATGTCCTTGCA - 3’
DNA_{in} guide with binding site for 2 biotin-conjugated DNA_{out}	5’ - GTCTCGTATCGCTACGT TTTTCCTTTT GTCTCGTATCGCTACGT TTTTCCTTTT GTCTCGATGTCCTTGCA - 3’
DNA_{in} guide with binding site for 3 biotin-conjugated DNA_{out}	5’ - GTCTCGTATCGCTACGT TTTTCCTTTT GTCTCGTATCGCTACGT TTTTCCTTTT GTCTCGTATCGCTACGT - 3’
DNA_{out} biotin-conjugated connector for use with DNA_{in} guide	5’ - CCTCGGACGTAGCGATATTTCTCTCTCTCT/3Bio/ - 3’
DNA_{out} unmodified connector for use with DNA_{in} guide	5’ - CCTCGGTGCAAGGACAT - 3’
antisense DNA_{out} 24 nt	5’ - AGAGAGAGAGAAATATCGCTACGT - 3’
antisense DNA_{out} 21 nt	5’ - GAGAGAGAAATATCGCTACGT- 3’
antisense DNA_{out} 19 nt	5’ - GAGAGAAATATCGCTACGT - 3’

6.4.2 Assembly of RNA-DNA hybrid nanoshapes

RNA-DNA hybrid nanoshapes were assembled by mixing stoichiometric amounts of nucleic acid components and annealing at 37°C for 10 minutes in the presence of 2 mM magnesium chloride. After annealing, samples were cooled on water ice for 5 minutes before using for gel electrophoresis analysis.

6.4.3 Assembly of RNA-DNA-Protein composite material

RNA-DNA-Protein was assembled in a multi-step protocol in the presence of 2 mM magnesium chloride: 1) Streptavidin and biotin-conjugated DNAout connector were mixed at a given ratio and incubated at 37°C for 1 hour before cooling on ice for 5 minutes. 2) To the mixture were added guide DNAin and unmodified DNAout connector followed by incubation at 37°C for 10 minutes. 3) RNA corner module oligonucleotides were added to the mixture and incubated 37°C for 50 minutes before cooling on water ice for 5 minutes.

6.4.4 Native polyacrylamide gel electrophoresis (PAGE)

Nucleic acid assemblies and composite material were analyzed on 5% native acrylamide/bisacrylamide (19:1) gels in 2X MOPS buffer (40mM 3-morpholinopropane-1-sulfonic acid, 10 mM sodium acetate) containing 2 mM magnesium chloride. Gel electrophoresis was performed at 220 V at 22 mA for 60-90 minutes.

6.4.5 Gel extraction

Gel-purified nano-sandwich composite was isolated by extraction from gel slices cut out around the individual band containing the composite after PAGE. The extracted band was cut into small pieces before soaking in 500 μL of 10mM sodium cacodylate buffer containing 2 mM magnesium chloride at 4°C for 5–7 days. Recovered solutions were concentrated on Amicon ultra 0.5 mL centrifugal filters (regenerated cellulose, 3,000 NMWL).

6.4.6 FRET experiments

FRET experiments were performed as described previously (21) on a Spectra Max Gemini monochromator plate reader (Molecular Devices) at room temperature. Cy5-modified RNA was at 100 nM concentration and Alexa Fluor 488-conjugated streptavidin was at 13.2 nM in 10 mM HEPES buffer (pH 7.0). Emission blocking filters were set at 550 and 665 nm. Alexa Fluor 488 was excited at 520 nm, and transferred fluorescence was read as Cy5 emission at 670 nm.

6.4.7 AFM Imaging

Freshly cleaved mica was modified with 50 mM solution of 1-(3-aminopropyl)-silatrane (APS) in deionized water by immersing strips for 30 min followed by rinsing with deionized water and drying in an Ar stream (22). Nucleic acid and composite samples were diluted at 4°C in assembly buffer (10 mM sodium cacodylate buffer, pH 6.5, for nucleic acid samples and 10 mM HEPES, pH 7.0, for sandwich composite) containing 2 mM magnesium chloride and immediately deposited onto APS-modified mica for 2 minutes. Typical sample concentration for deposition was 0.5–1.5 ng/μL. Samples were rinsed briefly with several drops of ice-cold water and dried with a gentle flow of argon. AFM images were collected with a MultiMode AFM Nanoscope IV system (Bruker Instruments) in Tapping Mode at ambient conditions. Silicon probes RTESPA-300 (Bruker Nano Inc.) with a resonance frequency of ~300 kHz and a spring constant of ~40 N/m were used for imaging at scanning rate of about 2.0 Hz. Images were processed using the FemtoScan software package (Advanced Technologies Center).

6.4.8 Cryo-TEM

Sample vitrification was performed with a Leica EMGP plunger (Leica Microsystems). Briefly, 3 ul of purified sandwich sample was applied to a glow-discharged Quantifoil grid (R1.2/1.3, Electron Microscopy Sciences). The grid was quickly plunged into liquid propane after

3.5 s blotting time at 95% humidity. Specimen was then transferred onto a Gatan cryo-transfer holder (Gatan Inc) and examined under a JEM2100F electron microscope (JEOL USA) with operation voltage at 200 kV. The images were recorded at electron dose less than 20 e/A2 and collected on a Gatan OneView CCD detector at pixel size of 2.8 Å at specimen space.

6.4.9 Single Particle Image Processing and 3D Reconstruction

Cryo-EM CCD images were imported into cryoSparc for image processing. After CTF correction, a total of 40764 particles were selected and 2D-classified for ab-initio initial models building under C1 symmetry. The initial model with three-layers density distribution was visually selected for further 3D refinements. The final density map was reconstructed by combining 6872 particles under superimposed D3 or C1 symmetry (Fig. S4). The density consistency for the final maps was calculated to be 5.79 Å by the GSFSC curve without any mask in cryoSparc.

6.5 Acknowledgment

The material in Chapter 6, in part, is currently submitted for a publication with Li Xing, Alba Monferrer and Thomas Hermann as co-authors. The dissertation author was the primary investigator and author of this material. Prof. Hermann was the corresponding author. The authors thank T. Wiryaman for help with analysis of cryo-EM data. The author thanks A. J. Lushnikov for help with AFM imaging.

Chapter 7: Conclusion and Future Perspectives

Nucleic acid nanotechnology that harnesses the strengths from both RNA's structural diversity and DNA's chemical stability has emerged as a promising research direction at the interface of biochemistry, biology and materials science. This dissertation describes the development of several fundamental assays, such as mix-and-match screening assay, for stable RNA-DNA hybrid nano-complexes and unique synthesis protocols, such as strand-exchange protocol and kinetic-trapping synthesis, for transformable RNA-DNA hybrid nano-complexes and hierarchical three-dimensional nanoparticles that incorporate RNA, DNA and proteins. All these assays and synthesis protocols provide powerful tools to discover self-assembling modular nanoshapes from small RNA and DNA modules, laying the foundation for the emerging nucleic acid nanotechnology field.

Future research directions in this field will largely remain in two research scopes: 1) design and prepare RNA-DNA hybrid nanoparticles with novel structural properties. This requires continuous research on RNA structures and folding, discovering novel RNA motifs with intrinsic structural diversities that serve as architectural joints of RNA-DNA hybrid nano-complexes. 2) prepare RNA-DNA hybrid nano-devices for materials and therapeutic applications. DNA modules that serve as functional groups or binding sites for other functional materials in the nano-devices will be the focus in this direction.

With increasing attention paying to the nucleic acid nanotechnology, RNA-DNA hybrid nanotechnology that develop novel modular nano-complexes self-assembling from small RNA and DNA modules will provide powerful tools to solve general challenges in the nanoengineering world.

Reference

1. Stillman B. Cell Cycle Control of DNA Replication. Science (80-). 1996 Dec 6;274(5293):1659 LP – 1663.

2. Sidorenkov I, Komissarova N, Kashlev M. Crucial Role of the RNA:DNA Hybrid in the Processivity of Transcription. Mol Cell. 1998;2(1):55–64.

3. Gorodkin J, Stricklin SL, Stormo GD. Discovering common stem–loop motifs in unaligned RNA sequences. Nucleic Acids Res. 2001 May 15;29(10):2135–44.

4. Westhof E, Auffinger P. RNA Tertiary Structure. Encyclopedia of Analytical Chemistry. 2006. (Major Reference Works).

5. Varani G, McClain WH. The G·U wobble base pair. EMBO Rep. 2000 Jul 1;1(1):18–23.

6. Giese MR, Betschart K, Dale T, Riley CK, Rowan C, Sprouse KJ, et al. Stability of RNA Hairpins Closed by Wobble Base Pairs. Biochemistry. 1998 Jan 1;37(4):1094–100.

7. Butcher SE, Pyle AM. The Molecular Interactions That Stabilize RNA Tertiary Structure: RNA Motifs, Patterns, and Networks. Acc Chem Res. 2011 Dec 20;44(12):1302–11.

8. Seeman NC. Nucleic acid junctions and lattices. J Theor Biol. 1982;99(2):237–47.

9. Mao C, Sun W, Seeman NC. Designed Two-Dimensional DNA Holliday Junction Arrays Visualized by Atomic Force Microscopy. J Am Chem Soc. 1999 Jun 1;121(23):5437–43.

10. Seeman NC. Structural DNA Nanotechnology BT - NanoBiotechnology Protocols. In: Rosenthal SJ, Wright DW, editors. Totowa, NJ: Humana Press; 2005. p. 143–66.

11. Seeman NC. An Overview of Structural DNA Nanotechnology. Vol. 37, Molecular Biotechnology. 2007. p. 246–57.

12. Rothemund PWK. Folding DNA to create nanoscale shapes and patterns. Nature. 2006;440(7082):297–302.

13. Marchi AN, Saaem I, Vogen BN, Brown S, LaBean TH. Toward Larger DNA Origami. Nano Lett. 2014 Oct 8;14(10):5740–7.

14. Chidchob P, Sleiman HF. Recent advances in DNA nanotechnology. Curr Opin Chem Biol. 2018;46:63–70.

15. Bathe M, Rothemund PWK. DNA Nanotechnology: A foundation for Programmable Nanoscale Materials. MRS Bull. 2017/12/08. 2017;42(12):882–8.

16. Seeman NC, Sleiman HF. DNA nanotechnology. Nat Rev Mater. 2017;3(1):17068.

17. Nummelin S, Kommeri J, Kostiainen MA, Linko V. Evolution of Structural DNA Nanotechnology. Adv Mater. 2018 Jun 1;30(24):1703721.

18. Madsen M, Gothelf K V. Chemistries for DNA Nanotechnology. Chem Rev. 2019 May 22;119(10):6384–458.

19. Westhof E, Masquida B, Jaeger L. RNA tectonics: towards RNA design. Fold Des. 1996;1(4):78–88.

20. Guo P, Zhang C, Chen C, Garver K, Trottier M. Inter-RNA interaction of phage phi29 pRNA to form a hexameric complex for viral DNA transportation. Mol Cell. 1998;2:149–55.

21. Shu D, Shu Y, Haque F, Abdelmawla S, Guo P. Thermodynamically stable RNA three-way junction for constructing multifunctional nanoparticles for delivery of therapeutics. Nat Nanotechnol. 2011;6(10):658–67.

22. Khisamutdinov EF, Li H, Jasinski DL, Chen J, Fu J, Guo P. Enhancing immunomodulation on innate immunity by shape transition among RNA triangle, square and pentagon nanovehicles. Nucleic Acids Res. 2014;42(15):9996–10004.

23. Jasinski DL, Khisamutdinov EF, Lyubchenko YL, Guo P. Physicochemically Tunable Polyfunctionalized RNA Square Architecture with Fluorogenic and Ribozymatic Properties. ACS Nano. 2014 Aug 26;8(8):7620–9.

24. Jasinski DL, Li H, Guo P. The Effect of Size and Shape of RNA Nanoparticles on Biodistribution. Mol Ther. 2017/12/22. 2018 Mar 7;26(3):784–92.

25. Khisamutdinov EF, Jasinski DL, Guo P. RNA as a Boiling-Resistant Anionic Polymer Material To Build Robust Structures with Defined Shape and Stoichiometry. ACS Nano. 2014 May 27;8(5):4771–81.

26. Sharma A, Haque F, Pi F, Shlyakhtenko LS, Evers BM, Guo P. Controllable self-assembly of RNA dendrimers. Nanomedicine Nanotechnology, Biol Med. 2016;12(3):835–44.

27. Khisamutdinov EF, Jasinski DL, Li H, Zhang K, Chiu W, Guo P. Fabrication of RNA 3D Nanoprisms for Loading and Protection of Small RNAs and Model Drugs. Adv Mater. 2016 Dec 1;28(45):10079–87.

28. Li H, Zhang K, Pi F, Guo S, Shlyakhtenko L, Chiu W, et al. Controllable Self-Assembly of RNA Tetrahedrons with Precise Shape and Size for Cancer Targeting. Adv Mater. 2016 Sep 1;28(34):7501–7.

29. Jedrzejczyk D, Chworos A. Self-Assembling RNA Nanoparticle for Gene Expression Regulation in a Model System. ACS Synth Biol. 2019 Mar 15;8(3):491–7.

30. Dibrov SM, Johnston-Cox H, Weng Y-H, Hermann T. Functional Architecture of HCV IRES Domain II Stabilized by Divalent Metal Ions in the Crystal and in Solution. Angew

Chemie. 2007;119(1–2):230–3.

31. Dibrov SM, McLean J, Parsons J, Hermann T. Self-assembling RNA square. Proc Natl Acad Sci U S A. 2011;108(16):6405–8.

32. Boerneke MA, Dibrov SM, Gu J, Wyles DL, Hermann T. Functional conservation despite structural divergence in ligand-responsive RNA switches. Proc Natl Acad Sci U S A. 2014;111(45):15952–7.

33. Boerneke MA, Dibrov SM, Hermann T. Crystal-Structure-Guided Design of Self-Assembling RNA Nanotriangles. Angew Chemie Int Ed. 2016 Mar 14;55(12):4097–100.

34. Liu D, Wang M, Deng Z, Walulu R, Mao C. Tensegrity: Construction of Rigid DNA Triangles with Flexible Four-Arm DNA Junctions. J Am Chem Soc. 2004 Mar 3;126(8):2324–5.

35. Yu J, Liu Z, Jiang W, Wang G, Mao C. De novo design of an RNA tile that self-assembles into a homo-octameric nanoprism. Nat Commun. 2015;6:5724.

36. Stewart JM, Viard M, Subramanian HKK, Roark BK, Afonin KA, Franco E. Programmable RNA microstructures for coordinated delivery of siRNAs †. Nanoscale. 2016;17542–50.

37. Afonin KA, Bindewald E, Yaghoubian AJ, Voss N, Jacovetty E, Shapiro BA, et al. In vitro assembly of cubic RNA-based scaffolds designed in silico. Nat Nanotechnol. 2010;5(9):676–82.

38. Afonin KA, Kasprzak W, Bindewald E, Puppala PS, Diehl AR, Hall KT, et al. Computational and experimental characterization of RNA cubic nanoscaffolds. Methods [Internet]. 2014;67(2):256–65.

39. Johnson MB, Halman JR, Satterwhite E, Zakharov A V, Bui MN, Benkato K, et al. Programmable Nucleic Acid Based Polygons with Controlled Neuroimmunomodulatory Properties for Predictive QSAR Modeling. Small. 2017 Nov 1;13(42):1701255.

40. Hong E, Halman JR, Shah AB, Khisamutdinov EF, Dobrovolskaia MA, Afonin KA. Structure and Composition Define Immunorecognition of Nucleic Acid Nanoparticles. Nano Lett. 2018 Jul 11;18(7):4309–21.

41. Bui MN, Brittany Johnson M, Viard M, Satterwhite E, Martins AN, Li Z, et al. Versatile RNA tetra-U helix linking motif as a toolkit for nucleic acid nanotechnology. Nanomedicine Nanotechnology, Biol Med. 2017;13(3):1137–46.

42. Liu D, Geary CW, Chen G, Shao Y, Li M, Mao C, et al. Branched kissing loops for the construction of diverse RNA homooligomeric nanostructures. Nat Chem. 2020;12(3):249–59.

43. Horiya S, Li X, Kawai G, Saito R, Katoh A, Kobayashi K, et al. RNA LEGO: Magnesium-Dependent Formation of Specific RNA Assemblies through Kissing Interactions. Chem

Biol. 2003;10(7):645–54.

44. Fujiya I, Harada K. Formation of dendrimeric RNA assemblies though RNA loop-loop interactions. Nucleic Acids Symp Ser. 2004 Nov 1;48(1):97–8.

45. Chworos A, Severcan I, Koyfman AY, Weinkam P, Oroudjev E, Hansma HG, et al. Building programmable jigsaw puzzles with RNA. Science (80-). 2004;306(5704):2068–72.

46. Grabow WW, Zakrevsky P, Afonin KA, Chworos A, Shapiro BA, Jaeger L. Self-Assembling RNA Nanorings Based on RNAI/II Inverse Kissing Complexes. Nano Lett. 2011 Feb 9;11(2):878–87.

47. Geary C, Chworos A, Verzemnieks E, Voss NR, Jaeger L. Composing RNA Nanostructures from a Syntax of RNA Structural Modules. Nano Lett. 2017 Nov 8;17(11):7095–101.

48. Wang P, Meyer TA, Pan V, Dutta PK, Ke Y. The Beauty and Utility of DNA Origami. Chem. 2017;2(3):359–82.

49. Geary C, Rothemund PWK, Andersen ES. A single-stranded architecture for cotranscriptional folding of RNA nanostructures. Science (80-). 2014;345(6198):799–804.

50. Jepsen MDE, Sparvath SM, Nielsen TB, Langvad AH, Grossi G, Gothelf K V, et al. Development of a genetically encodable FRET system using fluorescent RNA aptamers. Nat Commun. 2018;9(1):18.

51. Krissanaprasit A, Key C, Fergione M, Froehlich K, Pontula S, Hart M, et al. Genetically Encoded, Functional Single-Strand RNA Origami: Anticoagulant. Adv Mater. 2019 May 1;31(21):1808262.

52. Han D, Qi X, Myhrvold C, Wang B, Dai M, Jiang S, et al. Single-stranded DNA and RNA origami. Science (80-). 2017 Dec 15;358(6369):eaao2648.

53. Li M, Zheng M, Wu S, Tian C, Liu D, Weizmann Y, et al. In vivo production of RNA nanostructures via programmed folding of single-stranded RNAs. Nat Commun. 2018;9(1):2196.

54. Komura F, Takahashi Y, Inoue T, Takakura Y, Nishikawa M. Development of a Nanostructured RNA/DNA Assembly as an Adjuvant Targeting Toll-Like Receptor 7/8. Nucleic Acid Ther. 2019 Jul 18;29(6):335–42.

55. Afonin KA, Viard M, Martins AN, Lockett SJ, Maciag AE, Freed EO, et al. Activation of different split functionalities on re-association of RNA-DNA hybrids. Nat Nanotechnol. 2013;8(March):296–304.

56. Afonin KA, Desai R, Viard M, Kireeva ML, Bindewald E, Case CL, et al. Co-transcriptional production of RNA – DNA hybrids for simultaneous release of multiple split functionalities. 2014;42(3):2085–97.

57. Agarwal S, Franco E. Enzyme-Driven Assembly and Disassembly of Hybrid DNA–RNA Nanotubes. J Am Chem Soc. 2019;141:7831–41.

58. Jaeger L, Chworos A. The architectonics of programmable RNA and DNA nanostructures. Curr Opin Struct Biol. 2006;16(4):531–43.

59. Jasinski D, Haque F, Binzel DW, Guo P. Advancement of the Emerging Field of RNA Nanotechnology. ACS Nano. 2017 Feb 28;11(2):1142–64.

60. Hong F, Zhang F, Liu Y, Yan H. DNA Origami: Scaffolds for Creating Higher Order Structures. Chem Rev. 2017 Oct 25;117(20):12584–640.

61. Ke W, Hong E, Saito RF, Rangel MC, Wang J, Viard M, et al. RNA – DNA fibers and polygons with controlled immunorecognition activate RNAi , FRET and transcriptional regulation of NF- □ B in human cells. 2019;47(3):1350–61.

62. Afonin KA, Viard M, Kagiampakis I, Case CL, Dobrovolskaia MA, Hofmann J, et al. Triggering of RNA Interference with RNA–RNA, RNA–DNA, and DNA–RNA Nanoparticles. ACS Nano. 2015 Jan 27;9(1):251–9.

63. Monferrer A, Zhang D, Lushnikov AJ, Hermann T. Versatile kit of robust nanoshapes self-assembling from RNA and DNA modules. Nat Commun. 2019;10(1):608.

64. Chen S, Hermann T. RNA–DNA hybrid nanoshapes that self-assemble dependent on ligand binding. Nanoscale. 2020;12(5):3302–7.

65. Chen S, Zhang Z, Alforque E, Hermann T. Complex RNA-DNA hybrid nanoshapes from iterative mix-and-match screening. Nano Res. 2021;14(1):46–51.

66. Parlea L, Bindewald E, Sharan R, Bartlett N, Moriarty D, Oliver J, et al. Ring Catalog: A resource for designing self-assembling RNA nanostructures. Methods. 2016;103:128–37.

67. Kasprzak WK, Ahmed NA, Shapiro BA. Modeling ligand docking to RNA in the design of RNA-based nanostructures. Curr Opin Biotechnol. 2020;63:16–25.

68. Dibrov SM, Johnston-Cox H, Weng YH, Hermann T. Functional architecture of HCV IRES domain II stabilized by divalent metal ions in the crystal and in solution. Angew Chemie - Int Ed. 2007;46(1–2):226–9.

69. Shu D, Shu Y, Haque F, Abdelmawla S, Guo P. Thermodynamically stable RNA three-way junction for constructing multifunctional nanoparticles for delivery of therapeutics. Nat Nanotechnol. 2011;6(10):658–67.

70. Shu Y, Haque F, Shu D, Li W, Zhu Z, Kotb M, et al. Fabrication of 14 different RNA nanoparticles for specific tumor targeting without accumulation in normal organs. RNA. 2013 Jun 1;19(6):767–77.

71. Hao C, Li X, Tian C, Jiang W, Wang G, Mao C. Construction of RNA nanocages by re-

engineering the packaging RNA of Phi29 bacteriophage. Nat Commun. 2014;5(1):3890.

72. Schwarz-Schilling M, Dupin A, Chizzolini F, Krishnan S, Mansy SS, Simmel FC. Optimized Assembly of a Multifunctional RNA-Protein Nanostructure in a Cell-Free Gene Expression System. Nano Lett. 2018 Apr 11;18(4):2650–7.

73. Xiao F, Demeler B, Guo P. Assembly Mechanism of the Sixty-Subunit Nanoparticles via Interaction of RNA with the Reengineered Protein Connector of phi29 DNA-Packaging Motor. ACS Nano. 2010 Jun 22;4(6):3293–301.

74. Xu C, Li H, Zhang K, Binzel DW, Yin H, Chiu W, et al. Photo-controlled release of paclitaxel and model drugs from RNA pyramids. Nano Res. 2019;12(1):41–8.

75. Vantomme G, Meijer EW. The construction of supramolecular systems. Science (80-). 2019 Mar 29;363(6434):1396 LP – 1397.

76. Krishnan Y, Seeman NC. Introduction: Nucleic Acid Nanotechnology. Chem Rev. 2019 May 22;119(10):6271–2.

77. Afonin KA, Dobrovolskaia MA, Church G, Bathe M. Opportunities, Barriers, and a Strategy for Overcoming Translational Challenges to Therapeutic Nucleic Acid Nanotechnology. ACS Nano. 2020 Aug 25;14(8):9221–7.

78. Guo P. The emerging field of RNA nanotechnology. Nat Nanotechnol. 2010;5(12):833–42.

79. Jaeger L, Westhof E, Leontis NB. TectoRNA: Modular assembly units for the construction of RNA nano-objects. Nucleic Acids Res. 2001;29(2):455–63.

80. Ishikawa J, Furuta H, Ikawa Y. RNA Tectonics (tectoRNA) for RNA nanostructure design and its application in synthetic biology. Wiley Interdiscip Rev RNA. 2013;4(6):651–64.

81. Jiang F, Kumar RA, Jones RA, Patel DJ. Structural basis of RNA folding and recognition in an AMP-RNA aptamer complex. Nature. 1996;382(6587):183–6.

82. Guest Editorial: Nucleic Acid Nanotechnology. Acc Chem Res. 2014 Jun 17;47(6):1643–4.

83. Ohno H, Akamine S, Saito H. RNA nanostructures and scaffolds for biotechnology applications. Curr Opin Biotechnol. 2019;58:53–61.

84. Hermann T, Patel DJ. Adaptive Recognition by Nucleic Acid Aptamers. Science (80-). 2000 Feb 4;287(5454):820 LP – 825.

85. Khaled A, Guo S, Li F, Guo P. Controllable Self-Assembly of Nanoparticles for Specific Delivery of Multiple Therapeutic Molecules to Cancer Cells Using RNA Nanotechnology. Nano Lett. 2005 Sep 1;5(9):1797–808.

86. Douglas SM, Bachelet I, Church GM. A Logic-Gated Nanorobot for Targeted Transport of Molecular Payloads. Science (80-). 2012 Feb 17;335(6070):831 LP – 834.

87. O'Hara MJ, Marashi D, Morton S, Jaeger L, Grabow WW. Optimization of the Split-Spinach Aptamer for Monitoring Nanoparticle Assembly Involving Multiple Contiguous RNAs. Vol. 9, Nanomaterials . 2019.

88. Chopra A, Sagredo S, Grossi G, Andersen ES, Simmel FC. Out-of-plane aptamer Functionalization of RNA three-helix tiles. Nanomaterials. 2019;9(4).

89. Sakai Y, Islam MS, Adamiak M, Shiu SCC, Tanner JA, Heddle JG. DNA aptamers for the functionalisation of DNA origami nanostructures. Genes (Basel). 2018;9(12):1–20.

90. Panigaj M, Johnson MB, Ke W, McMillan J, Goncharova EA, Chandler M, et al. Aptamers as Modular Components of Therapeutic Nucleic Acid Nanotechnology. ACS Nano. 2019 Nov 26;13(11):12301–21.

91. Pei H, Liang L, Yao G, Li J, Huang Q, Fan C. Reconfigurable Three-Dimensional DNA Nanostructures for the Construction of Intracellular Logic Sensors. Angew Chemie Int Ed. 2012 Sep 3;51(36):9020–4.

92. Banerjee A, Bhatia D, Saminathan A, Chakraborty S, Kar S, Krishnan Y. Controlled Release of Encapsulated Cargo from a DNA Icosahedron using a Chemical Trigger. Angew Chemie Int Ed. 2013 Jul 1;52(27):6854–7.

93. Liu Z, Tian C, Yu J, Li Y, Jiang W, Mao C. Self-Assembly of Responsive Multilayered DNA Nanocages. J Am Chem Soc. 2015 Feb 11;137(5):1730–3.

94. Liao W-C, Lu C-H, Hartmann R, Wang F, Sohn YS, Parak WJ, et al. Adenosine Triphosphate-Triggered Release of Macromolecular and Nanoparticle Loads from Aptamer/DNA-Cross-Linked Microcapsules. ACS Nano. 2015 Sep 22;9(9):9078–86.

95. Azéma L, Bonnet-Salomon S, Endo M, Takeuchi Y, Durand G, Emura T, et al. Triggering nucleic acid nanostructure assembly by conditional kissing interactions. Nucleic Acids Res. 2018 Feb 16;46(3):1052–8.

96. Mitchell C, Polanco JA, DeWald L, Kress D, Jaeger L, Grabow WW. Responsive self-assembly of tectoRNAs with loop–receptor interactions from the tetrahydrofolate (THF) riboswitch. Nucleic Acids Res. 2019 Jul 9;47(12):6439–51.

97. Huizenga DE, Szostak JW. A DNA Aptamer That Binds Adenosine and ATP. Biochemistry. 1995 Jan 1;34(2):656–65.

98. Lin CH, Patel DJ. Structural basis of DNA folding and recognition in an AMP-DNA aptamer complex: Distinct architectures but common recognition motifs for DNA and RNA aptamers complexed to AMP. Chem Biol. 1997;4(11):817–32.

99. Hardin CC, Perry AG, White K. Thermodynamic and kinetic characterization of the dissociation and assembly of quadruplex nucleic acids. Biopolymers. 2000 Jan 1;56(3):147–94.

100. Seeman NC. DNA Nanotechnology at 40. Nano Lett. 2020 Mar 11;20(3):1477–8.

101. MCluskey JB, Clark DS, Glover DJ. Functional Applications of Nucleic Acid–Protein Hybrid Nanostructures. Trends Biotechnol. 2020;38(9):976–89.

102. Zhou K, Dong J, Zhou Y, Dong J, Wang M, Wang Q. Toward Precise Manipulation of DNA–Protein Hybrid Nanoarchitectures. Small. 2019 Jun 1;15(26):1804044.

103. Shibata T, Fujita Y, Ohno H, Suzuki Y, Hayashi K, Komatsu KR, et al. Protein-driven RNA nanostructured devices that function in vitro and control mammalian cell fate. Nat Commun. 2017;8(1):540.

104. Fu J, Wang Z, Liang XH, Oh SW, Iago-McRae E St., Zhang T. DNA-Scaffolded Proximity Assembly and Confinement of Multienzyme Reactions BT - DNA Nanotechnology: From Structure to Functionality. In: Fan C, Ke Y, editors. Cham: Springer International Publishing; 2020. p. 125–55.

105. Ge Z, Gu H, Li Q, Fan C. Concept and Development of Framework Nucleic Acids. J Am Chem Soc. 2018 Dec 26;140(51):17808–19.

106. Yan Y, Huang J, Tang BZ. Kinetic trapping – a strategy for directing the self-assembly of unique functional nanostructures. Chem Commun. 2016;52(80):11870–84.

107. Fan X, Wang J, Zhang X, Yang Z, Zhang J-C, Zhao L, et al. Single particle cryo-EM reconstruction of 52 kDa streptavidin at 3.2 Angstrom resolution. Nat Commun. 2019;10(1):2386.